The Dissertation Committee for Jeremiah Wayne Hanes Certifies that this is the approved version of the following dissertation:

THE ROLE OF THE HUMAN MITOCHONDRIAL POLYMERASE IN THE TOXICITY OF NUCLEOSIDE ANALOGS AND AGING

Committee:

Kenneth A. Johnson, Supervisor

Jon D. Robertus

Rick Russell

Kevin N. Dalby

Ernst-Ludwig Florin

THE ROLE OF THE HUMAN MITOCHONDRIAL POLYMERASE IN THE TOXICITY OF NUCLEOSIDE ANALOGS AND AGING

by

Jeremiah Wayne Hanes, B.S.

Dissertation

Presented to the Faculty of the Graduate School of

The University of Texas at Austin

in Partial Fulfillment

of the Requirements

for the Degree of

Doctor of Philosophy

The University of Texas at Austin

December, 2004

Dedication

To my soul mate, Serena L. Beller

Acknowledgements

I would like to thank my advisor, Kenneth Johnson for his willingness to educate and support me throughout my time in his lab. He taught me much more than biochemistry. I would also like to thank JoAnn Hunter Johnson for her support in the lab and many valuable lessons on life. Allison Johnson taught me many of the techniques used throughout this dissertation. I enjoyed many fruitful conversations with Harold Lee and Jarle Lillemoen on various topics of this work. Jeff Bartron maintained stocks of purified protein. Everyone in the lab, past and present, has been helpful and it has been a great experience to have worked with them. Thank you to my family for making my education possible and to Serena Beller for the sacrifices she made along the way.

THE ROLE OF THE HUMAN MITOCHONDRIAL POLYMERASE IN THE TOXICITY OF NUCLEOSIDE ANALOGS AND AGING

Publication No._____

Jeremiah Wayne Hanes, PhD

The University of Texas at Austin, 2004

Supervisor: Kenneth A. Johnson

The toxic side effects associated with the administration of nucleoside analogs used to treat HIV are correlated with the kinetics of incorporation by the human mitochondrial polymerase γ (Pol γ). The reconstitution of recombinant human enzyme has allowed for a detailed mechanistic analysis of the reactions governing nucleotide selectivity of the polymerase and the proofreading exonuclease. One nucleoside analog in particular, zidovudine (AZT), exhibits unique kinetics of incorporation by Pol γ. Evidence is presented supporting a model in which the kinetics of incorporation of AZT differ from that of natural nucleotides and other nucleoside analogs, in that phosphoryl transfer is reversibly linked to binding by way of a slower than normal enzyme isomerization following phosphoryl transfer. The implication of the unique reaction kinetics on the toxicity associated with the use of AZT is also discussed.

The most toxic nucleoside analog approved for treatment of HIV is zalcitabine (ddC). It was shown previously that the incorporation of ddC by Pol γ is relatively efficient and that the removal by the proofreading exonuclease was too slow to measure

under the conditions used. Both efficient incorporation and slow removal are likely to contribute to the observed clinical toxicity. I revisited this phenomenon by measuring the rate of excision more accurately and under various conditions in order to better understand the mechanistic basis for the slow removal of ddC.

In addition to a role in the toxicity of nucleoside analogs used to treat HIV, Pol γ may play an important part in the process of aging. The mitochondrial theory of aging states that electrons derived from the electron transport chain during normal respiration produce especially high levels of reactive oxygen species (ROS) in the mitochondria. These ROS can damage the mitochondrial genome, compromising its integrity. One of the most common products of oxidative damage to DNA is 8-oxodG. I have examined the kinetic parameters governing the replication of oxidatively damaged DNA by Pol γ and show that replication fidelity is reduced when incorporation is performed when 8-oxodG is the templating base. I provide evidence suggesting that oxidized free nucleotide (8-oxodGTP) may also be mutagenic.

Table of Contents

List of Tables

List of Figures

Chapter 1: Introduction

HUMAN MITOCHONDRIAL DNA POLYMERASE γ

The mitochondrial genome is approximately 16 kilobases in length and encodes genes for 13 proteins involved in oxidative phosphorylation, 22 tRNAs, and 2 rRNAs (*1;2*). The number of mitochondria per human cell varies from 100 to 1500 depending on tissue type and cell cycle phase (*3*). With two to ten copies of the mitochondrial genome per mitochondria, a single somatic cell can have thousands of copies (*4*). The mitochondrial DNA polymerase γ (Pol γ) is responsible for the replication of the mitochondrial genome. Initially, our interest in Pol γ stemmed from compounding evidence that many of the various toxic side effects associated with the administration of nucleoside analogs used for the treatment of Human Immunodeficiency Virus (HIV) are a result of mitochondrial DNA (mtDNA) depletion. Each of the U.S. Food and Drug Administration (FDA) approved nucleoside analogs terminate replication of the HIV genome by acting as substrates for HIV reverse transcriptase (RT). It soon followed that a similar mechanism of inhibition may be occurring during replication of the mitochondrial genome by inhibiting Pol γ.

Pol γ possesses 5′-3′ DNA dependent DNA polymerase activity and 3′-5′ exonuclease proofreading activity. The holoenzyme is thought to be a heterotrimer comprised of a catalytic subunit of approximately 140 kDa and two subunits of an accessory protein of about 54 kDa each (5). Both the catalytic and accessory subunits are nuclearly encoded and imported into the mitochondria (6). The catalytic subunit is encoded by the nuclear POLG gene mapped to human chromosome location 15q24 (7). Pol γ is a member of the family A DNA polymerases, along with T7 DNA polymerase and E. coli DNA polymerase I. Although currently the structure of Pol γ catalytic subunit

is unknown, it is presumed to follow the pattern of a right hand characteristic of family A DNA polymerases (8;9). The accessory subunit structure has been solved and forms a dimer with a structure related to glycyl-tRNA synthetase, but has no catalytic activity (5;10). Pol γ is in low abundance in human tissues (6), therefore, we and others have overexpressed the recombinant human Pol γ catalytic and accessory subunits to allow reconstitution of the holoenzyme (11-14). Work in our laboratory has revealed the role of the accessory subunit to be a nontraditional processivity factor, in that it does not increase the affinity of the polymerase for DNA as thioredoxin does for T7 DNA polymerase (15). The accessory subunit of Pol γ functions to increase processivity by increasing the rate of polymerization, but has little effect on the rate of dissociation of the polymerase from DNA (12). Throughout this dissertation the term Pol γ will be used to refer to the reconstituted holoenzyme formed with an excess of the accessory subunit.

Transient-state kinetic methods were used to characterize the replication of DNA by Pol γ. Kinetic studies on Pol γ, and every other DNA polymerase examined with natural deoxynucleoside triphosphate substrates (dNTP) have shown that the pre-steady-state burst of polymerization defines the rate of incorporation, and is followed by steady-state dissociation of DNA from the enzyme (12;16-22). By restricting our attention to the first turnover and examining reactions on a millisecond time scale, we circumvent the slower step (DNA dissociation), limiting steady-state measurements on these processive enzymes. Furthermore, kinetic parameters such as k_{cat} and K_m can be determined accurately with transient-state kinetic methods. Time dependent correct dNTP incorporation under single-turnover conditions (enzyme in excess of DNA) by Pol γ follows a single exponential rate to completion (kinetic mechanism shown below).

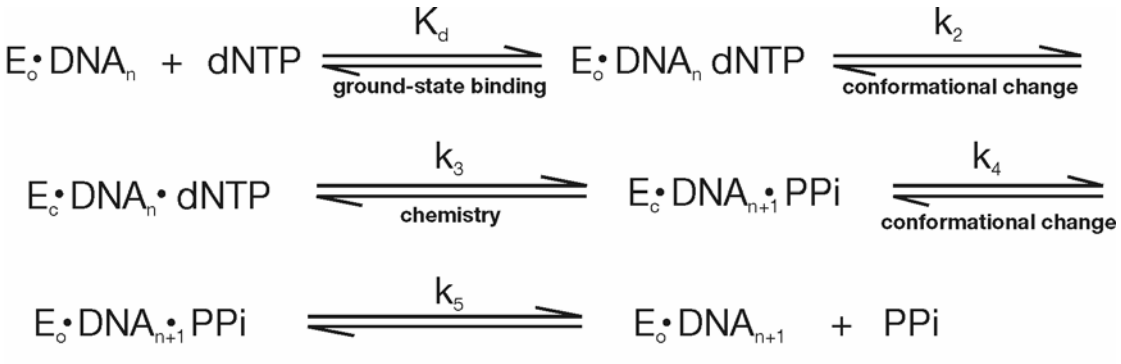

The rate of incorporation is dependent upon the concentration of nucleotide used, according to a hyperbolic relationship, which is indicative of a two-step process. The first step is a fast and reversible (K_d) collision of dNTP with E/DNA complex, allowing for a rapid equilibrium to be established, which is followed by an isomerization (k_2) of the enzyme, which results in both tighter binding and the proper alignment of the active site residues for catalysis(20;23). The observation of a saturable rate affords the measurement of the maximum rate of polymerization (k_{pol}) and the ground-state dissociation constant (K_d), which are equal to k_{cat} and K_m, because dNTP binding is a rapid equilibrium and is followed by a single rate-limiting step. Whether the conformational change or chemistry (phosphoryl transfer) defines k_{pol} for correct nucleotide incorporation by Pol γ has not been established, but for T7 DNA polymerase, mammalian DNA polymerase δ, and HIV RT evidence suggests that the conformational change prior to phosphoryl transfer is rate-limiting (18;24-26).

We have previously examined the kinetic parameters governing DNA replication by Pol γ (11;12;19;27). Figure 1.1 summarizes the results in a scheme redrawn from ref (27). Pol γ is able to copy the DNA at an average rate of 37 s^{-1}, with a processivity of 1,850 bases. The rate of excision of correctly paired DNA by Pol γ is 0.05 s^{-1}. Thus, the cost of proofreading is 0.05/(0.05+37) equal to 0.14%. This value is comparable to that reported for T7 DNA polymerase (0.06%) (28). The rate of incorporation to form a

mismatch varied from 0.01-1.2 s^{-1}, with the fastest rate recorded for the classic Watson-Crick wobble base pair G:T. The rate of excision of a single terminal mismatch increases to 0.4 s^{-1} compared to a correct terminal base pair, but the slow rate of polymerization over the mismatch (0.5 s^{-1}) or stalling is the key factor in increasing the probability of excision. Furthermore, stalling of polymerization continues beyond a mismatch (k_{pol} = 2 s^{-1}) and the rate of excision increases further to 3 s^{-1}, allowing proofreading to occur even when a mismatch is buried.

The rate-limiting step in the excision of a single terminal mismatch is the melting of the primer strand from the template strand. This was evidenced by an experiment showing that as the number of terminal mismatches was increased the rate of excision increased to a maximum rate of about 9 s^{-1} (7 terminal mismatches). Excision of a mismatch has been shown to occur largely (80%) through an intramolecular reaction, meaning that the primer strand is transferred to the exonuclease site, the terminal base is excised, and the strand is transferred back to the polymerase site before dissociation of the enzyme/DNA complex. An estimate of the overall error frequency, including the contribution of the 3′-5′ proofreading activity, is 1 error in 1 to 20 million bases copied (27). This error frequency is considerably higher than the error frequency reported for nuclear DNA replication (1 error in 10^9 to 10^{10} bases copied) and could account for the 5-100 fold higher rate of mutation in mitochondrial DNA relative to nuclear DNA (29;30). Accumulation of errors in the mitochondrial genome is thought to be related to aging. A recent study showed that mice expressing a proofreading-deficient version of Pol γ, prematurely developed numerous signs of aging, apparently as a result of a reduction in the fidelity of replication of the mitochondrial genome (31).

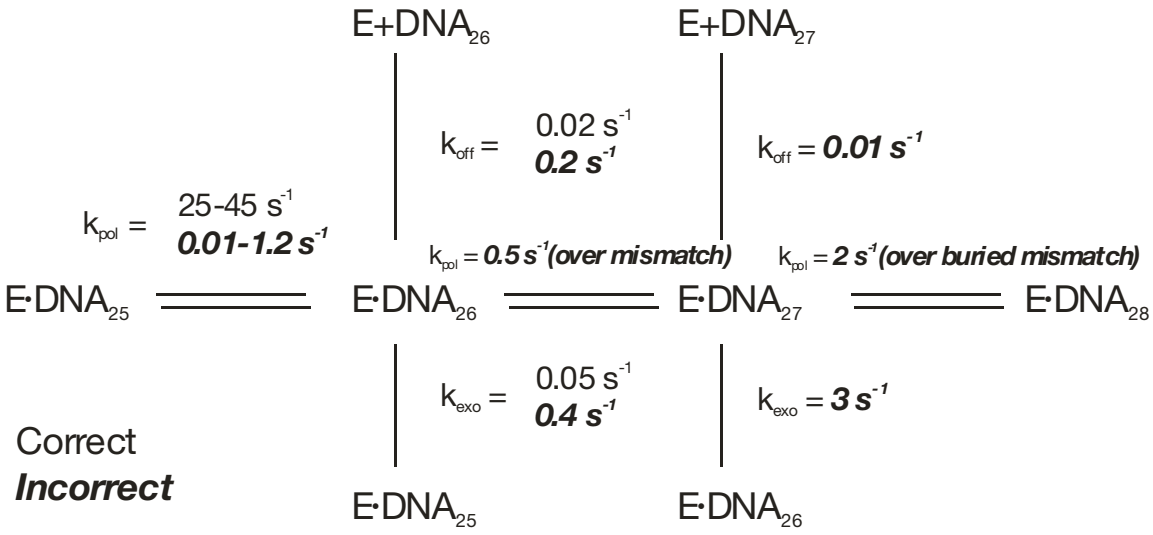

Figure 1.1: Kinetic parameters of polymerization by Pol γ.

The starting DNA used in this scheme was 25/45mer DNA, and the species of DNA at each step is designated by the resulting primer length (i.e. DNA_{25} signifies 25/45 DNA) (27).

TOXICITY OF NUCLEOSIDE ANALOGS

Current treatments for HIV include a cocktail of nucleoside analogs, nonnucleoside inhibitors with fusion, and protease inhibitors. Nucleoside analogs continue to be essential components of highly active antiretroviral therapy (HAART) combination regimens. The major limiting aspects of current treatments are the ability of HIV to develop resistance to the drugs and the toxicity of the nucleoside analogs (32). As a class, administration of nucleoside analogs, used as anti-HIV agents, cause duration-dependent mitochondrial dysfunction, which may be a result of three interrelated mechanisms: mtDNA depletion, oxidative stress, and mtDNA mutations. It has been proposed that these mechanisms work in a sequential manner beginning with energy decline resulting from mtDNA depletion leading to related events of oxidative stress which can cause damage to mtDNA, ultimately leading to mutations in the mitochondrial genome (33).

Effectiveness and toxicity of any given nucleoside analog are likely results of many factors including uptake, transport, metabolic activation, incorporation, and degradation (34-40). As a result of these many factors that influence bioavailability, toxicity is cell-, tissue-, and organ-specific. Patients treated with one or more nucleoside analogs may experience a variety of side effects including peripheral neuropathy, myopathy, pancreatitis, and bone marrow suppression (41). There are currently a total of eight FDA approved nucleoside analogs, given in order of approval: 3′-azido-2′,3′-dideoxythymidine (AZT); 2′,3′-dideoxyinosine (ddI); 2′,3′-dideoxycytidine (ddC); 2′, 3′-didehydro-2′,3′-dideoxythymidine (d4T); β-L-(-)-2′,3′-dideoxy-3′-thiacytadine (-3TC); (-)-cis-2-amino-1,9-dihydro-9-(4-hydroxymethyl)-(2-cyclopenten-1-yl)-6H-purine-6-1 (CBV); (R)-9-(2-phophonyl-methoxypropyl)adenine (PMPA); and 5-fluoro-1-(2R,5S)-

[2-(hydroxymethyl)-1,3-oxathiolan-5-yl]cytosine (FTC). The structures of these analogs are given in Figure 1.2, along with 1-(2′-deoxy-2′-fluoro-beta-D-arabinofuranosyl)-5-iodouridine (FIAU). PMPA, a nucleotide analog, is administered orally as the prodrug tenofovir disoproxil. This improves the lipophilicity of PMPA and increases diffusion across the plasma membrane (42). The structure of PMPA is shown without the hydrolysable lipophilic groups in Figure 1.2. In a similar view, 3% of ddI is intracellularly converted into its active form ddATP, (43;44), and CBV is given as the prodrug abacavir.

Each of the nucleoside analogs are administered orally in an inactive form and require subsequent phosphorylation by host cell kinases to the triphosphate, which can then act as substrates for RT (45). Nucleoside analogs are designed to target RT. They are incorporated into the viral genome during replication and cannot be removed because RT lacks a proofreading exonuclease function. Therefore, the specificity of nucleoside analogs towards RT results from discrimination between correct nucleotides and/or excision by proofreading of the host cellular DNA polymerase (32). As mentioned earlier, the nucleoside analogs approved by the FDA to date lack a 3′-OH group necessary to continue elongation, and thus they act as chain terminators to effectively inhibit viral replication, allowing patients to coexist with a low viral load for years when used in combination with nonnucleoside RT and protease inhibitors. Although such treatment extends patients' lives significantly, the toxicity that results is still limiting.

Side effects resulting from the toxicity of this class of drugs are, by and large, reminiscent of heritable mitochondrial diseases. In addition, *in vivo* studies with AZTTP have been shown to cause ultrastructural changes in mitochondria (46;47). In contrast to other nucleoside analogs AZT causes bone marrow toxicity, which is thought to be due to inhibition of one or more of the chromosomal DNA polymerases (48). In

nonproliferating cells nucleoside analogs, including AZT, have been documented to inhibit Pol γ specifically (48-52). Many of the nucleoside analogs designed for the treatment of HIV, hepatitis B virus (HBV), and other viruses are structurally similar.

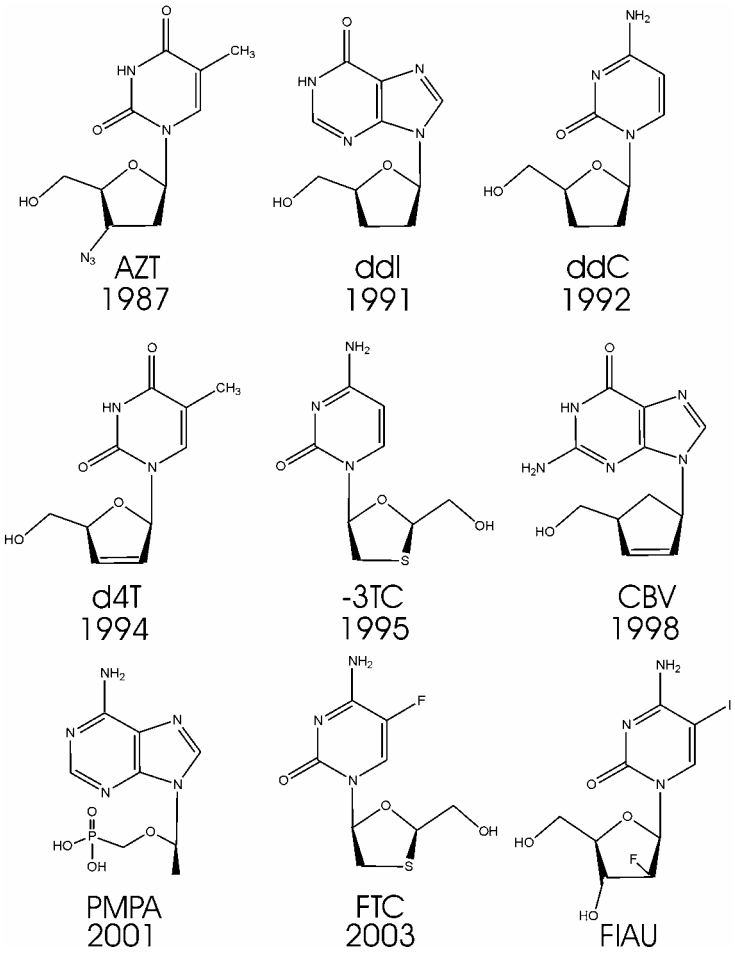

Figure 1.2: Structures and FDA approval dates of nucleoside analogs

The structures of eight approved nucleoside analogs in addition to FIAU are shown. FIAU is not a chain terminator. In an initial clinical trial with HBV infected patients treatment with FIAU resulted in delayed toxicity and eventually the death of five patients (53).

The initial clinical trial with FIAU on chronic HBV infected patients resulted in the death of five patients (54). The toxicity that arose from FIAU was manifest clinically by the presence of myopathy, lactic acidosis, pancreatitis, and hepatic steatosis (55). Based on the evident mitochondrial toxicity, a comparative *in vitro* study using mammalian DNA polymerases α, β, γ, δ, and ε purified from various tissues revealed that while FIAU was incorporated into the nascent DNA chain by all the polymerases, Pol γ was the most efficient (56). One significant difference between FIAU and other nucleoside analogs is the presence of a 3'-OH creating an opportunity for FIAU to be stably incorporated into the mitochondrial genome *in vivo* (57), and may explain the extreme toxicity seen. Studies in our laboratory revealed a k_{pol} of 24 s^{-1} for FIAUTP (TP designates triphosphate), identical to dTTP (58), and a K_d only five-fold weaker. Therefore, the ratio of specificity constants (discrimination) $((k_{pol}/K_d)_{correct}/(k_{pol}/K_d)_{incorrect})$ predicts that one in five template dAMPs, FIAU will be incorporated (assuming the concentration of competing substrates are equal, which is not a valid assumption for *in vivo* conditions). Furthermore, it was shown that there is a 68% probability that FIAU will be buried after incorporation rather than excised by the proofreading exonuclease. Once internalized into the mtDNA, FIAUMP may likely serve as a potent mutagen by altering dNTP selectivity or DNA topology (59).

Based on our kinetic studies examining the ability of Pol γ to discriminate against nucleoside analogs and also efficiency of proofreading, we defined a toxicity index to take into account the relative concentration of the analog triphosphate (AnaTP) compared to the natural dNTP, the rate of incorporation, and the rate of exonuclease removal (60). The toxicity index provides a method to rate compounds for their *potential toxicity*, and is defined as:

$$\text{toxicity index} = (k_{pol}/k_{exo})([\text{AnaTP}]/[\text{dNTP}])/4D$$

where, k_{pol} is the maximum rate of incorporation, k_{exo} is the rate of exonuclease removal, and D is discrimination. By this definition, the toxicity index gives the fractional increase in time required to replicate the mitochondrial genome. The toxicity index for nucleoside analogs examined in our laboratory is shown on a log scale as a bar graph in Figure 1.3 (adapted from ref (60)). The index was created assuming that the concentration of AnaTP and dNTP are equal, which is not generally the case, but is useful for illustrative purposes. The predicted toxicities vary over 6 orders of magnitude and generally follow the observed clinical side-effects. For example, dose-dependent peripheral neuropathy is the major treatment-limiting adverse effect of nucleoside analogs and is commonly seen following treatment with ddC, d4T and ddI, but not consistently with AZT, 3TC or CBV (26). It must be noted that this analysis does not account for the fact that cells replicating at higher rates may be more sensitive, and also that the bioavailability of each analog depends on many factors. In addition, the high copy number of the mitochondrial genome and any possible effect on gene expression resulting from chain termination are ignored. However, the toxicity index given here correlates well for clinically observed toxicities and should be useful to predict the toxicity of new compounds (32).

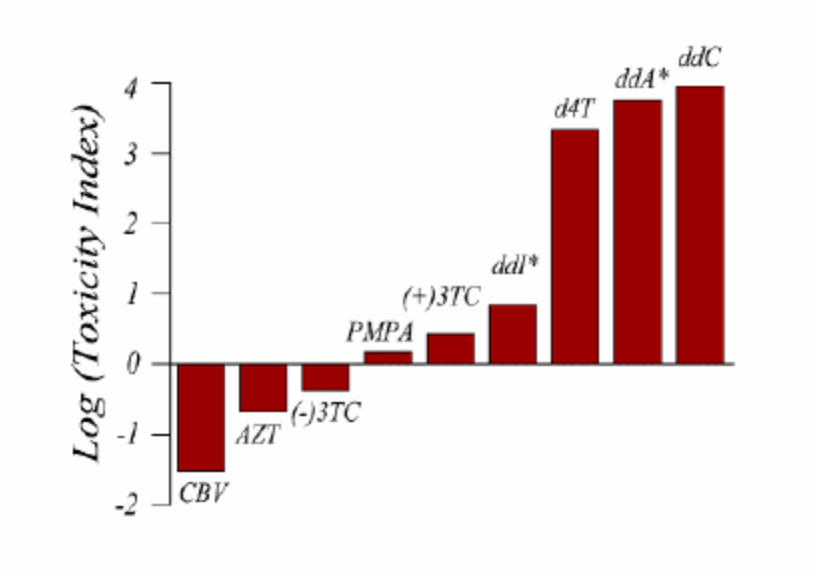

Figure 1.3: Toxicity index of nucleoside analogs

The toxicity index values calculated as described in the text are plotted on a log scale spanning 6 orders of magnitude. The index represents the fractional increase in time it takes to replicate the mitochondrial genome in the presence of an equal concentration of dNTP and nucleotide analog (in the triphosphate form). The concentrations of dNTP and nucleoside analog were assumed to be equal for comparative purposes only, and do not reflect physiological values. All drugs plotted except (+)3TC, and ddA (active form of ddI), have been approved by the FDA for use in the treatment of HIV positive individuals.

Of particular interest was the observation of qualitatively different incorporation of AZTTP by Pol γ. As stated earlier the rate of incorporation of correct nucleotides by Pol γ is dependent upon the concentration of nucleotide present in the experiment. This was also the case for all the nucleoside analogs, except AZTTP. Unlike other nucleotides the rate of AZTTP incorporation was relatively constant as concentration increased, but the amplitude was dependent according to a hyperbolic relationship. It was proposed that the underlying distinction for AZTTP incorporation was that binding could be reversibly linked to phosphoryl transfer (32), but this proposal remains to be tested. Another interesting nucleoside analog, ddC, exhibited a distinctive feature that could explain the severe toxicity seen clinically. The rate of excision of ddC was extremely slow compared to the other nucleoside analogs. This, in essence, reduces the comparison of effectiveness and toxicity to the abilities of RT and Pol γ to discriminate against ddCTP during incorporation, since neither polymerase has the ability to repair the termination. Further studies on the kinetics of the incorporation of AZT and the removal of ddC are part of this dissertation.

A detailed understanding of the mechanism by which antiviral drugs act to slow or inhibit mitochondrial replication is paramount in defining molecular attributes that cause and alleviate toxicity. More studies need to be undertaken in order to identify the exact structural features that take advantage of the differences in selectivity between Pol γ and HIV RT.

MITOCHONDRIAL THEORY OF AGING

According to the mitochondrial theory of aging, electrons from the electron transport chain, most likely from complex I are able to reduce O_2 to form superoxide anion radicals (O_2^-) during aerobic respiration. These reactive radicals go on to produce other reactive oxygen species (ROS) (61). ROS can be generated at a few cellular sites,

but in healthy tissues, the majority are a result of metabolism. ROS attack a variety of cellular macromolecules, including proteins, lipids and DNA. However, damage to mtDNA has been implicated as the most important in regard to aging, especially in postmitotic cells such as neurons (62-70).

One of the most common and significant products of oxidative DNA damage is 8-hydroxy-2′-deoxyguanosine (8-oxodG), which is mutagenic and is commonly used as biomarker for oxidative stress. Basal levels of 8-oxodG in mtDNA comparing different species correlate negatively with longevity in many mammals and birds, which is not the case with nuclear DNA (nDNA) (71). Moreover, as a result of the proximity of mtDNA to the electron transport chain, the levels of oxidative damage are significantly higher in all tissues of mammals and birds than in the nucleus (72).

The concern surrounding 8-oxodG stems from its mutagenic coding potential when copied by an assortment of mammalian and prokaryotic polymerases (73-75). For all studies done with DNA polymerases, dC and dA were inserted across from 8-oxodG with comparable efficiencies which potentially results in a G to T transversion mutation if gone unrepaired. The molecular mechanism for the lack of specificity afforded by 8-oxodG is thought to be due to the ability to form either a normal Watson-Crick hydrogen bonding arrangement with dCMP or a Hoogsteen base pair with dAMP by flipping to the *syn* conformation (76;77).

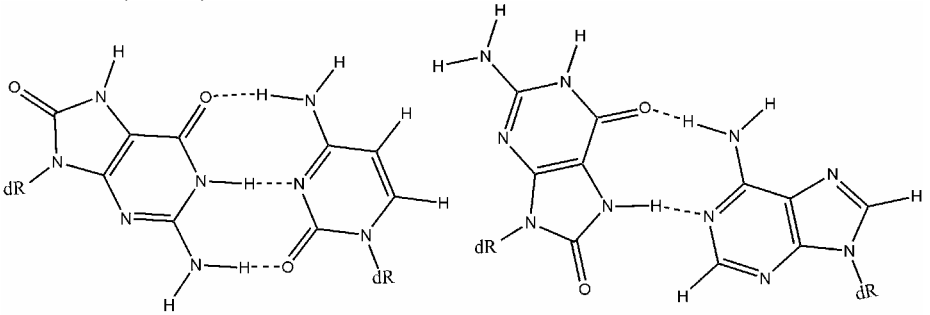

However, there are currently no detailed biochemical studies with the human mitochondrial polymerase γ examining the mutagenic potential of this oxidative lesion. Therefore, one chapter of this dissertation is devoted to the kinetic characterization of oxidatively damaged DNA replication by Pol γ

PROJECT SUMMARY

The projects reported in this dissertation can be divided into four main categories. Overexpression and purification of Pol γ holoenzyme using bacteria was carried out as an attempt to obtain a higher quality protein preparation (Chapter 2). A protocol was developed to separate and quantify products of single nucleotide incorporation reactions with a fluorescently labeled DNA substrate by capillary electrophoresis (Chapter 3). A detailed kinetic analysis of AZT incorporation by Pol γ was performed to explain the confusion regarding anomalous results obtained previously in our laboratory (Chapter 4). In line with this study was a brief examination of ddC excision in order to clarify the basis for inefficient removal (Chapter 5). The kinetic parameters governing the replication of oxidatively damaged DNA were obtained in order to contribute a much needed detailed study for the field of aging and age related diseases (Chapter 6).

Chapter 2: Expression and Purification of Pol γ Holoenzyme in Bacteria

INTRODUCTION

Previous attempts at the overexpression of recombinant Pol γ catalytic subunit in bacteria yielded poor results. A large quantity of protein was expressed, but it was wholly insoluble, which forced the use of a eukaryotic expression system employing a baculovirus vector and SF9 cells (11). Overexpression of the accessory subunit for Pol γ in bacteria was achieved, and the holoenzyme reconstituted with the two subunits (12). Bacterial expression systems have considerable advantages over the eukaryotic system we are currently using, namely, ease of site-directed mutagenesis, potentially better yield, lower cost, and less maintenance. The following research was an attempt to improve the expression of the catalytic subunit in bacteria by co-expressing the accessory subunit using a vector with two promoters and two cloning regions. It was hypothesized that the presence of the accessory protein could stabilize or aid in the folding process of the catalytic subunit during late stage synthesis. Additionally, degradation of the catalytic subunit was apparent in preparations from SF9 cells, and it is reasonable that the presence of the accessory subunit during expression and purification may reduce proteolysis.

MATERIALS AND METHODS

Bacterial overexpression of Pol γ holoenzyme

The large and small subunits were both inserted into the pETDuet-1 vector EMD Biosciences, Inc. (Madison, WI), designed for the co-expression of two target genes. The vector encodes two multiple cloning sites (MCS) each of which is preceded by a T7 promoter/lac operator and ribosome binding site (rbs). The vector also carries the pBR322-derived ColE1 replicon, *lacI* gene and ampicillin resistance gene. The small

subunit cDNA was inserted first because of restriction site limitations. PCR was used to create an insert with an Nco I site and a Methionine codon immediately prior to the 58th amino acid from the amino terminus along with a Afl II site on the carboxyl terminus of the cDNA. A six histidine tag was cloned in during PCR with a stop codon directly following the tag. The insert was then introduced into pETDuet-1 vector. The procedure was repeated for the large subunit insert, but with restriction digest sites of Mun I (N-terminus) and EcoR V (C-terminus). An N-terminal 68 amino acid truncation was cloned based on sequence analysis, based upon an estimate of the putative mitochondrial import signal sequence. This insert also contained a six histidine tag introduced during PCR followed by a stop codon. A vector map summarizing the cut sites and placement of cDNA is shown in Figure 2.1. The expression construct was transformed into BL21(DE3) cells. The transformed BL21(DE3) cells were grown to an OD_{600} of 0.4 in TB media including ampicillin at 100 μg/mL, at which time the temperature was reduced to 12^{o}C in either a 5 L Biostat fermenter, Sartorius AG (Goettingen, Germany) or a 16 L glass carboy equipped with an aerator (the carboy was placed in a refrigerated incubator to control the temperature for overexpression). Protein production was induced by the addition of isopropyl-D-thiogalactopyranoside to 0.5 mM. After 24 h of induction at 12^{o}C, the cells were harvested by centrifugation for 20 minutes at 3000 rpm in a Beckman JL-8 rotor at 4^{o}C. Cell pellets were then frozen in liquid nitrogen. The growth conditions in the fermenter were 600 rotations per minute, 1.5 L/min air (vacuum pump was used to deliver the air), and pH 7.2 @ 12^{o}C controlled with 0.5 M HCl and 0.5 M NaOH.

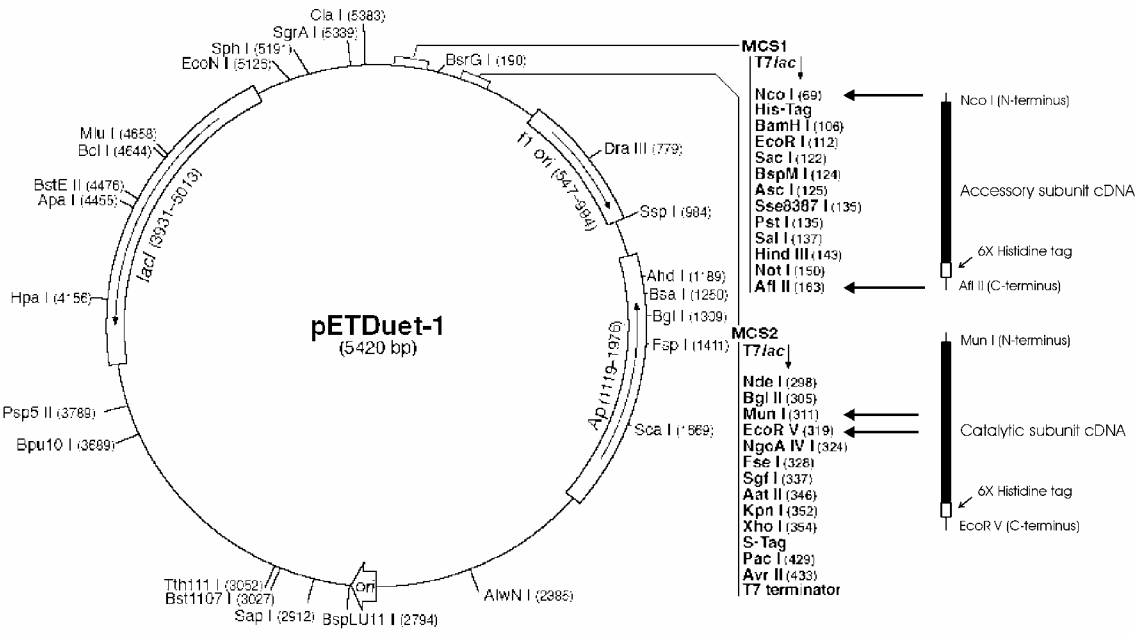

Figure 2.1: pETDuet-1 vector map

The cDNA for the accessory subunit (shown on the right hand side) was inserted into the vector prior to the catalytic subunit cDNA because the cut sites used were present in the cDNA for the catalytic subunit. A C-terminal 6X histidine tag just prior to a stop codon was cloned in during PCR for both the accessory subunit and the catalytic subunit. The cut sites used for cloning are shown on the right hand side with placement of the histidine tags. The map shown was modified from the pETDuet-1 vector map in the product literature published at: http://www.emdbiosciences.com/docs/docs/PROT/TB337.pdf

SDS-PAGE Analysis

All SDS-polyacrylamide gels were performed according to the method of Laemmli (78). A separating gel of 10% was used for all gels, and proteins were visualized with Coomassie blue R-250 (79).

Purification

All procedures were carried out at 4^{o}C unless otherwise specified. The bacterial cell pellets were thawed and resuspended in 5 volumes (mass to volume) of lysis buffer (20 mM Tris-Cl pH 8.0 @ 4^{o}C, 500 mM NaCl, 0.1% Triton X-100, 60 μg/mL lysozyme, 0.2 mM phenylmethylsulfonyl fluoride, and 0.7 μg/mL leupeptin). The suspension was stirred at 4^{o}C for 1 hour to lyse the cells. The lysate was sonicated on ice until it lost viscosity and then centrifuged for 40 min at 16,000 rpm in a Beckman JLA 16.250 rotor at 4^{o}C.

Chelating Sepharose Chromatography

Chelating Sepharose Fast Flow (Amersham Biosciences, Uppsala, Sweden) was prepared by washing 10 mL of resin with five volumes of distilled water, five volumes of 400 mM $NiSO_4$, and three volumes of binding buffer (20 mM Tris-HCl, pH 8.0, 500 mM NaCl, and 5 mM imidazole). As a result of the volume of lysis buffer used to resuspend the large mass of cell pellet (approximately 450 grams) the supernatant of the bacterial lysate was stirred with pre-equilibrated resin for 30 min instead of employing a traditional column. The mixture was centrifuged for 10 min in a Beckman JLA 16.250 rotor at 500 rpm to collect the resin. The resin was resuspended with 25 mL of binding buffer, and poured into a 50 mL column, which was then transferred to the FPLC. A flow rate of 2 mL/min was used for the nickel column. A gradient of 5-400 mM

imidazole was used to elute the protein. Fractions containing holoenzyme, as analyzed by SDS-PAGE and Western blot, were collected and dialyzed into buffer containing 50 mM Tris-HCl, pH 7.2, 50 mM NaCl, 5 mM EDTA, and 10% glycerol.

Single-Stranded DNA Cellulose Chromatography

A 10 mL single stranded DNA cellulose column (Sigma Aldrich) was poured and equilibrated with 50 mM Tris-HCl, pH 7.2, 50 mM NaCl, 1 mM DTT, 5 mM EDTA, and 10% glycerol (TDEG) buffer at pH 7.9 containing 50 mM NaCl. The dialysate from above was loaded onto this column at 1 mL/ min. The protein was eluted with a 100 mL gradient from 50 mM NaCl to 1 M NaCl in TDEG buffer at pH 7.9. Fractions containing holoenzyme were pooled and dialyzed against TDEG at pH 7.2 containing 50 mM NaCl for 4 hours in a 25,000 Dalton MWCO membrane.

Mono-S Chromatography

The dialysate from above was loaded at 1.0 mL/min onto a HR5/5 Mono-S column (Pharmacia, Uppsala, Sweden) that had been equilibrated with TDEG at pH 7.2 containing 50 mM NaCl. The column was washed with equilibration buffer until the A_{280} returned to baseline. The protein was eluted with a 10 mL gradient from 50 mM NaCl to 1 M NaCl in TDEG at pH 7.2 at 0.5 mL/min. The pooled fractions were dialyzed against TDEG (50% glycerol) at pH 8.4 containing 100 mM NaCl overnight. The dialyzed fractions were then frozen in liquid nitrogen and stored at -80°C. The protein concentration was measured by SDS gel electrophoresis Coomassie dye binding assay using BSA as a standard curve.

Preparation of DNA

A DNA primer and template of 25 and 45 nucleotides, respectively, was employed for the polymerase activity assay. The primer sequence was 5′-

GCCTCGCAGCCGTCCAACCAACTCA-3′, and the template sequence was 5′-GGACGGCATTGGATCGAGGGTGAGTTGGTTGGACGGCTGCGAGGC-3′. Primer was 5′-^{32}P-labeled using T4 polynucleotide kinase, according to the manufacturer's instructions (Life Technologies, Gaithersburg, MD). The reaction was terminated by incubation at 95°C for 5 minutes, and excess nucleotide was removed using a Bio-Spin 6 column (BioRad, Hercules, CA). Primer was annealed to 45-mer template by combining at an equimolar ratio, heating to 95 °C, and slowly cooling to room temperature.

Single nucleotide incorporation assay

A quench-flow apparatus (RFQ-3) from KinTek Corp. (Austin, TX) was used to rapidly mix and quench the reactions. Incorporation assays were performed at 37^{o}C in buffer containing 50 mM Tris-Cl, pH 7.5, 100 mM NaCl, 2.5 mM $MgCl_2$. Incorporation reactions were initiated by the addition of nucleotide and magnesium in the same reaction buffer at 37 °C and then quenched with 0.5 M EDTA. All concentrations given are concentrations after mixing. Products were separated on 15% denaturing polyacrylamide sequencing gels, imaged on a Molecular Dynamics Storm 860, and quantified using ImageQuaNT software (Amersham Biosciences, Uppsala, Sweden). Product formation as a function of time was fit to the burst equation ($[product] = A_1 * e^{-k_1 t} + k_{ss} t + C$), where A_1 is the amplitude, k_1 is the burst rate, and k_{ss} is the steady-state rate.

RESULTS

In an attempt to obtain soluble Pol γ holoenzyme using bacteria the pET-Duet-1 vector was employed because it was designed for the overexpression of two proteins simultaneously. It was thought that the accessory subunit, which has been successfully overexpressed in bacteria, may be able to stabilize the catalytic subunit, rendering it soluble and active. Sequencing results confirmed that cloning of the catalytic and

accessory subunit cDNA inserts into the pET-Duet-1 vector was successful and an induction trial was run (Figure 2.2) at 37^{o}C for four hours. The large subunit expressed at a high enough level to be visible in the total cell lysate, but when the lysate was cleared, greater than 95 percent pelleted with the cellular debris at 37^{o}C. Temperatures as low as 12^{o}C were attempted with a slightly better outcome, however such a small amount of protein was soluble that it could only be observed by western blot (Data not shown).

To look for the presence of soluble active Pol γ holoenzyme the volume of cell culture was scaled-up for preparation and purification of the two subunits. Large scale purification of the holoenzyme was performed by growing a 5 L culture in a fermenter and 16 L in a glass carboy. The overexpression of the holoenzyme was similar regardless of whether it was performed in a fermenter or a carboy. Expression was carried out for 24 hours at 12^{o}C and the pellets were combined for a total pellet mass of 450 grams. A batch method was used for the chelating sepharose affinity chromatography since the two subunits were his-tagged and there was a large volume of cleared lysate (detailed in the materials and methods section). A gradient of 5 mM to 400 mM imidazole was run rather than a step elution which is usually performed for this type of column to separate the holoenzyme from contaminants more effectively (Figure 2.3A). A faint band at the correct molecular weight was apparent on the Coomassie blue stained gel, which was confirmed by western blot. The remaining portion of the procedure was adapted from the protocol previously developed in our laboratory for the purification of the catalytic subunit alone which was overexpressed in a baculovirus-SF9 cell expression system (11). Briefly, ssDNA cellulose chromatography and Mono S cation exchange chromatography columns were run with success (Figure 2.3B). The two subunits co-eluted from the ssDNA column, but at slightly different salt concentrations. A control elution was run with holoenzyme reconstituted with catalytic subunit purified from the baculovirus

expression system and accessory subunit purified from bacteria with similar results (Data not shown). A steep gradient was run for the mono S column to concentrate the protein prior to final dialysis (Figure 2.3C). It is apparent from the gel that the preparation did not result in a homogenous mixture of the holoenzyme; furthermore the accessory subunit was in great excess of the catalytic subunit. However, the large excess of small subunit is not a significant issue for our kinetic assays, as we reconstitute the holoenzyme by adding a five molar excess of small subunit to the catalytic subunit. The approximate yield from 21 L (450 g cell pellet) of culture was 50 μg of catalytic subunit.

A rapid mixing experiment was performed with the holoenzyme under burst conditions (DNA in excess of enzyme) with the holoenzyme to examine its activity. A final concentration of only 12 nM could be achieved because the stock holoenzyme concentration was low. Therefore, 12 nM holoenzyme was preincubated with 300 nM DNA and mixed with Mg^{+2} and 100 μM dCTP (a single dC was to be inserted according to the template sequence) to start the reaction. The reaction was quenched with 0.5 M EDTA at specified time points (Figure 2.4). The amplitude of the burst was 6.4 ± 0.8 nM and the burst rate was 35 ± 7 s^{-1}. The amplitude of the incorporation reaction corresponds to the concentration of productively bound enzyme/DNA complex in solution; therefore, it was about 50 percent active and had a normal burst rate for dCTP incorporation. However, the steady-state rate was much faster (7.4 ± 1.1 s^{-1}) than previously observed (0.02 s^{-1}), which has been shown to be the rate of dissociation of the enzyme/DNA complex. The reason for the fast steady-state rate is unknown, but the rate measured previously with holoenzyme reconstituted from the catalytic subunit prepared from the baculovirus expression system was a construct that expressed 39 more amino acids on the N-terminus, possibly leading to a slower rate of dissociation.

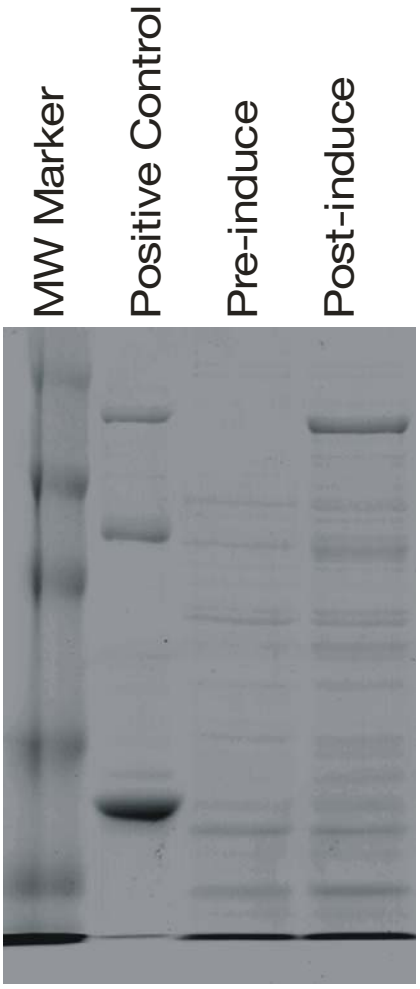

Figure 2.2: Bacterial expression of Pol γ induction trial

Shown is an induction trial for the co-expression of the catalytic and accessory subunits carried out at 37°C for 4 hours. The positive control has both the large and the small subunits, along with degradation products of the large subunit (middle band). The large subunit is obvious in the total cell lysate, and is slightly smaller than the control due to a larger truncation (29 versus 68 amino acid truncation).

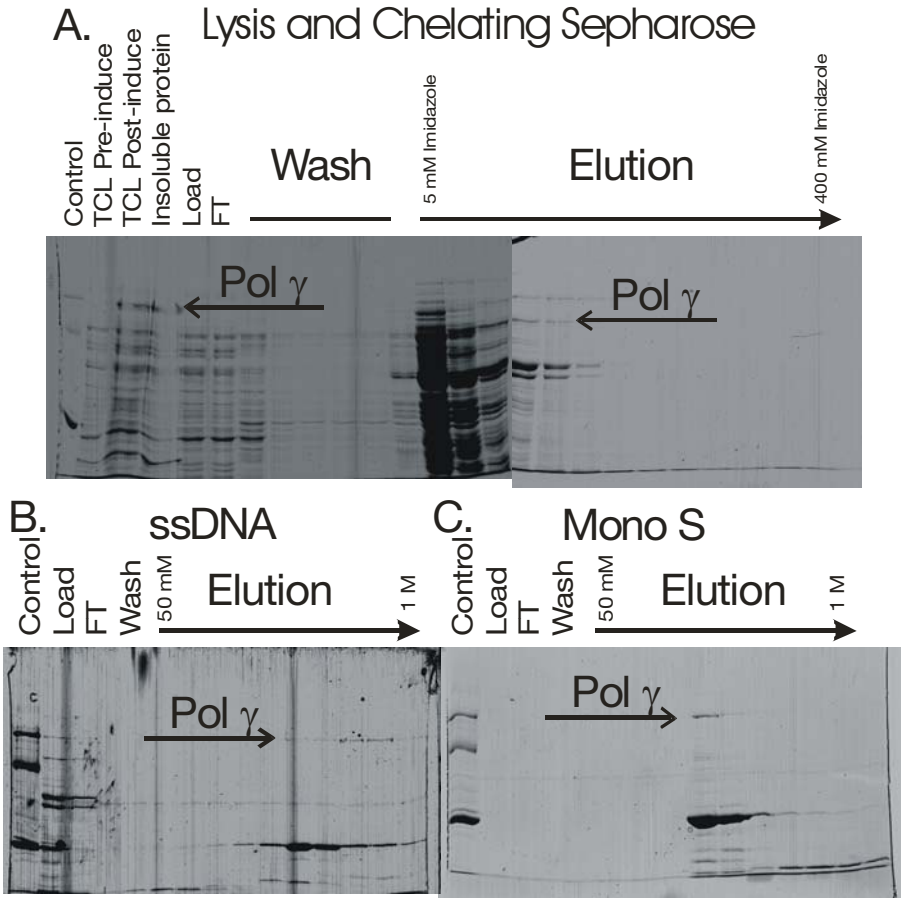

Figure 2.3: SDS-PAGE analysis of Pol γ purification

(A) SDS-PAGE analysis of cell lysis and chelating sepharose affinity chromatography. The large subunit of Pol γ is marked with an arrow, showing that most of the protein after clearing the lysate was in the pellet indicating that it was largely insoluble (upper left-hand gel). There is a small amount of soluble protein in the elution of the nickel column which was pooled and dialyzed for the next column (upper right-hand gel). **(B)** ssDNA affinity chromatography was effective at purifying the large and small subunits (lower left-hand gel). The small subunit is the most intense band in the elution. **(C)** Mono S cation exchange chromatography was used primarily to concentrate the protein.

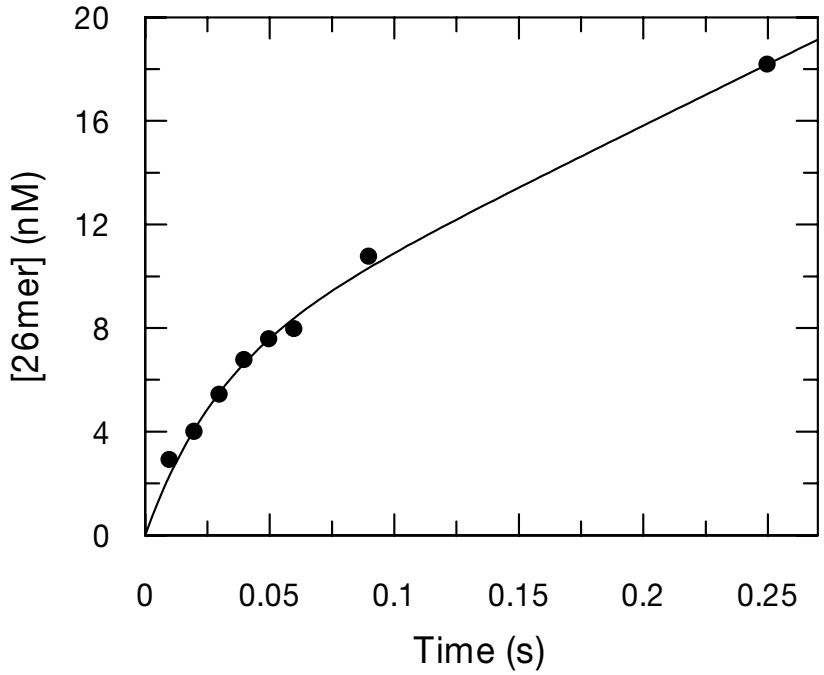

Figure 2.4: Single-nucleotide incorporation by Pol γ holoenzyme

Pol γ holoenzyme (12 nM) was preincubated with 300 nM DNA and rapidly mixed with dCTP and Mg^{+2} to start the reaction. At times plotted on the graph the reaction was quenched with 0.5 M EDTA. Product formation as a function of time was plotted and fit to a burst equation to obtain a burst amplitude of 6.4 ± 0.8 nM, a burst rate of 35 ± 7 s^{-1}, and a steady-state rate of 7.4 ± 1.1 s^{-1}, revealing that about 50 percent of the enzyme was active with a normal burst rate. A steady-state rate of 7.4 s^{-1} is 370-fold faster than we expected, as compared to our previously reconstituted holoenzyme (12).

DISCUSSION

It was shown that it is possible to obtain soluble active Pol γ holoenzyme by co-expressing the two subunits simultaneously in bacteria, whereas expression of the catalytic subunit alone results in no soluble protein. However, a yield of 50 μg per 21 L of cell culture is not sufficient to make the purification favorable over our previously established protocol. The percentage active sites was comparable to that obtained using the eukaryotic expression system as was the burst rate. However the steady-state rate of the single nucleotide incorporation reaction was 370-fold faster, which for most enzymes might indicate that the preparation was higher in quality, but in this case the fast turnover rate suggests that this particular truncation may have reduced the affinity for DNA. The same truncation used for our current studies (29 amino acids) was attempted using the pET Duet vector and identical purification conditions but the catalytic subunit was completely insoluble for unknown reasons.

Chapter 3: Analysis of Single Nucleotide Incorporation Reactions by Capillary Electrophoresis

INTRODUCTION

DNA polymerases are often processive enzymes, catalyzing the incorporation of thousands of bases before dissociating from the primer/template. The following method was developed with recombinant human mitochondrial polymerase γ holoenzyme (Pol γ), which catalyzes roughly 1850 nucleotides during a single DNA binding event (19). Because of this processivity, it is necessary to employ transient-state kinetic methods, using a rapid chemical quench flow, to quantify the incorporation of a single nucleotide under conditions where the polymerase and DNA are at a near stoichiometric ratio. Under conditions where DNA is in a 3-fold excess over Pol γ, a burst of product formation is observed followed by a linear phase, allowing the measurement of the pre-steady-state rate of incorporation, the absolute amount of productively bound enzyme-DNA complex, and the slower steady-state rate of turnover limited by the rate of dissociation of the enzyme-DNA complex (12). Traditionally, a small radio-labeled synthetic oligonucleotide primer annealed to a longer template is used for the extension reaction. Substrate (DNA_n) is then separated from product (DNA_{n+1}) using denaturing polyacrylamide gel electrophoresis (PAGE). In addition to the requirement of using a radiolabel, PAGE is labor intensive, time consuming and wasteful in terms of reagents.

Using laser-induced fluorescence (LIF) in combination with capillary electrophoresis (CE) alleviates some of the problems associated with PAGE and allows one to streamline, and automate product analysis. CE also allows one to eliminate the use of radioactive materials. An overview of the technique used for this report is shown in Figure 3.1. Moreover, a method that can detect fluorescence will allow for more

complex experimental designs using multiple fluorophores. Fluorescence methods are not without limitations beyond sensitivity and the resolution of products. For example, we have encountered problems due to non-specific interactions between the fluorophore-labeled DNA and the enzyme that inhibit polymerization. In addition resolution of the primer by CE has been hampered by the formation of heteroduplex with the template, present at stoichiometric concentrations. In the following report we will discuss our initial failed attempts to use published methods, our solutions to the technical difficulties, as well as the capabilities and limitations of the method.

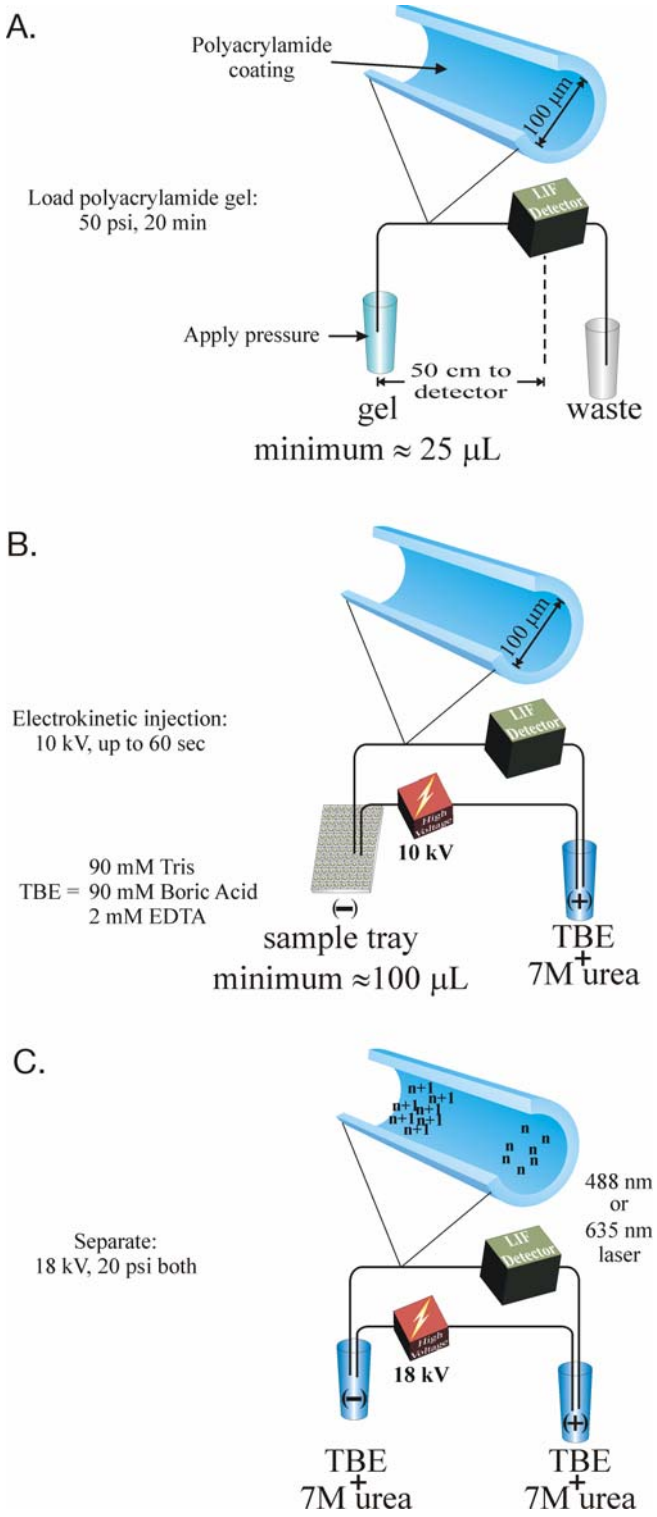

Figure 3.1: Overview of capillary electrophoresis technique

Figure 3.1: Overview of capillary electrophoresis technique

(A) To load the polyacrylamide gel into the capillary, 50 psi was applied to the left vial (gel) for 20 minutes. A capillary length of 50 cm, to the LIF window, was used with the best results. **(B)** Samples were electrokinetically injected with an electric potential of 10 kV for 60 seconds. **(C)** Separation was performed at an electric potential of 18 kV. Because of the relatively long capillary, more than a single sample can be loaded prior to the LIF window by "separating" the injected sample for only 5 minutes (simply to move the sample into the capillary a short distance) and then injecting a second sample as shown in (B) and separating again. A total of 12 points can be injected in this fashion. Then a final separation of about 75 minutes can be performed to record the fluorescence for all twelve points in a single electropherogram.

MATERIALS AND METHODS

Instrumentation

The P/ACE MDQ equipped with both the 488 and 635 nM laser modules was used for capillary electrophoresis (Beckman Coulter, Inc.). The eCAP^{TM} ssDNA 100-R kit, also available from Beckman Coulter, Inc., was used as a guide to begin the method development. Instead of using a 27 cm (20 cm to window) capillary, a 57 cm (50 cm to window) was needed. Experiments done with the 27 cm capillary did not resolve DNA_n from DNA_{n+1}, when DNA_{n+1} was less than 5 % of the total DNA (Data not shown). A 57 cm capillary required longer separation times, but this could be countered by sequential loading of multiple samples, followed by their individual resolution. Such sample stacking was performed by injecting multiple times with a 5 minute separation (18 kV) between each injection. Up to 12 samples were electrokinetically injected for 60 seconds at 10 kV and, after all the samples were injected, separated at 18 kV for 70-90 minutes. Separation time was variable because the migration time of the primer depended on the primer length and the viscosity of the ssDNA 100-R gel. The viscosity of the ssDNA 100-R gel provided with the eCAP^{TM} ssDNA 100-R kit varied for unknown reasons, but the resolution did not. After each 12-point time course was resolved, the gel was replaced and equilibrated. Gel loading and replacement times were extended 2-fold to 20 minutes, to compensate for the use of the 57 cm capillary. Transient-state polymerase reactions were performed using the RQF-3, rapid chemical quench-flow (www.kintek-corp.com).

Enzyme

Purification and characterization of the Pol γ catalytic subunit were as reported previously (11) using an exonuclease-deficient (E200A) enzyme. The accessory subunit

was purified and used to reconstitute the holoenzyme as reported previously (12). Pol γ catalytic subunit was pre-incubated on ice for 20 minutes with the accessory subunit at a stoichiometric ratio of 1:5 to reconstitute the holoenzyme.

DNA

All oligonucleotides were purchased from Integrated DNA Technologies, Coralville, IA, and were purified using 15% denaturing PAGE. The primer/templates used are shown in Figure 3.2. The two 5′-fluorescently labeled (Bodipy™ 630/650 and 6-FAM™) 25/45mer primer/templates were identical in sequence to the radiolabeled primer/template, except for a single T:A pair (G:C in the radioactive control) at the 5′-end. Since 5′-G is less efficiently labeled according to Integrated DNA Technologies, the sequence was modified. Purity of the fluorescently labeled primers was assessed by capillary electrophoresis (approximately 96 %) (Figure 3.3 inset). The concentrations of primer and template were obtained by measuring absorbance at 260 nm using the extinction coefficients provided by Integrated DNA Technologies. Labeled primer was combined with 45mer template at an equimolar ratio, heated to 95 °C, and annealed by slowly being cooled to room temperature.

Radiolabeled 25/45mer

5’-GCCTCGCAGCCGTCCAACCAACTCA
3’-CGGAGCGTCGGCAGGTTGGTTGAGTTGGAGCTAGGTTACGGCAGG

Fluorescently Labeled Primers

25/45mer

5’-Bodipy-TCCTCGCAGCCGTCCAACCAACTCA
3’-AGGAGCGTCGGCAGGTTGGTTGAGTTGGAGCTAGGTTACGGCAGG

25/45mer

5’-6-FAM-TCCTCGCAGCCGTCCAACCAACTCA
3’-AGGAGCGTCGGCAGGTTGGTTGAGTTGGAGCTAGGTTACGGCAGG

23/45mer

5’-6-FAM-CTCGCAGCCGTCCAACCAACTCA
3’-AGGAGCGTCGGCAGGTTGGTTGAGTTGGAGCTAGGTTACGGCAGG

27/45mer

5’-6-FAM-AAGCCTCGCAGCCGTCCAACCAACTCA
3’-CGGAGCGTCGGCAGGTTGGTTGAGTTGGAGCTAGGTTACGGCAGG

27/45mer mismatch

5’-6-FAM-AAGCCTCGCAGCCGTCCAACCAACTCA
3’-AGGAGCGTCGGCAGGTTGGTTGAGTTGGAGCTAGGTTACGGCAGG

Figure 3.2: Sequences of oligonucleotides

The sequences of primer/template combinations used for the experiments are shown. The 25/45mers were identical to the radioactive control, except for the 5′-base, where it was changed from G to T for more efficient labeling.

Preparation of radiolabeled DNA

Primer was 5′-^{32}P-labeled using T4 polynucleotide kinase, according to the manufacturer's instructions (Life Technologies, Gaithersburg, MD). The reaction was terminated by incubation at 95°C for 5 minutes, and excess nucleotide was removed using a Bio-Spin 6 column (BioRad, Hercules, CA).

Product Analysis

Polymerase assay reactions using radiolabeled DNA were separated using 15% denaturing polyacrylamide sequencing gels, imaged on a Molecular Dynamics Storm 860 and quantified using ImageQuaNT software (Amersham Biosciences, Uppsala, Sweden). To normalize data, the integrated amount of product (DNA_{n+1}) was divided by the sum of the substrate and product ($DNA_n + DNA_{n+1}$) and multiplied by the concentration of DNA used in the experiment. For assays using a fluorescent probe, peaks were analyzed by integration using the P/ACE system MDQ software, version 2.3 (Beckman Coulter, Inc.). To normalize data, the peak area of product (DNA_{n+1}) was divided by the sum of the peak area of substrate and product ($DNA_n + DNA_{n+1}$) and multiplied by the concentration of DNA used in the experiment. The time dependent changes in product concentration were fit to the burst equation ($[DNA_{n+1}] = A*e^{-kt} + k_{ss} + C$) using Grafit 5 software (Erithacus Software, Horley Surrey RH6 9YJ UK) where $[DNA_{n+1}]$ is the product concentration, A is the amplitude, k is the burst rate, k_{ss} is the steady-state rate, C is the offset, and, t is time.

Reagents

The eCAP^{TM} ssDNA 100-R kit purchased from Beckman Coulter Inc. included all the necessary materials and reagents for performing capillary electrophoresis, except for the formamide used in the sample buffer, which was purchased from Sigma Aldrich Corp

(St. Louis, MO). Unless otherwise stated, capillary electrophoresis materials and reagents were prepared according to product literature. All other reagents and chemicals were purchased from Sigma Aldrich Corp.

RESULTS

Our goal was to rapidly resolve products from single nucleotide incorporation reactions either under burst or single-turnover (enzyme in excess over DNA) conditions. Because the pre-steady-state incorporation reaction for natural nucleotides proceeds at an average rate of 37 s^{-1} for Pol γ, it is necessary to use a rapid chemical quench-flow to mix and quench the reaction in the millisecond time scale. To form the enzyme-DNA complex, Pol γ holoenzyme was mixed with 5′-fluorescently labeled primer annealed to a 45mer nucleotide template, and allowed to equilibrate on ice for 20 minutes. A solution of the next correct nucleotide (with Mg^{+2}) was prepared separately. After mixing E-DNA with Mg-dNTP 1:1 in the quench-flow instrument, the mixture contained 100 nM Pol γ holoenzyme, 300 nM DNA, 100 μM nucleotide, 50 mM tris (hydroxymethyl)-aminomethane (Tris), 100 mM NaCl, 5mM $MgCl_2$, and 0.1 mg/mL bovine serum albumin (BSA), pH 7.4 @ 37°C. A reaction volume of 30 μL was quenched with 80 μL of 0.5 M ethylene-diamine-tetra-acetic acid (EDTA) and then mixed with 80 μL sample buffer containing 50% formamide. Samples were then loaded into a 96-well plate and heated to 95°C for 5 minutes. Figure 3.3A shows an electropherogram of the reaction mixture at zero time. We expected to observe one peak corresponding to substrate (27mer in this case), but two were present. Figure 3.3B shows an electropherogram after a 0.12 s reaction. A portion of substrate was expected to be converted to product, which is seen to the left of the electropherogram, where there is a group of two peaks corresponding to DNA_n and DNA_{n+1}, but following those peaks were two other peaks. It was clear that some of the primer was migrating as duplex. Surprisingly, sample buffers

containing either 8 M urea or 100% formamide were unable to eliminate the second set of peaks, even though the ssDNA 100-R gel was prepared with 7 M urea and run at 30^{o}C. The two peaks representing primer migrating as duplex were ultimately eliminated by the addition of unlabeled ssDNA complementary to the template to displace the fluorescently labeled primer.

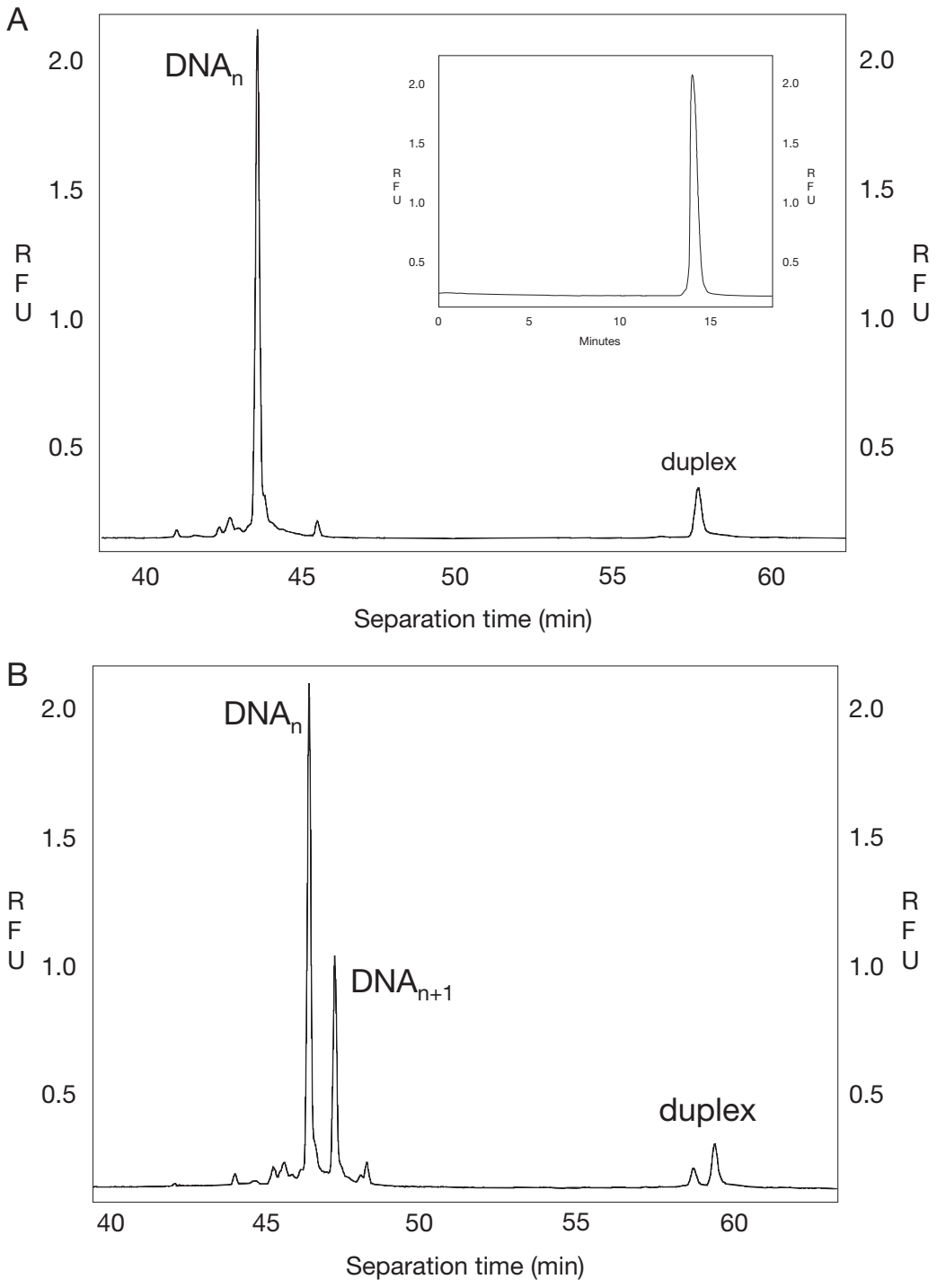

Figure 3.3: Resolution of an oligonucleotide primer, DNA_n, and DNA_{n+1}

Figure 3.3: Resolution of an oligonucleotide primer, DNA_n, and DNA_{n+1}

(A) An electropherogram of a sample that was quenched with 0.5 M EDTA before nucleotide was added (zero time), with final reaction conditions of 300 nM DNA and 100 nM Pol γ holoenzyme. At zero time we expected only a single peak corresponding to substrate, DNA_n. **(Inset)** An electropherogram depicting a 27mer oligonucleotide 5′-6-FAM™ labeled, which was purified using 15% denaturing PAGE. This oligonucleotide was 96% pure. **(B)** A single nucleotide incorporation reaction was performed under the same conditions as in (A), but quenched after 0.12 s reaction. The duplex could not be eliminated by increasing the stringency of melting with higher percentages of formamide or an equal volume of 7-8 M urea.

Such long separation times present a problem for the method to compete with traditional PAGE. Elimination of the contaminating duplex, allowed us to stack the samples onto the gel by sequentially injecting for 60 seconds, separating for 5 minutes, injecting again, and so on. Figure 3.4 is a representative electropherogram of a 12-point time course for single nucleotide incorporation under burst conditions. It shows a decrease in substrate and, concomitantly, an increase in product as a function of reaction time corresponding to the sequential injections. The overall time required for this method, from quenching the last time point to resolving the time course, was approximately 3.5 hours. The actual injection and separation time required for each 12-point time course was 2.5 hours.

We were concerned with possible interactions between the 5′-fluorescent label and the polymerase. Results obtained using two commercially available labels differed kinetically when used in single nucleotide incorporation assays. Bodipy^{TM} 630/650, which has a good signal when excited with the 635 nM laser, was linked to the 5′ end of a 25mer primer and annealed to a 45mer template. Figure 3.5 shows the results of two burst experiments performed in the presence of 100 nM Pol γ holoenzyme and 300 nM DNA reacting with 100 μM dTTP. When fit to a burst equation, the rate of the burst was not significantly different from the experiment performed using the radiolabeled primer, but the amplitude of the reaction was only 30%. The burst amplitude is important because it quantifies the concentration of active E-DNA complexes. The underlying cause for the lower amplitude is unknown, but it seems logical that the highly hydrophobic label may interact with the polymerase to weaken the DNA binding affinity, interfere with proper alignment of the DNA on the enzyme, or both. Bodipy^{TM} labeled DNA was abandoned at this time in the interest of finding a probe that gave results kinetically similar to those obtained using a radioactive label. The possibility of an

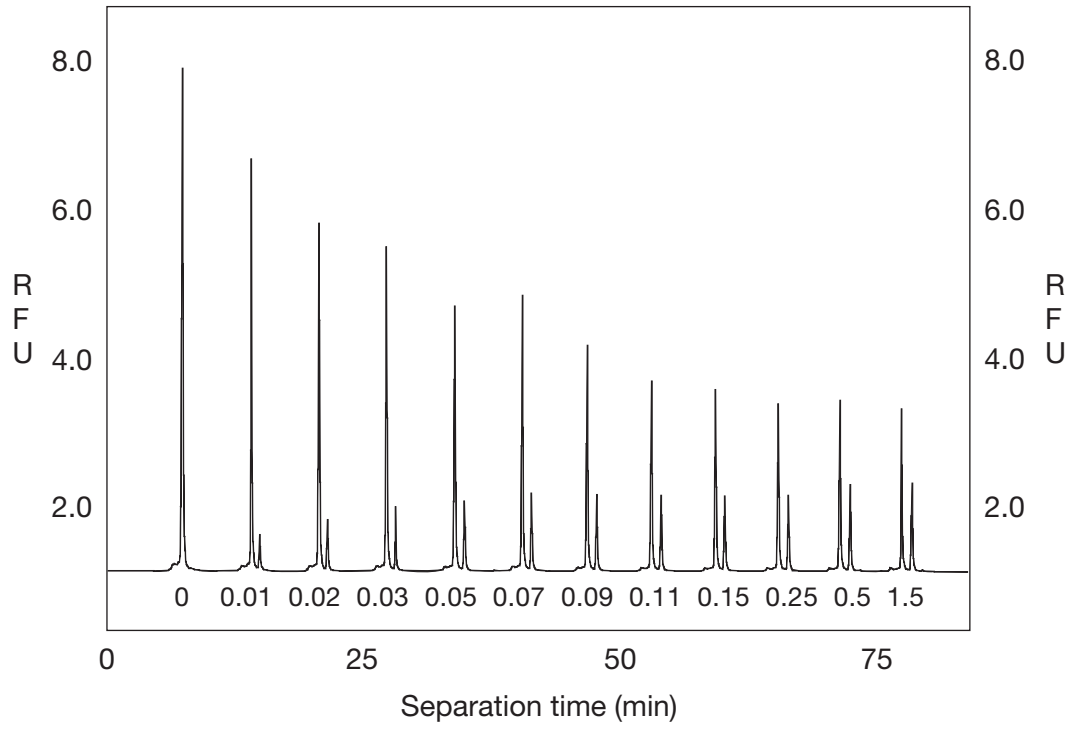

Figure 3.4: Electropherogram of a 12-point burst experiment

The separation of a 12-point pre-steady-state burst experiment (0 - 1.5 seconds) was carried out, where the samples were injected every 5 minutes, and then resolved sequentially. With the elimination of duplex, the samples separated cleanly and were easily analyzed by integration (all points in a single electropherogram). The single peak to the far left was a zero time point, where there was no DNA_{n+1}. In the following peaks there was a decrease in DNA_n, and a corresponding increase in DNA_{n+1}, until approximately 30 % of DNA_n was consumed.

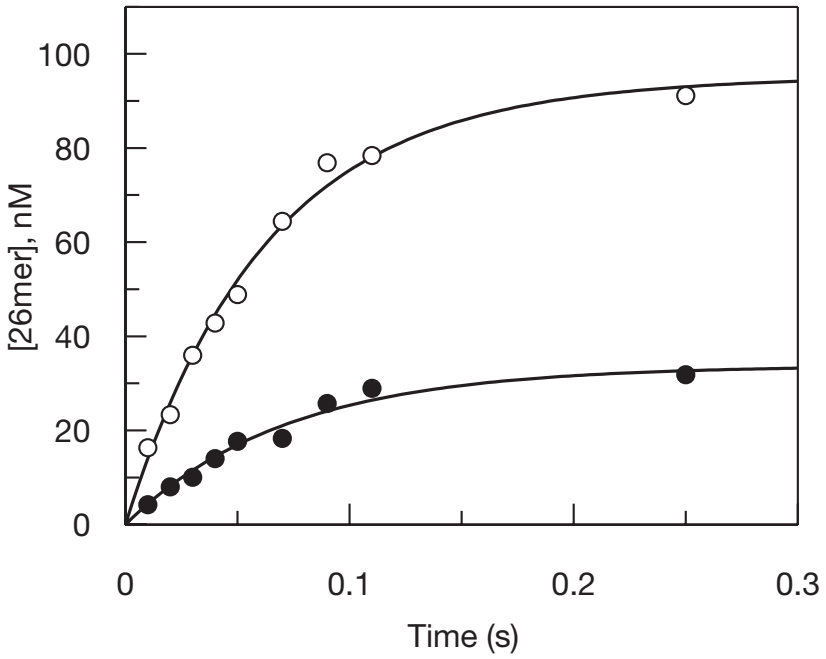

Figure 3.5: Bodipy^{TM} 630/650 labeled primer showed a significant kinetic difference in a burst experiment

Two burst experiments were performed under identical conditions (100 nM Pol γ holoenzyme and 300 nM DNA), except for the 5′-labels. Parallel reactions were performed using radiolabeled primer (○) and a 5′-Bodipy^{TM} 630/650 label (●). The rates are identical, but the reaction with the fluorescently labeled DNA had an amplitude of only 33 ± 1 nM, compared to 93 ± 3 nM for the control.

interaction between the label and the polymerase prompted a brief study probing for possible interactions with 5′-6-carboxyfluorescein (6-FAM™) using the 488 nM laser. Along with a change in the 5′-label from Bodipy™ to 6-FAM™ on the 25mer, two other primers were examined which were of differing lengths. The sequences are shown in Figure 3.2; two were 27/45mers (one with a G:A mismatch at 3′ of the template), which have a two base pair overhang, one was a 23/45mer, which has a two base pair recessed end.

Figure 3.6 shows the results of a series of pre-steady-state burst experiments under identical conditions, except for the sequence and length of the primers used. The rates of the four were relatively normal, but there are significant differences in the reaction amplitudes. The 25/45mer showed normal rate and amplitude. The reason for lower amplitudes obtained with DNA containing an overhang and recessed ends was not examined because the 25/45mer DNA gave a promising result. A parallel experiment performed with a radiolabeled primer is shown in Figure 3.7; the results obtained using the two methods were nearly identical. Further experiments with this primer/template combination showed that single-turnover experiments (90 nM DNA) could be performed with accuracy (data not shown). However, under the conditions outlined here, the limit of detection did not allow for accurate analysis of reactions containing concentrations less than 90 nM 5′-6-FAM™ labeled DNA (2.7 pmol primer per well).

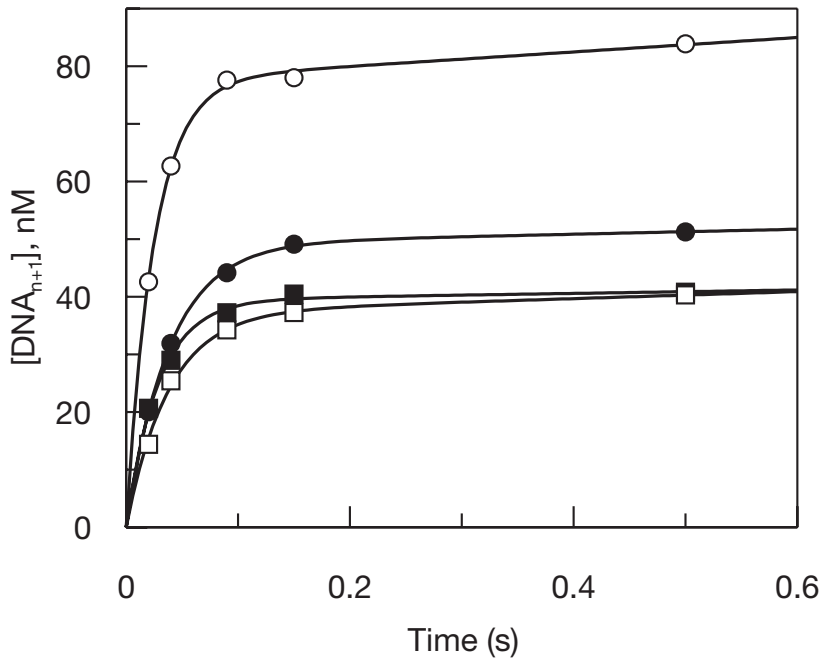

Figure 3.6: Experiments with 5′-6-FAM^{TM}-labeled DNA

Four pre-steady-state experiments were performed under identical conditions, except for the DNA used. Figure 1 depicts the particular sequence for experiments performed with a 23/45mer with a 5′-2 base recess (□), a 27/45mer with a 5′-AA overhang (■), or a 27/45mer with a 5′-AA overhang and a G:A (●) and compared to an experiment performed with a radiolabeled 25/45mer (○), which showed the highest reaction amplitude (77 ± 1 nM).

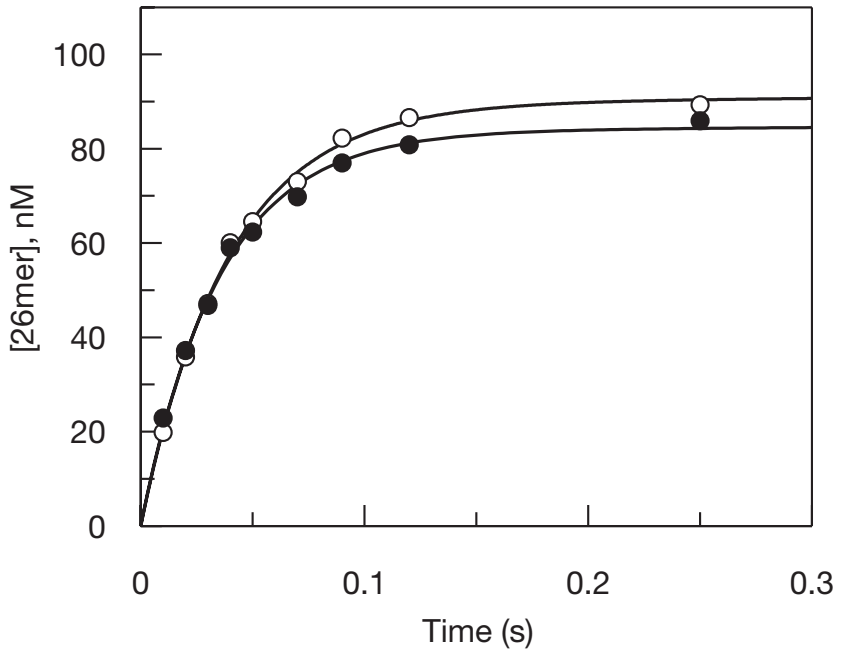

Figure 3.7: 5′-6-FAM™ labeled DNA compared to a radioactive control

The two reactions were performed in parallel, under identical conditions, except that one was done using a 5′-6-FAM labeled 25/45mer (○), whereas the other was done traditionally with a 5′-^{32}P-labeled 25/45mer (●). The experiment with fluorescently labeled DNA had a rate of 26 ± 1 s^{-1} and an amplitude of 89 ± 1 nM, which was similar to the rate and amplitude of the experiment with ^{32}P-labeled DNA (28 ± 1 s^{-1} and 84 ± 1 nM, respectively).

DISCUSSION

We began this work with the goal of developing a method that would allow us to quickly and accurately analyze the products from single nucleotide incorporation experiments without using radiolabels. It was hoped that this would allow more complex experiments to be executed using multiple fluorescent reporters. The main problem(s) we encountered were due to a fraction of the primer migrating in heteroduplex with the template, limiting sensitivity, and fluorophore-protein interactions. Addition of excess unlabeled ssDNA complementary to the template freed the labeled primer, which, in turn, allowed injecting multiple samples and resolving them during a single separation. While the sensitivity limited our ability to accurately analyze samples from reactions containing less than 90 nM 6-FAM™ labeled primer, it was sufficient to allow use of concentrations typically used with radiolabeled primer. It may be possible to go to lower DNA concentrations than examined here by loading undiluted samples into the 96-well plate if the reaction volume is not a concern. Furthermore, labels other than 6-FAM™ may give better signal, which was the case for Bodipy™ 630/650 in these experiments, but it is important to be certain that the fluorescent label reports results comparable to the radioactive label. Capillary life seemed to vary greatly, and with the small sample size, we can not reliably quote a figure, but it is possible for a capillary to last for one hundred 12-point time course separations (1200 data points).

The benefits of the method over traditional PAGE are numerous, in that, radioactive material is eliminated, one time course can be analyzed within 4 hours, samples can be retained much longer, it is far less labor intensive, and is dramatically less wasteful in terms of reagents and laboratory space. It is likely that this method will be useful for many DNA and RNA polymerases, whether examining single, double, or triple

nucleotide incorporation reactions. Multiple incorporation events are common when examining fidelity, where reaction times are much longer, such that, more than one mismatch can be formed. In addition, the technique can be used to inspect the kinetic parameters of incorporation of nucleoside analog chain terminators, as is pertinent for Pol γ.

Chapter 4: Kinetics of AZTTP Incorporation by the Human Mitochondrial Polymerase γ

INTRODUCTION

Current treatments for HIV include various combinations of nucleoside analog reverse transcriptase inhibitors (NRTI), nonnucleoside RT inhibitors (NNRTI), protease inhibitors, and a fusion inhibitor. Nucleoside analogs continue to be essential components of highly active antiretroviral therapy (HAART). The major limiting aspects of current treatments are the ability of HIV to develop resistance on one hand and the toxicity of the nucleoside analogs on the other (32). It has been established that mitochondrial dysfunction observed with the use of nucleoside analogs is largely a result of inhibition of Pol γ during mitochondria DNA replication. There have been a variety of reports for the toxicity of 3'azido-2',3'-dideoxythymidine (AZT) and not all agree on the site of toxicity, leading to some confusion in regard to the clinical side-effects observed for AZT (32).

The incorporation of all nucleoside analogs examined, except AZTTP, exhibited a concentration dependent rate of incorporation. For AZTTP incorporation the amplitude was dependent on concentration according to a hyperbolic relationship, but the rate remained approximately constant, which complicated our interpretation of AZT toxicity (32). We proposed that phosphoryl transfer (k_3) is reversibly linked to binding (kinetic mechanism shown in the introduction). That is to say that phosphoryl transfer is reversible (pyrophosphorolysis) for AZTTP incorporation. This is an interesting prospect given the fact that AZTTP is the second least toxic nucleoside analog according to our toxicity index (Figure 1.3) and could be valuable information to aid the design of novel low toxicity inhibitors with similar incorporation kinetics. This chapter is devoted to

understanding the kinetics of incorporation of AZTTP by Pol γ and how it relates to the mitochondrial dysfunction observed.

MATERIALS AND METHODS

Nucleoside analog triphosphates

AZTTP and d4TTP were obtained from Moravek Biochemicals (Brea, CA). AZATP, AZCTP, and AZGTP were purchased from TriLink Biotechnologies (San Diego, CA).

Pol γ expression and purification

Overexpression and purification of recombinant human Pol γ were previously described (11;12). Holoenzyme was reconstituted at a 1:5 ratio of catalytic subunit to accessory subunit. All of the studies on the kinetics of incorporation of nucleoside analog triphosphates were conducted using an exonuclease-deficient mutant (E200A).

Preparation of DNA

A DNA primer/template of 25 and 45 nucleotides, respectively, was employed for all experiments except when terminated with AZTMP or dTMP for pyrophosphorolysis reactions, in which case they were 26 and 45 nucleotides, respectively. The primer sequence was 5′-GCCTCGCAGCCGTCCAACCAACTCA-3′, and the template sequence was 5′-GGACGGCATTGGATCGAGG**X**TGAGTTGGTTGGACGGCTGCGAGGC-3′, where the bold **X** in the template was modified to provide desired base pair for the particular experiment being conducted. Primer was 5′-^{32}P-labeled using T4 polynucleotide kinase, according to the manufacturer's instructions (Life Technologies, Gaithersburg, MD). The reaction was terminated by incubation at 95°C for 5 minutes, and excess nucleotide was removed using a Bio-Spin 6 column (BioRad, Hercules, CA). Primer was annealed to 45-mer template by combining at an equimolar ratio, heating to

95 °C, and slowly cooling to room temperature. Primers containing 3′-terminal AZTMP were created to examine pyrophosphorolysis. A polymerase reaction was performed using 1 μM HIV-1 RT, 3 μM duplex DNA (containing appropriate template base opposite the 26th primer position), and 50 μM AZTTP in standard reaction buffer (50 mM Tris-Cl, pH 7.5, 100 mM NaCl, 2.5 m $MgCl_2$). The reaction mixture was incubated at 37 °C for 30 min, and then the product was gel-purified to obtain the AZTMP-terminated primer. Primer was labeled, and DNA duplex was annealed as described above.

Incorporation and pyrophosphorolysis reaction conditions

For reactions too fast to measure by benchtop mixing a quench-flow apparatus (RFQ-3) from KinTek Corp. (Austin, TX) was used. All incorporation assays were performed at 37^{o}C in a buffer containing 50 mM Tris-Cl, pH 7.5, 100 mM NaCl, 2.5 mM $MgCl_2$. In some reactions $MgCl_2$ was substituted by $MnCl_2$ as noted in the text and Figure legends. The Pol γ holoenzyme was reconstituted by incubating the two protein subunits for 5 min on ice in reaction buffer lacking magnesium. DNA was then added to the proteins, and the mixture was incubated for an additional 5 min on ice. Incorporation reactions were initiated by the addition of nucleotide and magnesium in the same reaction buffer at 37 °C and then quenched with 0.5 M EDTA. Alternatively, the pyrophosphorolysis reactions were initiated by the addition of PPi and magnesium. All concentrations given are concentrations after mixing. Products were separated on 15% denaturing polyacrylamide sequencing gels, imaged on a phosphorimager, Molecular Dynamics Storm 860, and quantified using ImageQuaNT software (Amersham Biosciences, Uppsala, Sweden).

K_d and maximum rate of incorporation for nucleoside analogs or dTTP

Single nucleotide incorporation assays were performed with various concentrations of analog to examine the nucleotide concentration dependence of incorporation rate or amplitude. Single-turnover conditions were employed where the concentration of enzyme was greater than the concentration of DNA. Specific reaction conditions are listed in each Figure legend. A time course was performed for each concentration of nucleotide or analog. To normalize data, the integrated amount of product (DNA_{n+1}) was divided by the sum of the substrate and product ($DNA_n + DNA_{n+1}$) and multiplied by the concentration of DNA used in the experiment. The concentration of extended product 26mer DNA was plotted against time and fit to a single ([product] = $A_1*e^{-k_1t}$ +C), double ([product] = $A_1*e^{-k_1t} + A_2*e^{-k_2t}$ + C), or triple ([product] = $A_1*e^{-k_1t} + A_2*e^{-k_2t} + A_3*e^{-k_3t}$ + C) exponential equation (as described in the Figure legends and results section). The observed amplitudes were then plotted against nucleotide or analog concentrations, and the data were fit to a hyperbola (observed rate (or amplitude) = k_{pol} (or A_{max}) * [dNTP]/(K_d + [dNTP]) to obtain the K_d and k_{pol} or maximum amplitude (A_{max}) for each nucleoside analog triphosphate or dTTP. For cases where the rate was not dependent on the concentration of the nucleotide analog, the rate was estimated by the reaction rate at the higher concentrations where a higher amplitude allowed a more accurate rate measurement.

Determination of K_d by competition with dTTP

Single exponential rates of dTTP incorporation in the presence of AZTTP were plotted as a function of AZTTP concentration. The data were first fit to a hyperbola and then analyzed with the equation $K_{dapp}=K_{d,AZTTP}(1+([dTTP]/K_{ddTTP}))$, defining competitive inhibition parameters.

Stopped-flow measurement of PPi release

A SF 2004 series stopped-flow apparatus from KinTek Corp. (Austin, TX) was used for the measurements. Exonuclease-deficient holoenzyme (100 nM) was preincubated for 5 minutes with 2.5 mM Mg^{+2}, 90 nM 25/45mer DNA, 1.5 μM E. coli phosphate binding protein (PBP) mutant labeled at Cys197 with N-[2-(1-maleimidyl)ethyl]-7-(diethylamino)coumarin-3-carboxamide (MDCC), 100 μM 7-methylguanosine, 0.02 units/mL purine nucleotide phosphorylase, and 0.005 units/μL pyrophosphatase. The solution was then rapidly mixed in the stopped flow apparatus at 20°C with 2.5 mM Mg^{+2}, 50 μM dTTP, 100 μM 7-methylguanosine, and 0.02 units/mL purine nucleotide phosphorylase. The sample was excited at 425 nm and a 450 nm long pass filter was used to observe emission. The enzyme coupled assay for phosphate detection was previously established (80). Control experiments verified that the rate of conversion of pyrophosphate to phosphate by pyrophosphatase was faster than the observed reaction.

Synthesis of γ ^{32}P labeled AZTTP

Nucleoside diphosphate kinase (NDP kinase) was purchased from Sigma Aldrich Corp. (St. Louis, MO). γ ^{32}P-labeled ATP was from Perkin Elmer (Wellesley, MA). AZTDP was purchased from Moravek Biochemicals (Brea, CA). The reaction was carried out in standard Pol γ buffer at room temperature for 1 hour with 600 nM γ ^{32}P-labeled ATP (3000 Ci/mmol), 600 nM AZTDP, and 0.1 units/μL NDP kinase, at which time, conventional rat kinesin was added to a final concentration of 5 μM to rid the reaction of unreacted γ ^{32}P-labeled ATP. The sample was loaded onto a 1 mL DEAE Sepharose FF (Amersham Biosciences (Piscataway, NJ)) column at flow rate of 1 mL/min and a gradient of 0.1-1M triethylammonia (pH 7.5) was run to elute γ ^{32}P-labeled AZTTP. Elution of product was monitored by counting 10 μL of each fraction using a

scintillation counter. Peak fractions were lyophilized and resuspended in 10 mM Tris-Cl, pH 7.5. Labeled and unlabeled AZTTP were combined at a ratio of 1:10,000 for a stock concentration of 3 mM.

Measurement of PPi release during AZTTP incorporation

Reactions were performed by manual mixing on the benchtop under single-turnover conditions (exact reaction conditions are listed in the Figure legend). The Pol γ/DNA complex was mixed with γ ^{32}P-labeled AZTTP and Mg^{+2} to start the reaction. At each time point a 40 μL aliquot was taken and passed through a BioSpin 30 (BioRad, Hercules, CA) gel filtration column by centrifuging for 30 seconds @ 4,000 RPM. The elution from each time point was spotted onto a PEI Cellulose F 20 × 20 cm glass backed TLC plate (EM Science) along with a standard curve of various amounts of γ ^{32}P-labeled AZTTP to generate a standard curve. Imaging was performed using a phosphorimager, Molecular Dynamics Storm 860, and quantified using ImageQuaNT software (Amersham Biosciences, Uppsala, Sweden).

RESULTS

AZTTP incorporation by Pol γ

Shown in Figure 4.1A are the results of a single-turnover experiment, starting with a preincubated solution of exonuclease-deficient Pol γ and 25/45mer DNA substrate (single T incorporation) and rapidly mixed with increasing concentrations of AZTTP. This experiment is a repeat of an experiment already published and was an effort to obtain more accurate data (32). Again, it was the amplitude that was dependent on the concentration of nucleotide used (Figure 4.1B). However, the rate of incorporation decreased as the concentration of AZTTP increased (Figure 4.1C). The dependence of the amplitude on concentration was fit to a hyperbola using non-linear regression yields a

K_d of 160 ± 40 μM. A k_{pol} of 0.2 s^{-1} can be estimated from the rate of incorporation at higher concentrations of AZTTP. The rates obtained at lower amplitudes exhibit relatively high errors because the total product formation is approaching the experimental limit for accurate analysis.

Pyrophosphorolysis of AZTMP

The most direct method to examine the possibility of pyrophosphorolysis occurring during AZTTP incorporation was to perform the reaction in the reverse direction. For this experiment a 26mer primer 3′-terminated with AZTMP was annealed to a 45mer template. It was expected that pyrophosphorolysis would be observed by mixing the Pol γ/DNA complex with various concentrations of PPi. To the contrary, no degradation was observed under the conditions examined (Figure 4.2).

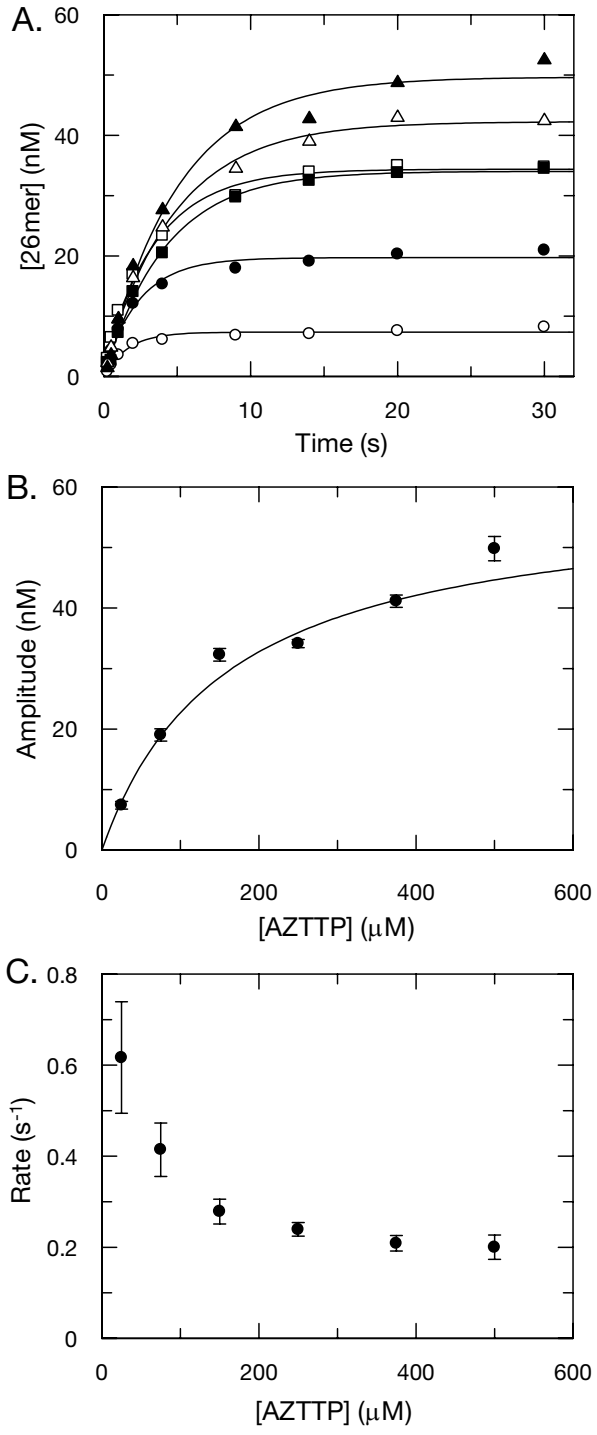

Figure 4.1: Kinetics of incorporation of AZTTP by Pol γ

Figure 4.1: Kinetics of incorporation of AZTTP by Pol γ

(A) Exonuclease-deficient holoenzyme (100 nM) was preincubated with 90 nM 25/45mer DNA and then rapidly mixed with Mg^{+2} and various concentrations of AZTTP (25 (○), 75 (●), 150 (□), 250 (■), 375 (△), and 500 μM (▲)). Each data set was fit to a single exponential to obtain the amplitude of the single exponential. **(B)** The single exponential amplitudes were plotted as a function of AZTTP concentration. The fit of the data to a hyperbola yields a K_d of 160 ± 40 μM. **(C)** The single exponential rates were plotted against AZTTP concentration. The maximum polymerization rate of 0.2 s^{-1} was estimated from the rate of incorporation at higher AZTTP concentrations.

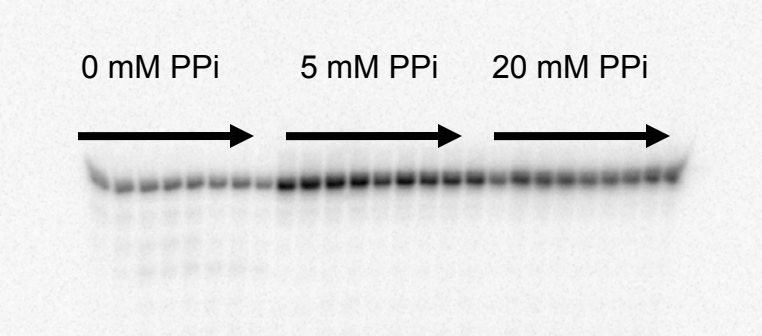

Figure 4.2: Pyrophosphorolysis reaction of AZTMP-terminated primer

Exonuclease-deficient holoenzyme (100 nM) was preincubated with 90 nM 26/45mer DNA terminated with AZTMP and mixed with Mg^{+2} and various concentrations of PPi as depicted in the gel image. No Pyrophosphorolysis was observed in reactions carried out to 25 minutes. The arrows depict increasing reaction times, (0, 1, 2, 4, 6, 10, 15, and 25 minutes).

The lack of detectable pyrophosphorolysis using an AZTMP-terminated primer did not agree with our hypothesis of reversible phosphoryl transfer and prompted an experiment designed as a positive control using a primer terminated with the natural nucleotide, dTMP.

Pyrophosphorolysis of dTMP

An experiment was performed under conditions similar to the previous experiment, except that the primer was designed to be a 26mer, with dTMP at the 3′-terminus. Figure 4.3A shows the result of the experiment performed by mixing a preformed complex of Pol γ and dTMP-terminated DNA with increasing concentrations of PPi. It is apparent in the upper left hand time course designated "0 mM PPi", there was a slow rate of background degradation of the primer. In reactions containing PPi, the rate of loss of substrate (26mer) increased along with apparent extension of the substrate, indicating the production of dNTP as a result of pyrophosphorolysis during the course of the reaction. It was not a surprise that pyrophosphorolysis would occur with a naturally terminated primer as it has been previously accomplished using T7 DNA polymerase (22). The time course of loss of substrate for each concentration of PPi was fit to a single exponential (Figure 4.3B) and the rates obtained were plotted versus pyrophosphate concentration and fit to a hyperbola plus a constant. The constant was included to account for the rate of degradation of the 26mer with no pyrophosphate present (Figure 4.3C). The maximum rate of pyrophosphorolysis was $0.75 \pm 0.09\ s^{-1}$ and the K_d was $80 \pm 65\ \mu M$. The pyrophosphorolysis reactions did not go to completion due to the formation of dNTP and illustrates an equilibrium between the forward and reverse reactions.

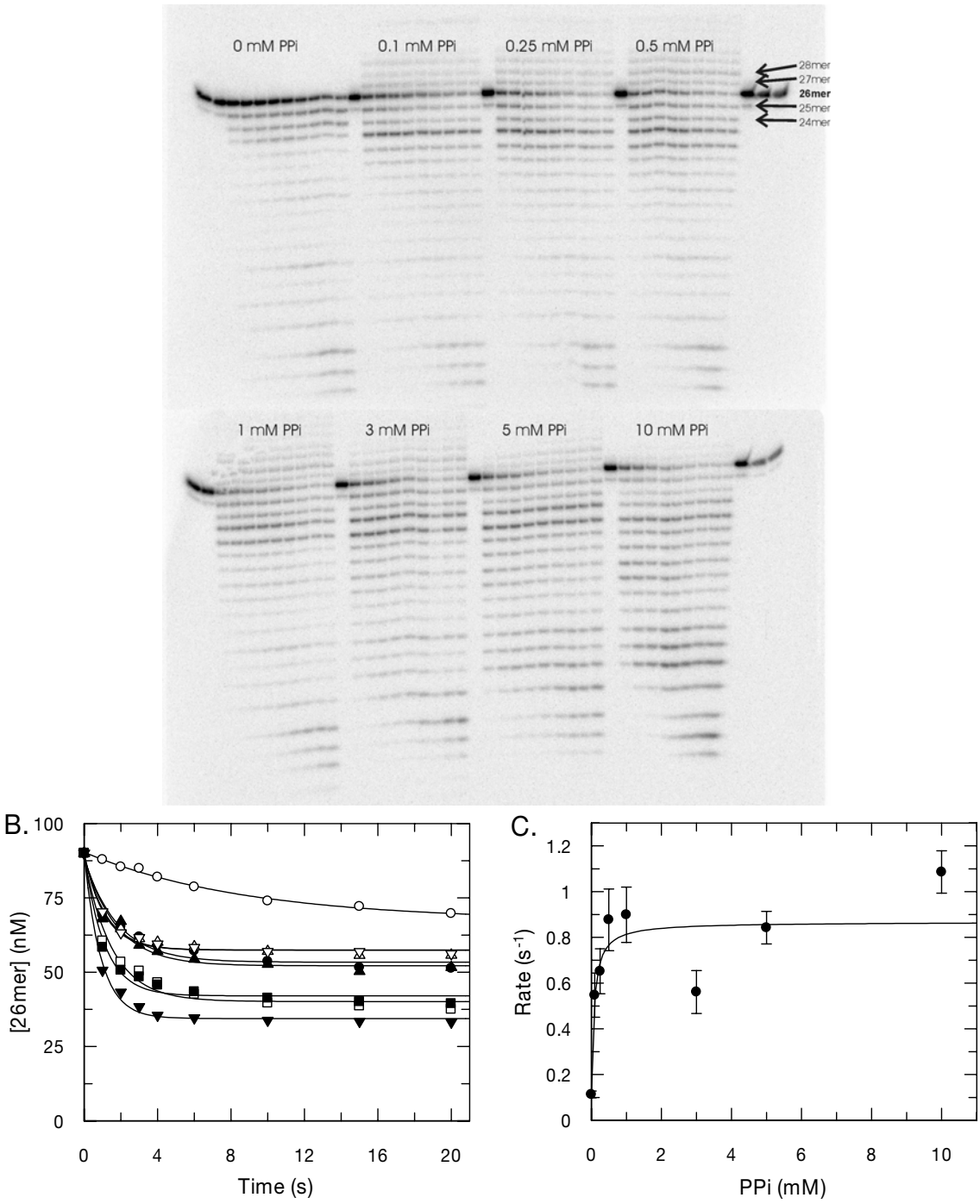

Figure 4.3: Pyrophosphorolysis of dTMP-terminated primer

Figure 4.3: Pyrophosphorolysis of dTMP-terminated primer

(A) Exonuclease-deficient holoenzyme (100 nM) was preincubated with 90 nM 26/45mer DNA terminated with dTMP and was mixed with Mg^{+2} and various concentrations of PPi (depicted on the phosphorimage of the gel.). Reactions were carried out for 25 seconds. It is apparent from the gel that pyrophosphorolysis is occurring due to the accumulation of both shorter and longer DNA products. Longer products could only be a result of pyrophosphorolysis because of the production of the dNTP during the reaction. **(B)** The concentration of substrate 26mer was plotted as a function of time and fit to a single exponential equation to obtain the reaction rates. Each reaction was performed at a different concentration of PPi (0 (○), 0.1 (●), 0.25 (□), 0.5 (■), 1 (△), 3 (▲), 5 (▽), and 10 (▼) mM. **(C)** The reaction rates were plotted versus the concentration of PPi used in the experiment and fit to a hyperbola (plus a constant) to yield a K_d of 80 ± 65 μM, a maximum rate of pyrophosphorolysis of 0.75 ± 0.09 s^{-1}, and a background rate of exonuclease activity of 0.11 ± 0.03 s^{-1}.

AZTTP incorporation in the presence of PPi or pyrophosphatase

Another approach used to examine the role of pyrophosphate in the polymerization reaction with AZTTP was to either include or exclude pyrophosphate from solution during the incorporation reaction. To exclude pyrophosphate from solution, we included a sufficient concentration of yeast pyrophosphatase in the reaction mixture to convert pyrophosphate to phosphate within the time scale of the experiment. The time dependence of polymerization in the presence of yeast pyrophosphatase was identical to the control experiment (Figure 4.4A). In AZTTP incorporation reactions where pyrophosphatase was replaced with increasing concentrations of pyrophosphate, no significant decrease in the amplitude of the reaction was observed until the concentration reached 100 μM (Figure 4.4A). However, at PPi concentrations near that expected to be formed during the incorporation reaction (~40 nM), there was no statistically significant difference in the data obtained in the presence or absence of PPi. A reduction in the amplitude of incorporation at concentrations of 100 μM or greater was likely to be the result of degradation of substrate 25mer at a rate comparable to the rate of incorporation of AZTTP (Figure 4.4B).

Hydrolysis of AZTTP in the active site

Unable to observe a role for pyrophosphorolysis on the concentration dependent amplitude of incorporation of AZTTP from the above experiments, we believed a different approach was needed. Rather than the enzyme catalyzing the pyrophosphorolysis reaction at a rate fast enough to explain our results, we considered the possibility that AZTMP was hydrolyzed from the primer at a substantial rate in the active site. Instead of AZTTP returning to solution due to pyrophosphorolysis after incorporation, AZTMP would accumulate as the product of an enzyme catalyzed

hydrolysis reaction. In order to test this postulate, a single-turnover experiment was performed at a concentration of 75 μM AZTTP. At zero time an aliquot was taken and separated using a salt gradient on a DEAE column, measuring absorbance at 254 nm (Figure 4.5A). The longest time point analyzed was carried out to 110 minutes and did not reveal any detectable hydrolysis of AZTTP to AZTMP (Figure 4.5B).

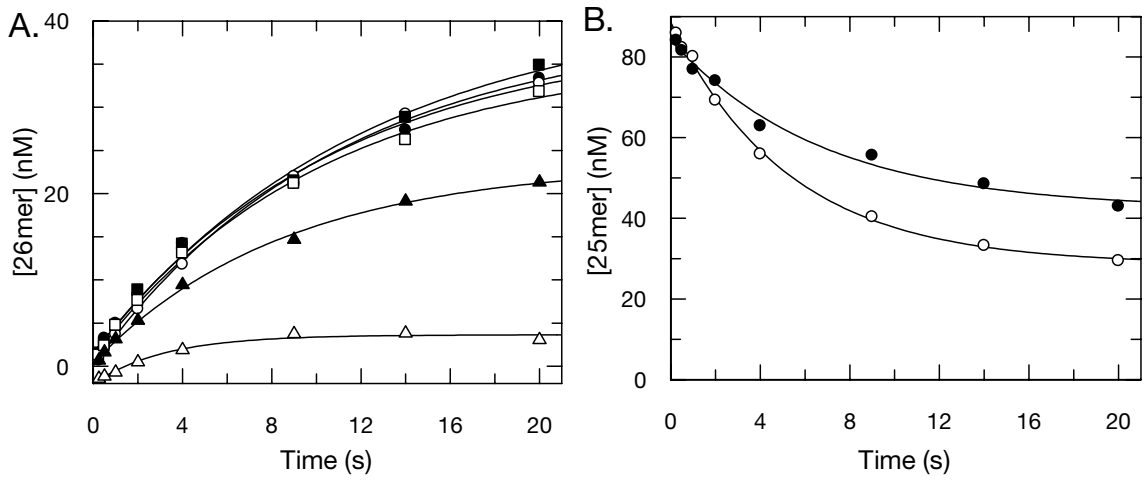

Figure 4.4: Incorporation of AZTTP in the presence of PPi or pyrophosphatase

(A) Exonuclease-deficient holoenzyme (100 nM) was preincubated with 90 nM 25/45mer DNA and mixed with Mg^{+2} and 200 μM AZTTP alone (●) or in the presence of 0.5 units of yeast pyrophosphatase (○), or varying concentrations of PPi (0.2 (■), 1 (□), 100 (▲), or 500 (△) μM). Including pyrophosphatase in the reaction had little to no effect. Only in reactions containing 100 or 500 μM PPi was the amplitude reduced, which was likely due to the loss of 25mer substrate DNA in the reaction at about the same rate as the incorporation of AZTMP (~0.2 s^{-1}). **(B)** Shown is a plot of the amount of 25mer during the course of the reactions containing 100 (●) and 500 (○) μM PPi. A fit to a single exponential obtained rates of loss of 25mer at 0.19 ± 0.01 s^{-1} and 0.15 ± 0.03 s^{-1}, respectively.

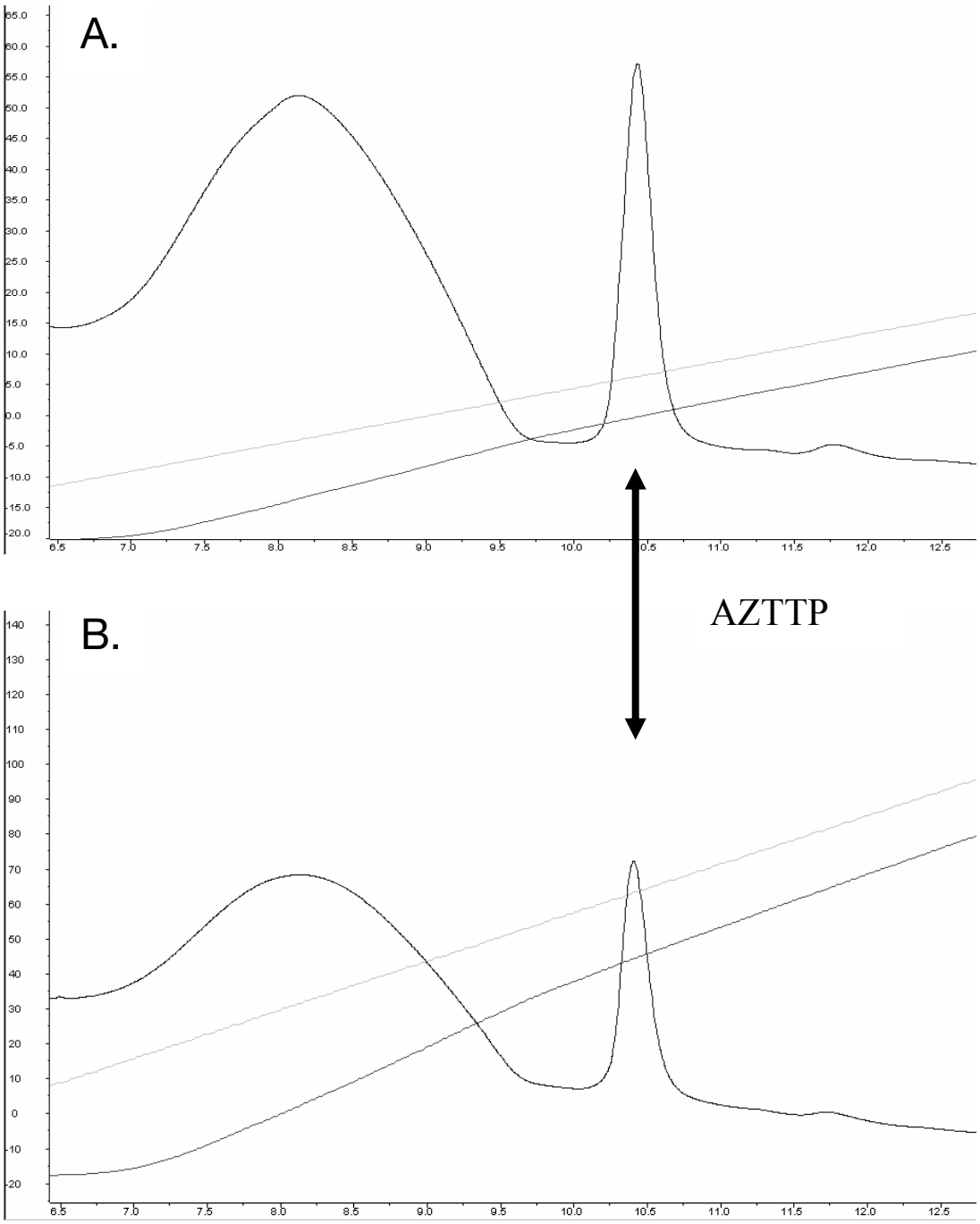

Figure 4.5: Hydrolysis of AZTTP during incorporation reaction

Figure 4.5: Hydrolysis of AZTTP during incorporation reaction

(A) Exonuclease-deficient holoenzyme was preincubated with 90 nM 25/45mer DNA and mixed with Mg^{+2} and 75 μM AZTTP. The trace shown is a gradient elution (0.02-1M NaCl in 0.02M tris-hydroxymethylaminoethane (Tris) buffer, pH 7.7 @ $4^{o}C$) of the reaction at zero time from a DEAE fast flow chromatography column measuring absorbance at 254 nm. Control experiments of AZTTP and AZTMP showed that the peak labeled is AZTTP (Data not shown). **(B)** A trace of a reaction stopped at 110 minutes under the same experimental conditions as (A) shows that the AZTTP used in the reaction was not hydrolyzed to AZTMP.

dTTP chase experiment

To examine the amount of enzyme/DNA complex at equilibrium during AZTTP incorporation, a chase experiment was designed, where a single-turnover reaction with AZTTP was carried out for 15 second (long enough to reach equilibrium), then dTTP was added and a reaction time course was taken. Since AZTTP incorporation was at equilibrium at the time of the dTTP addition, any immediate product formation had to be occurring with enzyme/DNA complex that was free of AZTTP (Figure 4.6). According to the K_d for DNA binding, and many previous single-turnover experiments (correct incorporation reactions with 100 nM holoenzyme and 90 nM DNA), an amplitude of 60 nM is normal. The first time point taken after the addition of dTTP was at two seconds, at which time, the amount of product was 60 nM, which can be interpreted as the sum of AZTMP and dTTP incorporation. If the amount had been significantly lower than 60 nM, then our approximation of the K_d for AZTTP binding would have been incorrect. The seemingly linear increase in the amount of product formed over time after the addition of dTTP is due to the binding of free enzyme and un-reacted DNA followed by incorporation and precludes any detailed analysis.

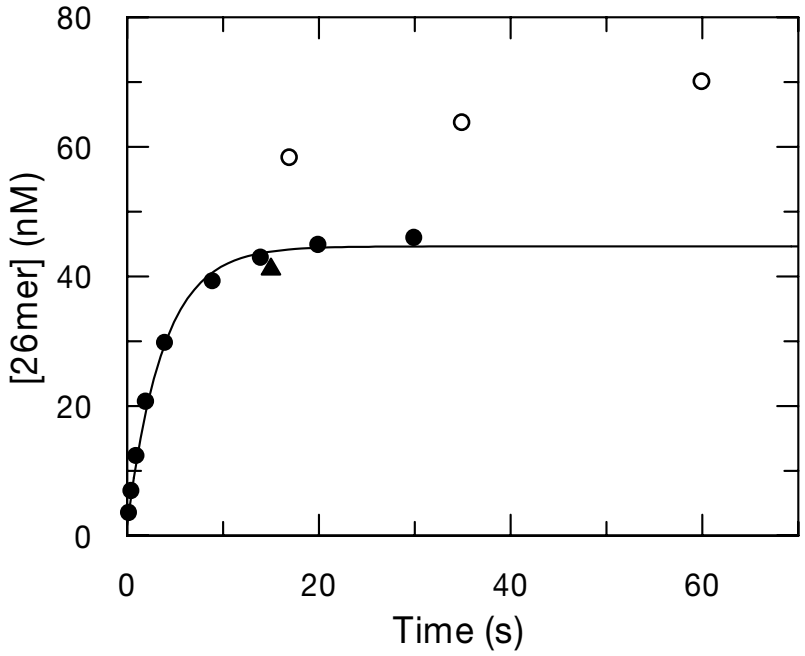

Figure 4.6: AZTTP incorporation followed by a chase with TTP

Two reactions were performed in parallel for this experiment: First, exonuclease-deficient holoenzyme (100 nM) was preincubated with 90 nM 25/45mer DNA and then mixed with Mg^{+2} and 200 μM AZTTP and allowed to react for up to 30 seconds for a control (●), Second,: the same starting reaction conditions as in the control was allowed to react for 15 seconds with 200 μM AZTTP and a single time point taken (▲) at which time 50 μM dTTP was added and allowed to react for two seconds before the first time point was taken (corresponding to 17 seconds on the graph)(○). The amount of product 2 seconds after the addition of dTTP was about 60 nM, and illustrates that there was about 18 nM free enzyme/DNA complex in solution when dTTP was added.

Determination of the K_d for AZTTP by competitive inhibition

An additional method was employed in order to determine the K_d for AZTTP binding, because of the unusual way in which the K_d was obtained previously. An unambiguous measurement of the K_d was performed by direct competition of dTTP and AZTTP. In order to accomplish this, we measured the rate of dTTP incorporation in the presence of varying concentrations of AZTTP under single-turnover conditions (Figure 4.7A). This was possible because of the large difference between the maximum rates of incorporation (25 $s^{-1}$for dTTP and 0.2s^{-1} for AZTTP). The K_d determined was 30 ± 16 μM, and was about 5-fold tighter than the K_d obtained earlier (160 ± 40 μM) by fitting the amplitude dependence (Figure 4.7B). The underlying reason for such a tight true K_d cannot be explained at this time and may require further investigation.

Incorporation of dTTP in the presence of Mn^{+2}

Mn^{+2} has been shown to dramatically reduce the fidelity of DNA polymerases and is the basis for error prone PCR. Neither correct nor incorrect incorporation had been studied with Pol γ using Mn^{+2} instead of Mg^{+2}; therefore, we felt it to be a worthwhile endeavor to examine the incorporation of dTTP and AZTTP with manganese present. It was thought that substitution of the divalent cation could help clarify the abnormal incorporation kinetics of AZTTP. Under single-turnover conditions, we measured product formation for dTTP incorporation as a function of time at a final Mn^{+2} concentration of 2.5 mM (Figure 4.8A). The data from the four highest concentrations of dTTP were best fit to a double exponential equation, whereas the data from the lower two dTTP concentrations were fit with a single exponential equation. The rate of the fast phase of incorporation from the four highest concentrations of dTTP and the rate from the two lower concentrations (single exponentials) were plotted versus dTTP concentration

and fit to a hyperbola (Figure 4.8B) to obtain a k_{pol} of 170 ± 20 s^{-1}, and a K_d of 3.6 ± 0.7 μM. The reason underlying the two phase reaction is unknown, but is likely the result of a small amount of free enzyme and DNA (according the K_d for DNA binding) at the start of the reaction and going on to react more slowly as a function of the rate of DNA binding. At lower concentrations of dTTP the two phases of the reaction were not resolved and the resulting single exponential rate is, in essence, an average of the two unresolved phases. One interesting result not expected from this experiment was the dramatic rate enhancement from 25 s^{-1} in the presence of Mg^{+2} to 170 s^{-1} in the presence of Mn^{+2}. However, the ground state dissociation constant increased by about the same magnitude resulting in no overall change in the specificity constant (Table 4.1).

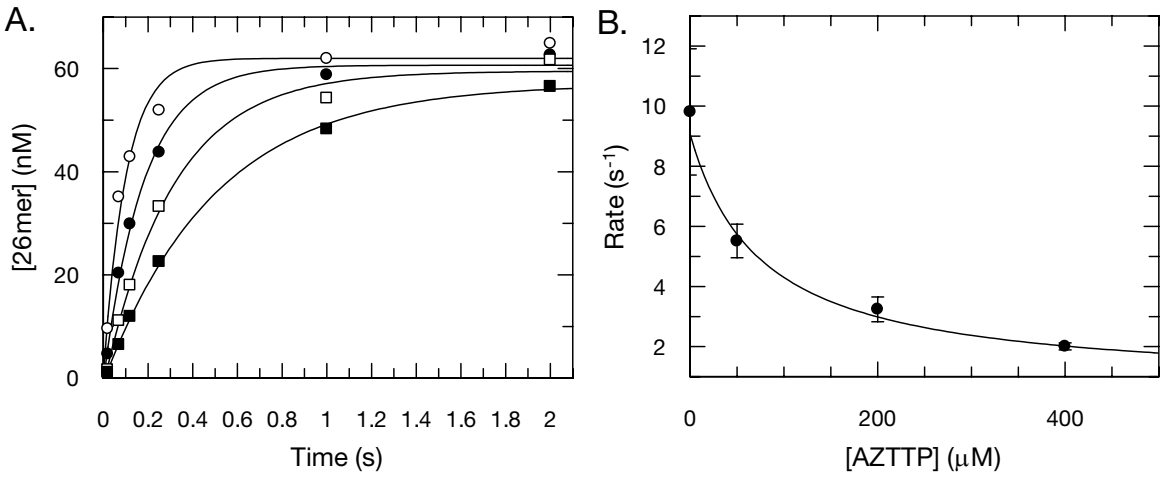

Figure 4.7: Determination of the K_d for AZTTP by competitive inhibition

(A) Exonuclease-deficient holoenzyme (100 nM) was preincubated with 90 nM 25/45mer DNA and then rapidly mixed with Mg^{+2}, 1 μM dTTP and various concentrations of AZTTP (0 (○), 50 (●), 200 (□), and 400 (■) μM). Each data set was fit to a single exponential to obtain the rate of the single exponential. **(B)** The single exponential rates were plotted as a function of AZTTP concentration. Data were fit to a hyperbola to obtain an apparent K_d of 76 ± 42 μM and analyzed with the equation $K_{dapp}=K_{dAZTTP}(1+([dTTP]/K_{ddTTP}))$, defining competitive inhibition parameters to yield a true K_d of 30 ± 16 μM.

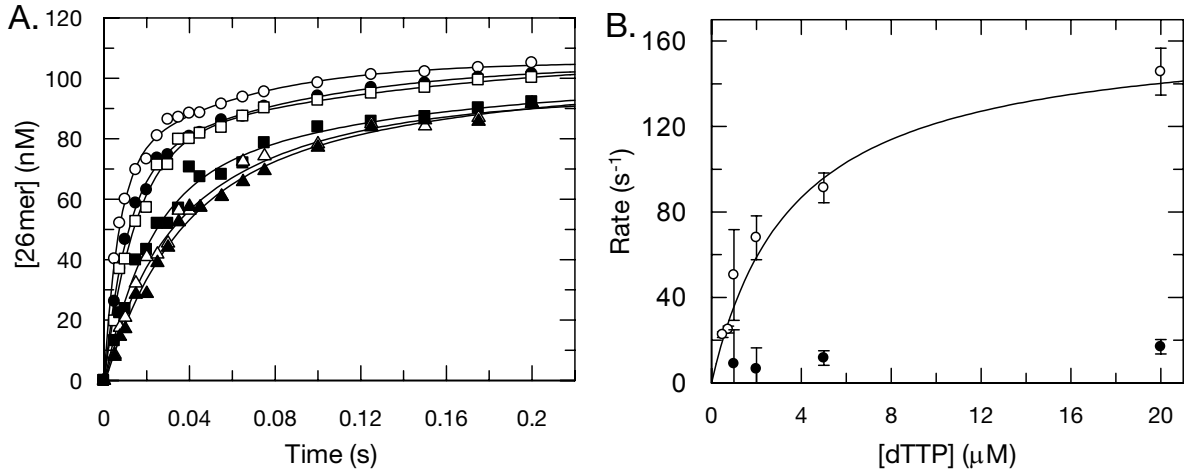

Figure 4.8: Incorporation of dTTP in the presence of Mn^{+2}

(A) Exonuclease-deficient holoenzyme (150 nM) was preincubated with 140 nM 25/45mer DNA and then rapidly mixed with 2.5 mM Mn^{+2} and various concentrations of dTTP (0.5 (○), 0.75(●), 1(□), 2(■), 5(△), and 20 μM (▲)). Each of the four highest data sets were fit to a double exponential to obtain the rates of incorporation, but the lower two concentration data sets were best fit to a single exponential. **(B)** The fast phase of the double exponential fits (highest four concentrations of dTTP) and the single exponential rates (lowest two concentrations of dTTP) were plotted as a function of dTTP concentration(○) and a fit of the data to a hyperbola yields a K_d of 3.6 ± 0.7 μM and a maximum rate of incorporation of 170 ± 20 s^{-1}. The slow phases are nearly constant, at a rate of approximately 10 s^{-1} (●).

Incorporation of AZTTP in the presence of Mn^{+2}

Single-turnover experiments were performed exactly as in the previous experiment, but with AZTTP (Figure 4.9A). Of significance, unlike incorporation of AZTTP in Mg^{+2} where the amplitude was dependent on concentration, the rate varied with concentration of AZTTP incorporation with Mn^{+2} present (Figure 4.9B). Data were fit to a hyperbola to obtain a K_d of 23 ± 5 μM and a k_{pol} of 0.043 ± 0.004 s^{-1}. The trend of faster incorporation and looser binding for dTTP (Mn^{+2} versus Mg^{+2}) was reversed in the case of AZTTP. The rate for AZTTP incorporation in the presence of Mn^{+2} was 5-fold slower and the K_d 7-fold tighter compared to incorporation in the presence of Mg^{+2}, resulting in no statistically significant change in specificity constants (Table 4.1). A change from a concentration dependent amplitude of incorporation in the presence of Mg^{+2} to a concentration dependent rate of incorporation in the presence of Mn^{+2} is not fully understood, but suggests that there may be an unusual interaction between the azide group and Mg^{+2} or other metal ion-dependent change in the interaction of AZT with the enzyme.

Discrimination against AZTTP in the presence of Mn^{+2}

Surprisingly, discrimination against AZTTP is not greatly reduced when the incorporation reaction is performed in the presence of Mn^{+2} compared to Mg^{+2} (32,000 and 25,000, respectively) (Table 4.1). A discrimination of 32,000 predicts that, at equal concentrations of dTTP and AZTTP, Pol γ is 32,000 times more likely to insert the natural nucleotide. The fact that we did not see a large reduction in discrimination against AZTTP in the presence of Mn^{+2} is puzzling, and may warrant further investigation. Other polymerases, notably T7, Taq, and Klenow show a marked reduction in fidelity with the use of Mn^{+2} in the place of Mg^{+2} (81;82).

	k_{pol} (s^{-1})	K_d (μM)	Specificity (k_{pol}/K_d)	Discrimination[a]
dTTP/Mg^{+2}	25 ± 2	0.6 ± 0.2	42± 14	32000
AZTTP/Mg^{+2}	~0.2[b]	160 ± 40	0.0013 ± 0.0003	
dTTP/Mn^{+2}	170 ± 20	3.6 ± 0.7	47 ± 11	25000
AZTTP/Mn^{+2}	0.043 ± 0.004	23 ± 5	0.0019 ± 0.0004	

[a] Discrimination = $(k_{pol}/K_d)_{correct}/(k_{pol}/K_d)_{analog}$, where the values for dTTP incorporation in the presence of Mg^{+2} were taken from Ref (19)
[b] A value of 0.2 s^{-1} was estimated from the rate of incorporation at higher concentrations of AZTTP.

Table 4.1: Comparison of the incorporation of dTTP and AZTTP in the presence of Mg^{+2} and Mn^{+2}

Data obtained from the incorporation reactions with the natural nucleotide dTTP in the presence of Mg^{+2} and Mn^{+2} are compared to data obtained from the incorporation of AZTTP in the presence of Mg^{+2} and Mn^{+2}. Surprisingly, discrimination against AZT is not greatly reduced when the incorporation reaction is performed in the presence of Mn^{+2}.

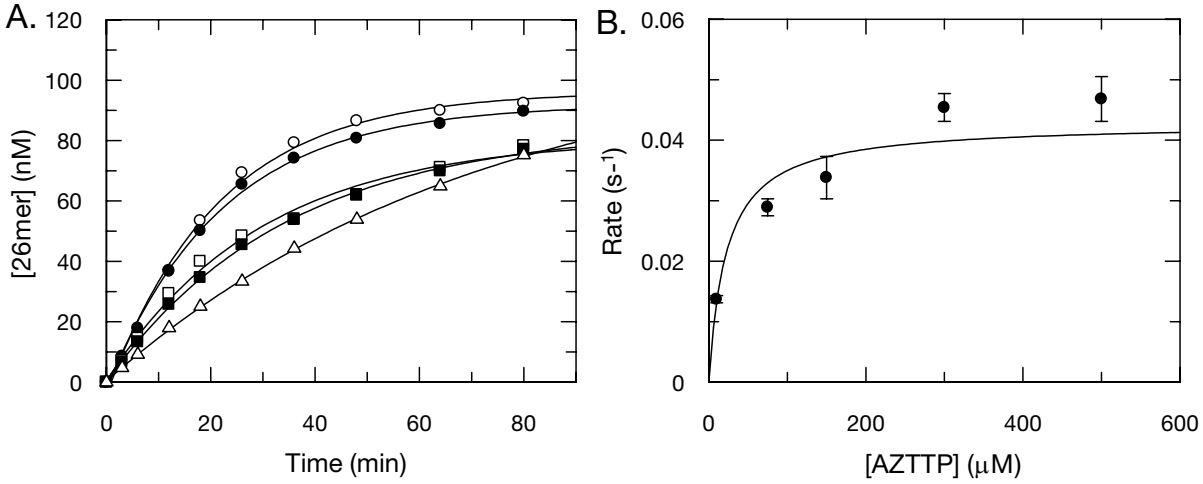

Figure 4.9: Incorporation of AZTTP in the presence of Mn^{+2}

(A) Exonuclease-deficient holoenzyme (150 nM) was preincubated with 140 nM 25/45mer DNA and then rapidly mixed with 2.5 mM Mn^{+2} and various concentrations of AZTTP (10 (○), 75 (●), 150 (□), 300 (■), and 500 (△) μM). Each data set was fit to a single exponential to obtain the rate of incorporation. **(B)** The single exponential rates of incorporation were plotted as a function of AZTTP concentration (●) and a fit of the data to a hyperbola yields a K_d of 23 ± 5 μM and a k_{pol} of 0.043 ± 0.004 s^{-1}.

Incorporation of d4TTP in the presence of Mn^{+2}

The thymidine analog d4T has been approved by the FDA for use in the treatment of HIV. Structurally, d4T differs from thymidine and AZT only on the 2′ and 3′ carbons. d4T has no functional group on the 3′ carbon, but rather has a double bond connecting the 2′ to the 3′ carbon. This structural similarity gave us the opportunity to examine the incorporation of d4TTP in the presence of Mn^{+2}, in an attempt to better understand the results obtained with AZTTP. The result of a single-turnover experiment is shown in Figure 4.10A. The amplitude of the reaction is dependent upon concentration of d4TTP reveals a hyperbolic relationship, but in this case the substoichiometric concentration of d4TTP used in the experiment limits overall product formation. (Figure 4.10B). The amplitude of the reaction was fit to a quadratic to yield a K_d of 3 ± 5 nM. A plot of the rate of reaction against d4TTP concentration is fairly linear, also signifying an extremely tight K_d (Figure 4.10B). Under the conditions we normally use to measure ground state dissociation constants for nucleotides, it is difficult to obtain reliable data for such tight binding substrates. However a fairly accurate assessment of the maximum rate of incorporation can be estimated from the data and is approximately 2 s^{-1}. Using these values and comparing them to data obtained for the incorporation of d4TTP in the presence of Mg^{+2} (32), the K_d is about 15-fold tighter and the k_{pol} is about 8-fold faster resulting in about an 120-fold reduction in discrimination against d4TTP (0.1). This result contrasts with the largely unchanged discrimination against AZTTP in the presence of Mn^{+2} versus Mg^{+2}.

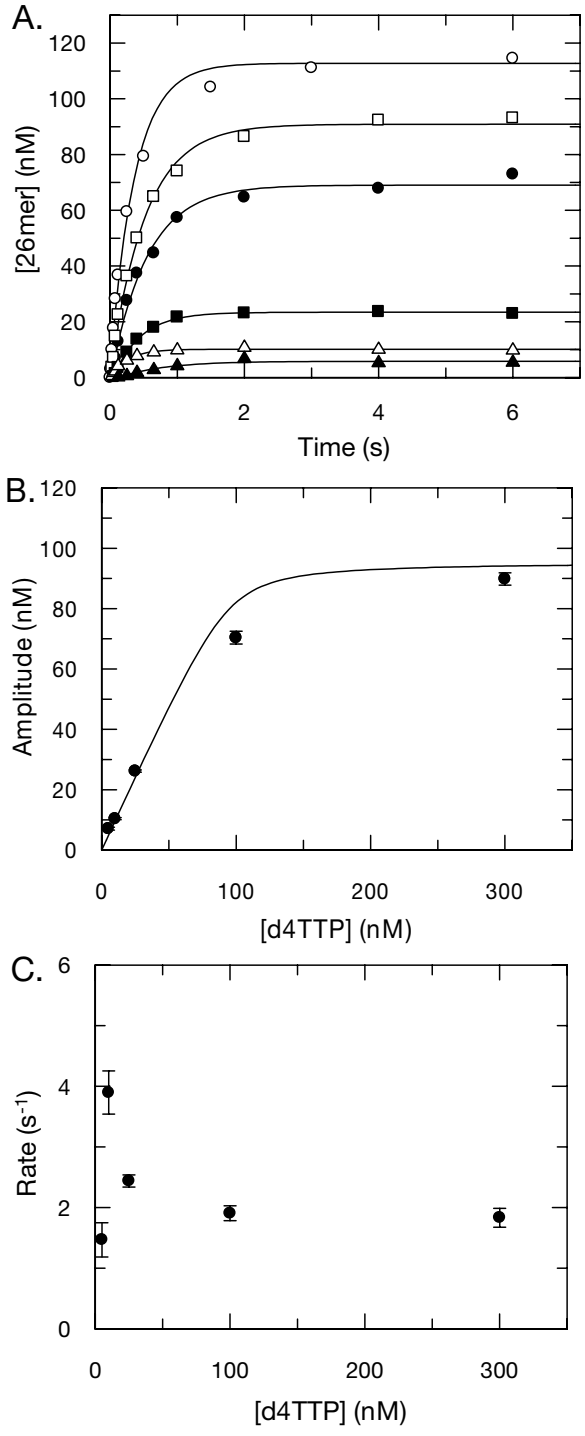

Figure 4.10: Incorporation of d4TTP in the presence of Mn^{+2}

Figure 4.10: Incorporation of d4TTP in the presence of Mn^{+2}

(A) Exonuclease-deficient holoenzyme (150 nM) was preincubated with 140 nM 25/45mer DNA and then rapidly mixed with 2.5 mM Mn^{+2} and various concentrations of d4TTP (0.005 (○), 0.01 (□), 0.025 (●), 0.1 (■), 0.3 (△), and 50 (▲) μM). Each data set was fit to a single exponential to obtain the rate and amplitude of incorporation. **(B)** The amplitudes were plotted as a function of d4TTP concentration and fit to a quadratic equation to obtain a K_d of 3 ± 5 nM.. The maximum obtainable amplitude was limited by the amount of d4TTP added to the reaction at low concentrations and is so tight that it is difficult to measure using this technique. **(C)** The rate of incorporation was plotted as a function of d4TTP concentration. The rates were more or less linear with concentration, which likely means that, at concentrations of d4TTP required to obtain lower rates of incorporation, there is too little product for measurement.

Steady-state kinetic parameters for the incorporation of AZTTP

We measured the steady-state kinetic parameters for AZTTP incorporation because it is possible that the steady-state kinetic parameters could reveal a change on the overall rate-limiting step of the reaction compared to correct nucleotide incorporation. Since we were unable to observe the reverse reaction by adding PPi to a preformed complex of enzyme/DNA (terminated with AZTMP), it is likely that a step following phosphoryl transfer is not readily reversible. The most likely explanation for the reaction to appear reversible regarding the incorporation reaction (amplitude dependence) but not be able to observe the reverse reaction is that the conformational change (opening of the enzyme) after phosphoryl transfer may not be occurring at a fast rate. If the enzyme remains in the closed conformation after AZT incorporation and the rate of opening is slower than DNA release then the steady-state rate may be slowed in comparison to DNA release during a correct nucleotide incorporation reaction. Shown in Figure 4.11A is the result of a steady-state experiment in which increasing concentrations of AZTTP were added to a reaction with DNA in a 15-fold molar excess over enzyme. A plot of rate versus AZTTP concentration follows a Michalis-Menton relationship of initial velocities and was fit to the hyperbola to obtain a k_{cat} of 0.001 ± 0.0001 s^{-1} and a K_m of 280±70 μM (Figure 4.11B). Significantly, the k_{cat} of 0.001 s^{-1} for AZTTP incorporation was 20-fold slower than the k_{cat} of 0.02 s^{-1} for a correct incorporation under the same conditions (12). It is important to note that the incorporation of AZTTP under single turnover conditions occurs at a 200-fold faster rate (0.2 s^{-1}) than the k_{cat}, which likely means that there is a step following phosphoryl transfer that is rate limiting in the steady-state. The rate-limiting step is most likely the conformational change following phosphoryl transfer or DNA release, but cannot be identified exclusively from this experiment.

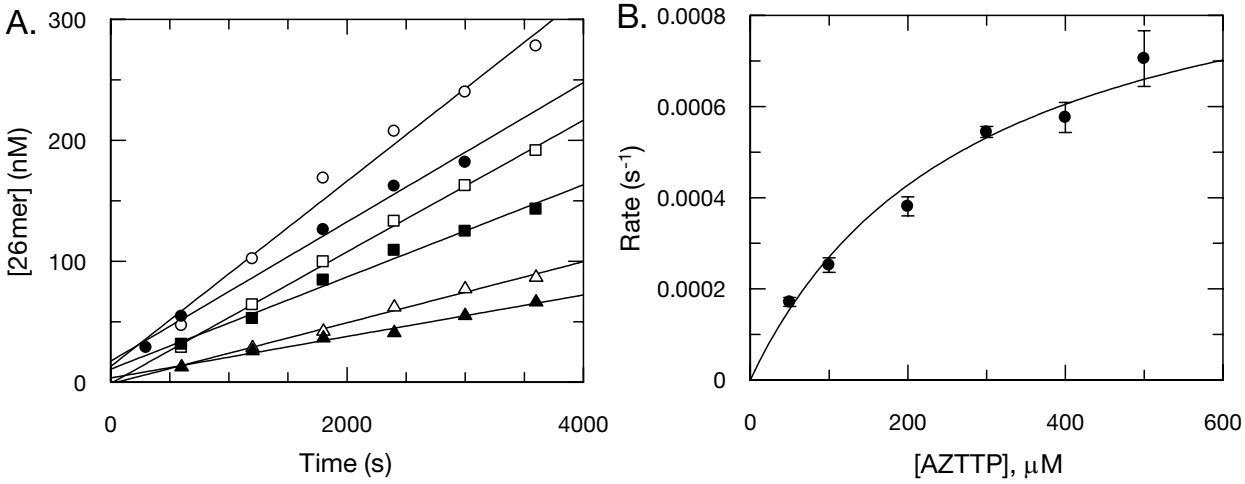

Figure 4.11: Steady-state incorporation of AZTTP

(A) Exonuclease-deficient holoenzyme (100 nM) was preincubated with 1.5 μM 25/45mer DNA and mixed with Mg^{+2} and various concentrations of AZTTP (50 (○), 100 (●), 200 (□), 300 (■), 400 (△), and 500 (▲) μM). Data obtained was fit by linear regression and the slope divided by enzyme concentration to obtain the rate of turnover. **(B)** The rate of turnover was plotted against AZTTP concentration and data were fit to the Michalis-Menton equation to obtain K_m and k_{cat} values. The K_m for AZTTP incorporation was found to be 280±70 μM and the k_{cat} was 0.001 ± 0.0001 s^{-1}. The value of 0.001 s^{-1} for k_{cat} was 20-fold slower than the rate of dissociation of the enzyme/DNA complex (0.02 s^{-1}), found previously for normal incorporation reactions (12).

AZTMP-terminated DNA dissociation

To get a better grasp on the basis for the reduced steady-state rate of AZTTP incorporation as compared to that for a natural nucleotide, we attempted to measure the release from the enzyme active site of DNA terminated with AZTMP. Two separate experiments were performed: (1) Pol γ, was mixed with excess DNA (radiolabeled), the correct nucleotide (dCTP in this case), and Mg^{+2} (Figure 4.12A) to measure the steady-state rate of incorporation; and (2) Pol γ was preincubated with a 2-fold excess of AZTMP-terminated DNA (non-radiolabeled) before mixing with the same contents as in (1). The first reaction was performed in order to obtain an expected value for the steady-state rate of turnover while the second reaction was limited by the rate of release of AZT-terminated DNA from the enzyme (Figure 4.12B). In the second reaction starting with a preincubated solution of Pol γ and AZT-terminated DNA, one might expect to see a lag defining an exponential increase in the steady-state turnover rate as the reaction proceeded, because of the dissociation of the enzyme/AZTMP-terminated DNA complex leading to free enzyme to catalyze incorporation onto the excess labeled DNA template. Product formation for the first experiment was plotted versus time and fit to a burst equation to obtain the rate and amplitude of the burst phase and also the linear steady-state rate. The amplitude of burst phase was 87 ± 3 nM (100 nM enzyme was used in the reaction) and the rate was 2.5 ± 0.2 s^{-1}. The steady-state rate was obtained by dividing the slope of the linear phase by the enzyme concentration and was 1.24 ± 0.5 s^{-1}. The turnover rate for the reaction containing AZT-terminated DNA was linear with a rate of 0.08 ± 0.004 s^{-1}. This slow linear rate of product formation in the experiment can be accounted for as a function of the 6 nM free enzyme during the experiment, calculated by dividing the turnover rate of the control experiment by the turnover rate of the experiment

containing AZT-terminated DNA. Computer simulation of this experiment shows that the rate of AZTMP-terminated DNA dissociation from the enzyme is likely to be less than 0.004 s^{-1}, but cannot be assigned a definitive value.

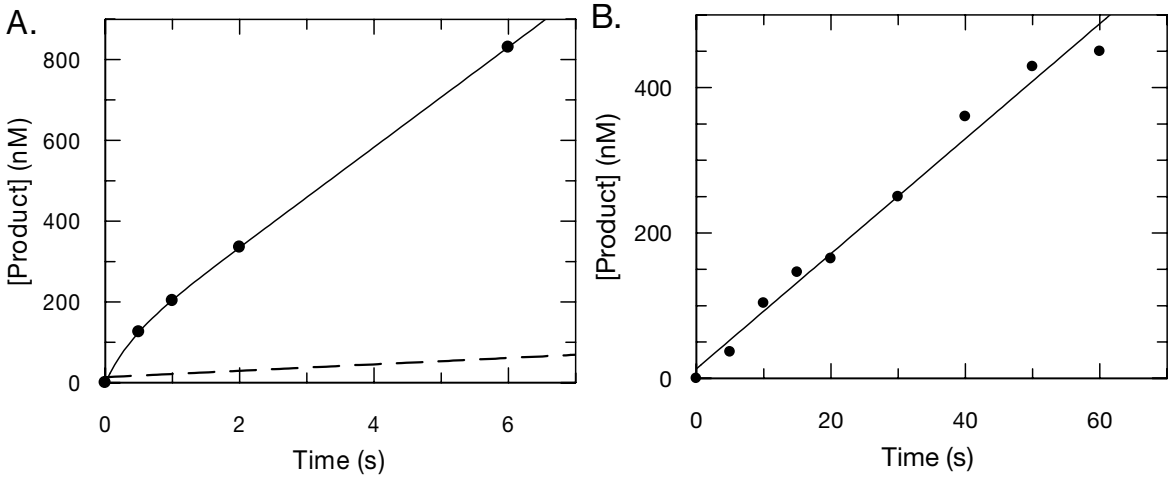

Figure 4.12: Dissociation of enzyme from DNA terminated with AZTMP

(A) Exonuclease-deficient holoenzyme (100 nM) was rapidly mixed with Mg^{+2}, 5 μM dCTP, and 2 μM 25/45mer DNA (coding for dCTP incorporation). Product formation for the control was plotted versus time and fit to a burst equation to obtain the rate and amplitude of the burst phase and also the linear steady-state rate. The amplitude of burst phase was 87 ± 3 nM and the rate was 2.5 ± 0.2 s^{-1}. The steady-state rate was obtained by dividing the slope of the linear phase by the enzyme concentration and was 1.24 ± 0.5 s^{-1}. The dashed line is the linear fit of the data in the following experiment. **(B)** Exonuclease-deficient holoenzyme (100 nM) preincubated with 200 nM 26/45mer terminated with AZTMP was rapidly mixed with Mg^{+2}, 5 μM dCTP, and 2 μM 25/45mer DNA (coding for dCTP incorporation). Product formation was plotted versus time and was fit by linear regression to obtain the slope. The steady-state rate was obtained by dividing the slope of the linear phase by the enzyme concentration and was 0.08 ± 0.004 s^{-1}. A linear rate instead of an exponential increase in rate signifies that little to none of the enzyme in complex with AZTMP-terminated DNA dissociated (becoming free to react) during the reaction.

Rate of pyrophosphate release during dTTP incorporation

From previous experiments it was established that the rate of dissociation of AZTMP-terminated DNA from Pol γ was slower than expected regardless of whether PPi was present in the active site. Therefore, it was of interest to measure the rate of PPi release from Pol γ during both dTTP and AZTTP incorporation reactions. To measure PPi release during dTTP incorporation we designed an experiment taking advantage of MDCC-labeled phosphate binding protein (PBP), which exhibits large fluorescence increase upon phosphate binding (80). PPi does not induce a fluorescence change with MDCC-labeled PBP, so PPi was hydrolyzed to phosphate (Pi) during the reaction with a high concentration of yeast pyrophosphatase. Because Pi is a wide spread contaminant, a "Pi mop" consisting of 7-methylguanosine and purine nucleoside phosphorylase was used to reduce the concentration of contaminant Pi for each experiment (80). The first experiment was done with dTTP to get the results shown in Figure 4.13. The data obtained from 7 individual time traces was averaged and fit to a triple exponential equation by nonlinear regression. The three phases of the exponential, starting with the fast phase, had rates of 15 ± 0.08 s^{-1}, 0.722 ± 0.007 s^{-1}, and 0.060 ± 0.001 s^{-1}, respectively (Figure 4.13A). The first two phases of the reaction can be accounted for by our knowledge of this reaction. The first phase is likely the rate of release of PPi as a function of the rate of dTTP incorporation and the second phase is a function of the rate of free enzyme and DNA binding since under these conditions enzyme is not completely saturated with DNA upon mixing. We do not know what the third phase of the reaction represents. The amplitude of the fast phase of the reaction was determined to be 54 nM by using a PPi standard curve performed in the stopped-flow on the same day of the experiment (Figure 4.13B). As a control experiment, a reaction using radiolabeled DNA

was performed in the quench-flow under the same conditions (superimposed on the stopped-flow data Figure 4.13A). The data also fit a triple exponential. The three phases of the exponential had rates of 22 ± 2 s^{-1}, 0.9 ± 0.3 s^{-1}, and 0.09 ± 0.09 s^{-1}, respectively. Correspondingly, amplitudes of the three phases were 33 ± 2 nM, 13 ± 2 nM, and 20 ± 4 nM, respectively. The differences in the rates and amplitudes of the two experiments stems from the difficulty of measuring a triple exponential reaction in the quench-flow apparatus where the three phases are not defined well, but the rate of the fast phase of the two experiments agree fairly well (15 s^{-1} in the stopped-flow and 22 s^{-1} in the quench-flow). It is likely that the slower rate obtained in the stopped-flow was due to the slightly larger amplitude of the fast phase (54 versus 33 nM), which would account for a reduction in the rate. These data indicate that PPi release is fast following incorporation. Similar experiments were performed with AZTTP but failed, for reasons stated below.

Rate of pyrophosphate release during AZT incorporation

To examine the rate of release of pyrophosphate by Pol γ during the slower AZTTP incorporation reaction, a different experimental approach was needed. γ-^{32}P-AZTTP was prepared from AZTDP using nucleotide diphosphate kinase and γ^{32}P-ATP. A preincubated solution of enzyme/DNA (single-turnover conditions) was mixed with γ-^{32}P-AZTTP to start the reaction. For each time point, an aliquot was taken and, as quickly as possible, centrifuged through a gel filtration column. The elution was spotted onto a TLC plate prepared with a standard curve for absolute PPi concentration determination, and quantified by fluorography. When passed through the gel filtration column, only the enzyme-bound PPi should be present in the elution. As shown in Figure 4.14 there is a transient rise and fall in the concentration of enzyme bound PPi. The concentration of PPi in the elution was plotted versus time and fit to a double exponential equation. The rate and amplitude of the fast phase were 1.2 ± 0.3 min^{-1} and 700 ± 70 nM,

respectively. The rate and amplitude of the slow exponential decrease in product formation were 0.007 ± 0.002 min^{-1} and 700 ± 50 nM, respectively. As evidenced by the data, PPi is not released from the active site during the incorporation of AZTTP (0.2 s^{-1}). The release rate of PPi is 1700-fold slower than AZTTP incorporation.

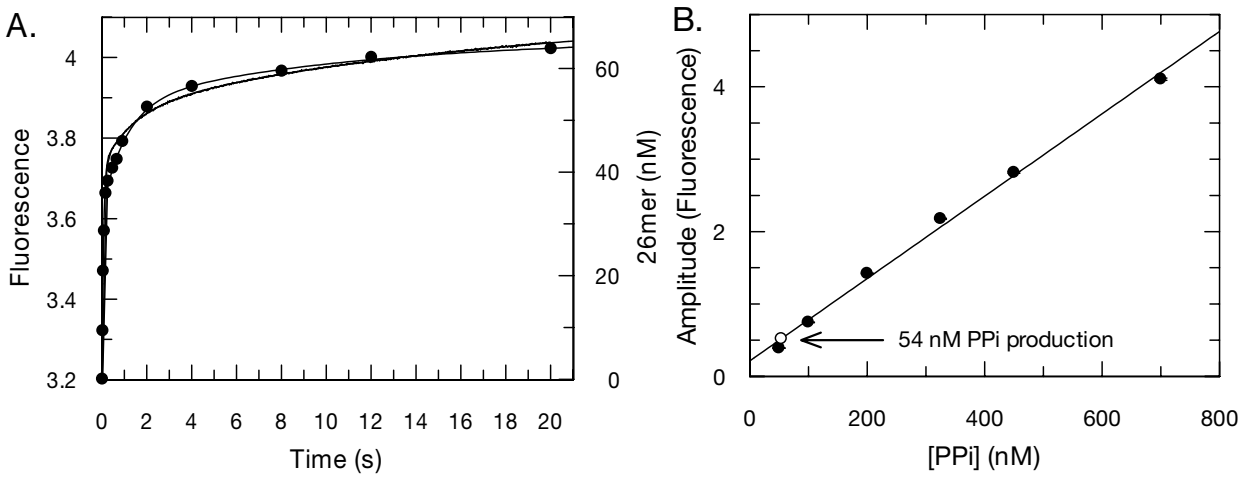

Figure 4.13: Rate of PPi release during dTTP incorporation

(A) Exonuclease-deficient holoenzyme (100 nM) was preincubated for 5 minutes with 2.5 mM Mg^{+2}, 90 nM 25/45mer DNA, 1.5 μM E. coli PBP mutant labeled at Cys197 with MDCC, 100 μM 7-methylguanosine, 0.02 units/mL purine nucleotide phosphorylase, and 0.005 units/μL pyrophosphatase and then rapidly mixed in the stopped-flow apparatus at 20°C with 2.5 mM Mg^{+2}, 50 μM dTTP, 100 μM 7-methylguanosine, and 0.02 units/mL purine nucleotide phosphorylase. The sample was excited at 425 nm and a 450 nm long pass filter was used to observe emission. The data obtained from 7 individual time traces was averaged and fit to a triple exponential equation by nonlinear regression. The three phases of the exponential, starting with the fast phase, had rates of 15 ± 0.08 s^{-1}, 0.722 ± 0.007 s^{-1}, and 0.060 ± 0.001 s^{-1}, respectively. Superimposed on the same graph is a control experiment performed in the quench-flow as follows (●). Identical conditions as in the stopped-flow, except that the reaction was done with radiolabeled DNA as the reporter. Amount of product formation was plotted on the same graph and fit to a triple exponential equation to obtain rate and amplitude information. The three phases of the exponential had rates of 22 ± 2 s^{-1}, 0.9 ± 0.3 s^{-1}, and 0.09 ± 0.09 s^{-1}, respectively, and had

amplitudes of 33 ± 2 nM, 13 ± 2 nM, and 20 ± 4 nM, respectively. **(B)** Shown is a standard curve for determination of PPi concentration produced in the stopped-flow. The reactions were performed under similar reaction conditions as above, except that dTTP was substituted with increasing concentrations of PPi. Shown is a plot of the amplitude obtained in the individual time traces and plotted versus concentration of PPi (●). The amplitude of the fast phase in (A) was determined to be 54 nM.

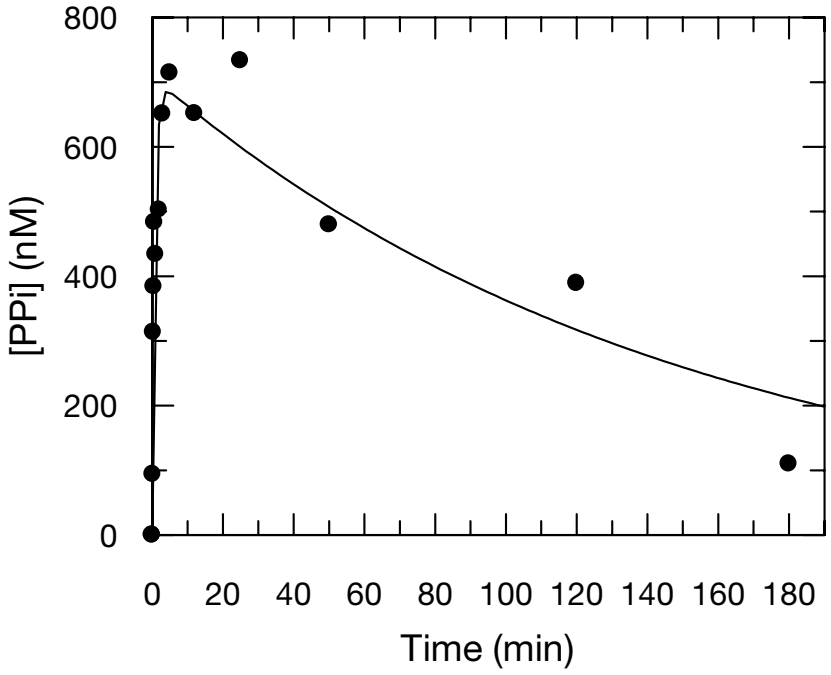

Figure 4.14: Rate of pyrophosphate release during AZT incorporation

Exonuclease-deficient holoenzyme (1 μM) was preincubated with 900 nM 25/45mer DNA and mixed with Mg^{+2}, 300 μM γ-^{32}P-labeled AZTTP, then at each time point an aliquot was taken and passed through a gel filtration column. The elution was spotted on a TLC plate and quantified by fluorography and compared to a standard curve to obtain absolute concentration of PPi remaining in the active site of the enzyme. The amount of PPi in the elution was plotted versus time and fit to a double exponential equation. The rate and amplitude of the fast phase were 1.2 ± 0.3 min^{-1} and 700 ± 70 nM, respectively. The rate and amplitude of the slow exponential decrease in product formation were 0.007 ± 0.002 min^{-1} and 700 ± 50 nM, respectively.

Kinetics of incorporation of AZATP by Pol γ

The interesting results obtained for AZTTP incorporation prompted a series of experiments examining 3′-azido-2′,3′-dideoxyadenosine-5′-triphosphate (AZATP), 3′-azido-2′,3′-dideoxycytidine-5′-triphosphate (AZCTP), and 3′-azido-2′,3′-dideoxyguanosine-5′-triphosphate (AZGTP) incorporation reactions. Figure 4.15A shows the time dependent incorporation of AZATP under single-turnover conditions. The data were fit to a double exponential. The amplitude for fast phase of each reaction was plotted as a function of AZATP concentration and fit the hyperbola to obtain a K_d of 800 ± 120 μM, which is about 4-fold greater than that of AZTTP (Figure 4.15B). The rate of the fast phase of each reaction was plotted against AZATP concentration in Figure 4.15C to illustrate that the trend for AZATP incorporation was similar to that of AZTTP. A maximum rate of polymerization of 0.75 s^{-1} was estimated from the rate of incorporation at higher AZATP concentrations. One significant difference between AZATP and AZTTP incorporation is that AZATP incorporation was biphasic on the time scale examined. The underlying reason for biphasic incorporation will be addressed in the discussion section.

Kinetics of incorporation of AZCTP by Pol γ

The incorporation of AZCTP followed a biphasic trend (Figure 4.16A) similar to that of AZATP, but a K_d of 96 ± 6 μM determined from a hyperbolic fit of the concentration dependent amplitude change was about 2-fold tighter (Figure 4.16B). The maximum rate of incorporation, estimated from the rate of incorporation at higher concentrations of AZCTP was 2 s^{-1}, which is over 2-fold faster than AZATP, and 10-fold faster than AZTTP incorporation.

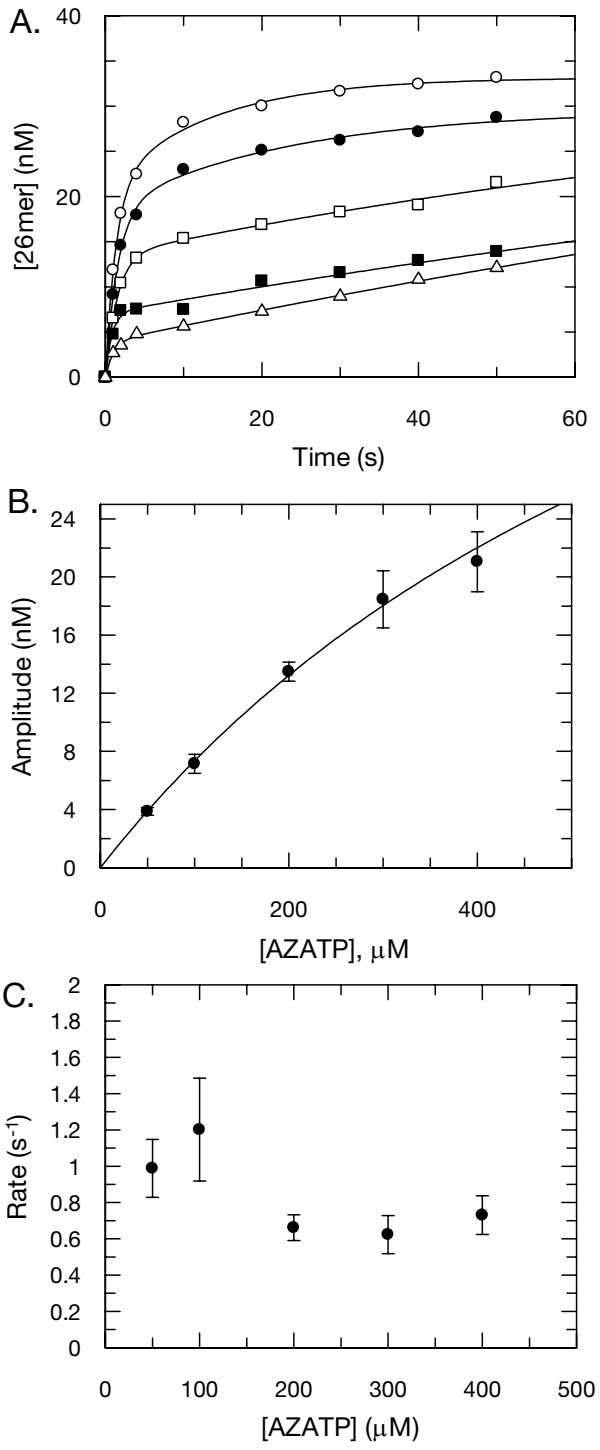

Figure 4.15: Kinetics of incorporation of AZATP by Pol γ

Figure 4.15: Kinetics of incorporation of AZATP by Pol γ

(A) Exonuclease-deficient holoenzyme (100 nM) was preincubated with 90 nM 25/45mer DNA and then rapidly mixed with Mg^{+2} and various concentrations of AZATP (50 (○), 100 (●), 200 (□), 300 (■), and 400 μM (△)). Each data set was fit to a double exponential. **(B)** The amplitude for fast phase of each reaction was plotted as a function of AZATP concentration. A fit of the data to the hyperbola yields a K_d of 800 ± 120 μM. **(C)** The rate of the fast phase of each reaction was plotted against AZATP concentration. A maximum rate of polymerization of 0.75 s^{-1} can be estimated from the rate of incorporation at higher AZATP concentrations.

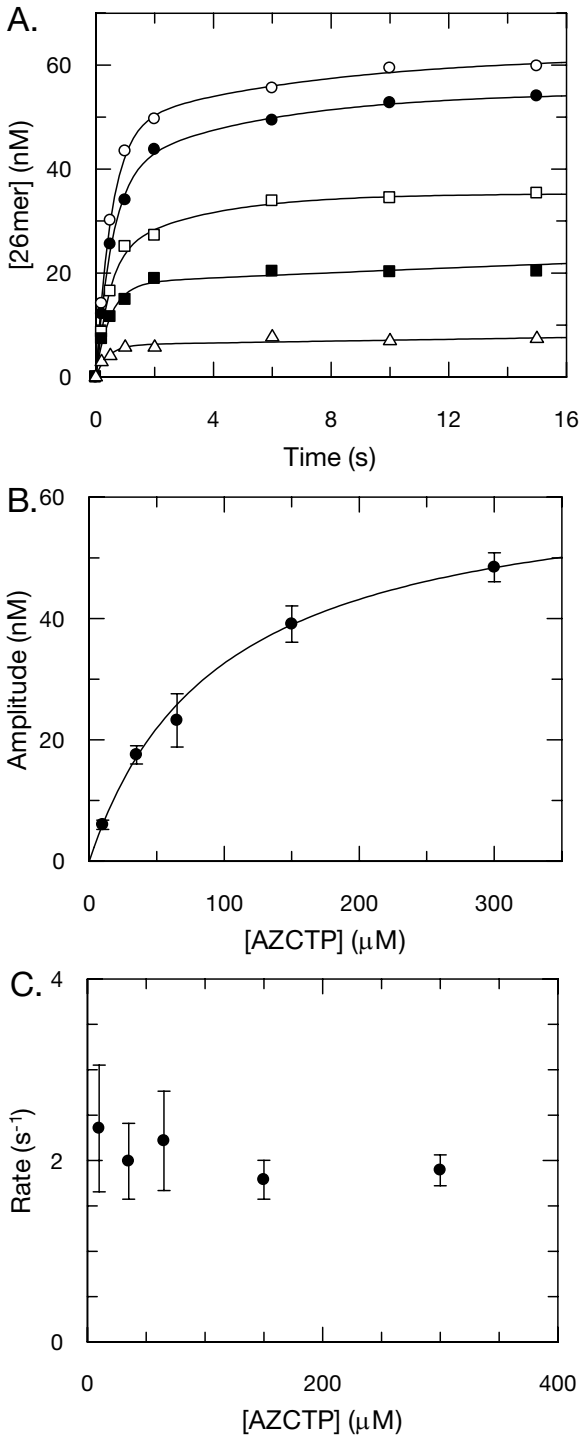

Figure 4.16: Kinetics of incorporation of AZCTP by Pol γ

Figure 4.16: Kinetics of incorporation of AZCTP by Pol γ

(A) Exonuclease-deficient holoenzyme (100 nM) was preincubated with 90 nM 25/45mer DNA and then rapidly mixed with Mg^{+2} and various concentrations of AZCTP (10 (○), 35 (●), 65 (□), 150 (■), and 300 μM (△)). Each data set was fit to a double exponential. **(B)** The amplitude for fast phase for each reaction condition was plotted as a function of AZCTP concentration. A fit of the data to the hyperbola yields a K_d of 96 ± 6 μM. **(C)** The rate of the fast phase of each reaction was plotted against AZCTP concentration. A maximum rate of polymerization of 2 s^{-1} can be estimated from the rate of incorporation at higher AZCTP concentrations.

Kinetics of incorporation of AZGTP by Pol γ

AZGTP incorporation differed significantly from the other azide analogs examined both qualitatively and quantitatively. The time dependent incorporation of AZGTP was fit to a single exponential (Figure 4.17A) and the amplitude of each reaction was plotted against AZGTP concentration (Figure 4.17B). The dissociation constant from a hyperbolic fit of the amplitude was 50 ± 10 μM, about 3-fold tighter than AZTTP. The most interesting aspect of AZGTP incorporation by Pol γ was that the maximum rate of polymerization was nearly 200-fold slower than AZTTP incorporation (0.07 min^{-1} as estimated from the highest concentration of AZGTP used) (Figure 4.17C). Furthermore, the rate increased linearly with concentration suggesting that the rate followed a simple one step binding model, $k_{obs} = k_{on}[AZGTP] + k_{off}$. An off rate of 0.028 ± 0.002 min^{-1} and an apparent second order rate constant of 7.5 ± 0.5 x 10^{-5} $\mu M^{-1}min^{-1}$, were obtained from the y-intercept and slope of the best fit line, respectively. It should be noted that the values obtained by a linear fit may not be interpreted correctly because the amplitude dependence upon concentration skews the fitted rates. The rate of an exponential is a reflection of the time it takes a reaction to reach equilibrium, therefore the low amplitudes at lower concentrations of AZGTP will tend to cause the fitted rates to increase, and consequently the straight line could be an artifact of the amplitude dependence.

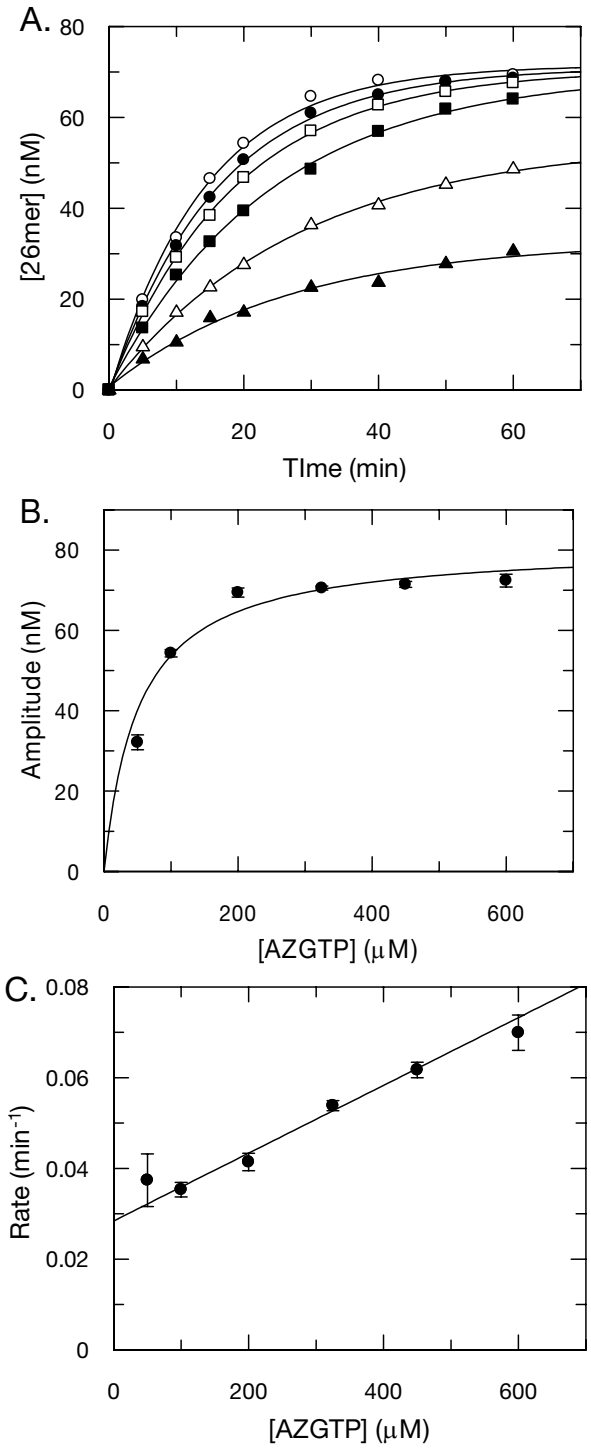

Figure 4.17: Kinetics of incorporation of AZGTP by Pol γ

Figure 4.17: Kinetics of incorporation of AZGTP by Pol γ

(A) Exonuclease-deficient holoenzyme (100 nM) was preincubated with 90 nM 25/45mer DNA and then rapidly mixed with Mg^{+2} and various concentrations of AZGTP (50 (○), 100 (●), 200 (□), 325 (■), 450 (△) and 600 μM (▲)). Each data set was fit to a single exponential. **(B)** The amplitude for each reaction condition was plotted as a function of AZGTP concentration. The fit of the data to a hyperbola yields a K_d of 50 ± 10 μM. **(C)** The rate of each reaction was plotted against AZGTP concentration and was fit by linear regression to obtain a y-intercept (k_{off}) of 0.028 ± 0.002 nM and a slope of (second order rate constant) 7.5 ± 0.5 x 10^{-5} $\mu M^{-1}min^{-1}$.

	k_{pol} (s^{-1}) [b]	K_d (μM)	Specificity (k_{pol}/K_d)	Discrimination[a]
AZTTP	0.2	160 ± 40	$1.3 \pm 0.3 \times 10^{-3}$	32,000
AZATP	0.75	800 ± 120	$9.4 \pm 1.4 \times 10^{-4}$	44,000
AZCTP	2	96 ± 6	$2.1 \pm 0.1 \times 10^{-2}$	2,200
AZGTP	0.001	50 ± 10	$2 \pm 0.4 \times 10^{-5}$	2,300,000

[a] Discrimination = $(k_{pol}/K_d)_{correct}/(k_{pol}/K_d)_{analog}$, where the values for dNTP incorporation in the presence of were taken from Ref (19)

[b] Values of rates of incorporation were estimated from the rate of incorporation at higher concentrations of AZNTP.

Table 4.2: Summary of the kinetics of incorporation of AZNTP by Pol γ

DISCUSSION

The kinetics of incorporation of AZTTP are unusual, in that the rate stays approximately constant at various concentrations of nucleotide (~ 0.2 s^{-1}) while the amplitude increases with concentration. Similar results were found with each of the 3′-azide analogs and are summarized above in Table 4.2.

The amplitude of single-turnover polymerization reactions defines the amount of enzyme-DNA product complex that is rapidly formed during the first turnover. The relationship between amplitude and concentration suggests that the phosphoryl transfer is reversibly linked to binding, such that, increasing concentrations of AZTTP drive the formation of product at equilibrium in the active site.

Instead of fitting the rate dependence on concentration, a fit of the concentration dependence of the amplitude yields an apparent ground state dissociation constant of 160 ± 40 μM, the weakest binding of all nucleoside analogs examined in our laboratory to date. The maximum rate of incorporation was simply taken to be 0.2 s^{-1}, since there was little variation with concentration.

The measured rate of pyrophosphate release of 0.007 min^{-1} suggests that the conformational change after phosphoryl transfer may be rate-limiting. It is also possible that the release of pyrophosphate itself is rate-limiting; however it was shown that the DNA terminated with AZTMP dissociates more slowly than normal DNA. Since there was no pyrophosphate present during that measurement, it appears that the 3′-azide group may interfere with the relaxation of the enzyme to an open conformation, thereby slowing the dissociation of PPi and DNA from the active site. Furthermore, the inability to observe pyrophosphorolysis of DNA terminated with AZTMP by adding PPi from solution may suggest that the enzyme is largely in the closed conformation or that the rate

of closure is very slow. The most probable cause for the equilibrium observed for AZTTP incorporation is that after incorporation the enzyme remains in the closed conformation for an extended period of time with the active site residues aligned for catalysis with pyrophosphate remaining in position for the reaction, thus allowing the reaction to be reversible, and reach equilibrium on the time scale of a few seconds.

Shown in Figure 4.18 are simulated data generated using KinTekSim computer simulation software using an initial collision (K_d) of 400 μM, a rate of 0.4 s^{-1} for the forward phosphoryl transfer reaction, a rate of 0.2 s^{-1} for the reverse (pyrophosphorolysis) reaction, and a rate of 0.007 min^{-1} for the conformational change following phosphoryl transfer. The mechanism used for the simulation is shown in the following scheme (Figure 4.18 legend) along with the rates used for generating the data. The mechanism was truncated in that the step representing the conformational change preceding phosphoryl transfer was omitted because it appears to be kinetically silent. The K_d experimentally measured was about 160 μM and, according to this model, is the product of at least four steps in the reaction (on and off rates and forward and reverse phosphoryl transfer rates). The values used for the simulation can be used to calculate the measured apparent K_d.

$$K_d = \frac{k_{off} k_{reverse}}{k_{on} k_{forward}} = \frac{400 \times 0.2}{1 \times 0.4} = 200 \mu M$$

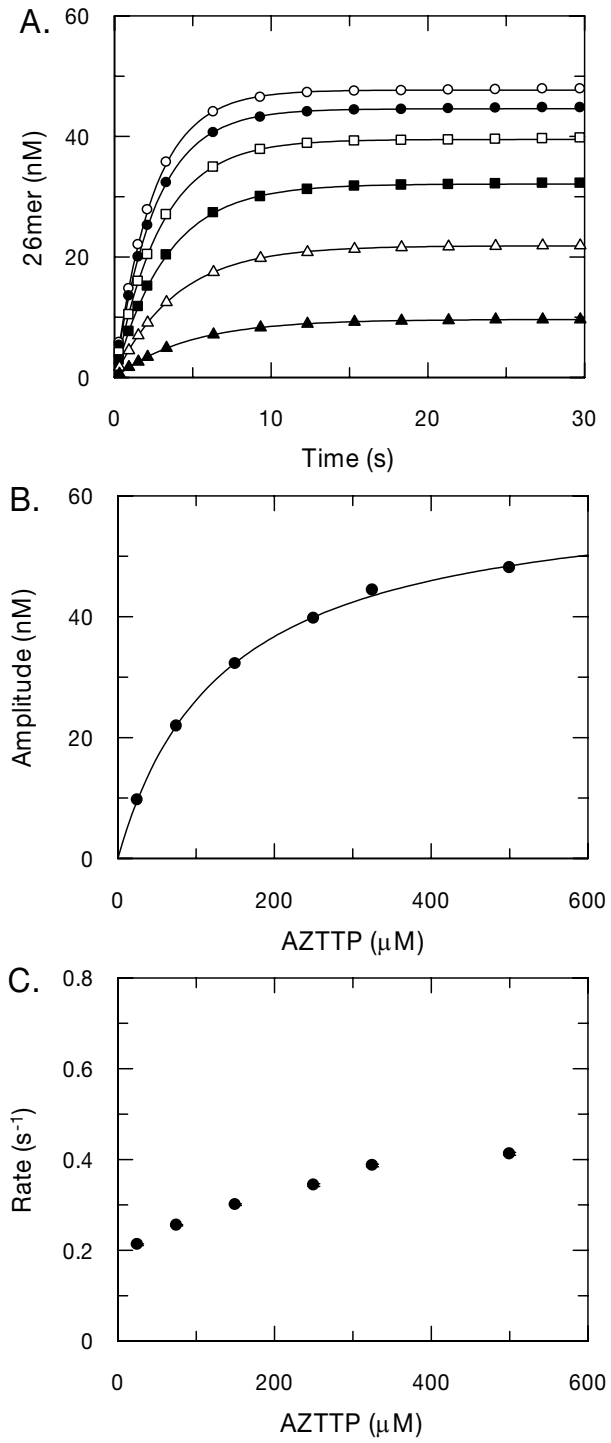

Figure 4.18: Simulation of AZTTP incorporation by Pol γ

Figure 4.18: Simulation of AZTTP incorporation by Pol γ

(A) Shown are data points generated from KinTekSim computer simulation software using the mechanism and numbers in the scheme below for the incorporation of various concentrations of AZTTP (25 (▲), 75 (△), 150 (■), 250 (□), 325 (●), and 500 (○) μM) under single turnover conditions. Data were plotted as a function of time and fit to a single exponential equation. **(B)** The single exponential amplitudes were plotted as a function of concentration and fit to a hyperbola to yield a theoretical K_d of 135 μM, which agrees well with the experimentally measured K_d of about 160 μM. **(C)** The single exponential rates were plotted as a function of concentration to illustrate that they do not vary greatly with concentration. The experimentally obtained data was plotted previously in Figure 4.1.

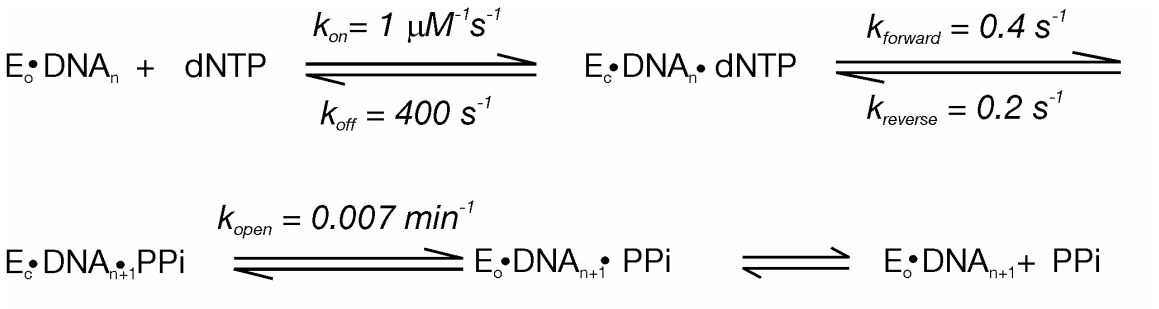

The incorporation of the other 3′-azide analogs revealed that, except for AZGTP, they also exhibit similar reaction kinetics, suggesting that an azide group on the 3′ carbon has a profound effect on the conformational change following phosphoryl transfer. The results for AZGTP were somewhat different, in that the amplitude and rate varied with concentration and cannot be explained in detail at this time. The incorporation of AZGTP was about 170-fold slower than AZTTP, possibly masking the equilibrium of phosphoryl transfer somewhat, due to the rate of incorporation being comparable to the rate of the conformational change following phosphoryl transfer.

We are now confident that the calculation of the toxicity index for AZTTP is accurate as calculated from the apparent K_d obtained by fitting the single exponential amplitude of AZTTP incorporation (160 ± 40 μM). AZTTP is the second least toxic analog (according to the toxicity index) we examined due, in large part, to the weak apparent binding compared to the other analogs. PMPA had a K_d of 40.3 ± 5.7 μM (32), the second lowest binding affinity of the inhibitors inspected. However, questions remain regarding the clinical toxicity that is observed for AZT, although minor compared to ddC, d4T and ddI. Studies *in vivo* with AZTTP have shown it to cause ultrastructural changes in mitochondria (83;84), but other studies have shown that AZT causes bone marrow toxicity, in contrast to other nucleoside analogs. Therefore AZT toxicity is thought to be due to inhibition of one or more of the chromosomal DNA polymerases (48). In nonproliferating cells, nucleoside analogs, including AZT, have been documented to inhibit Pol γ specifically (48;85-88). Recent studies with HepG2 cells have shown that AZT can reduce oxidative phosphorylation without reducing the amount of mtDNA (89), and that oxidative damage to mtDNA was increased in muscle and liver tissues of mice treated with AZT (90;91), suggesting that AZT causes mitochondrial dysfunction by some mechanism other than inhibition of mtDNA synthesis (92). Such a large array of

reports has lead to confusion regarding AZT toxicity, but simply taken at face value our experiments suggest that the clinical toxicity of AZT is not due to inhibition of Pol γ specifically.

Chapter 5: Exonuclease Removal of ddC and incorporation of Acyclovir-TP and dd2APyTP by Pol γ

INTRODUCTION

Incorporation of nucleoside analogs by the mitochondrial DNA polymerase γ has been implicated as the primary cause underlying many of the toxic side effects of these drugs in HIV therapy. Recently, we have accomplished a detailed mechanistic analysis of the reactions governing nucleotide selectivity of the mitochondrial polymerase and its proofreading exonuclease. The toxic side effects of nucleoside analogs are correlated with the kinetics of incorporation by Pol γ, varying over 6 orders of magnitude in the sequence zalcitabine (ddC) > didanosine (ddI metabolized to ddA) > stavudine (d4T) > lamivudine (3TC) > tenofovir (PMPA) > zidovudine (AZT) > abacavir (metabolized to carbovir, CBV) (32;60). Of the nucleoside analogs examined, ddCTP was the least effectively discriminated against by Pol γ with a discrimination of only 2.9, in that ddCTP was incorporated 70-fold more slowly, but bound 27-fold more tightly than the natural nucleotide, dCTP (93). In addition, the rate of excision of ddC was reported to be too slow to measure, suggesting that ddC is effectively a suicide inhibitor of mitochondrial DNA synthesis (94). In this chapter we reinvestigate this apparently anomalous result.

Peripheral neuropathy is the primary dose-limiting adverse effect observed with the long term use of ddC and other nucleoside analogs (95;96). Cell culture experiments that quantify the potencies of inhibition of mtDNA synthesis have shown ddC to cause almost complete depletion of mtDNA after 9-days of incubation at a concentration of 30 μM, leading to a virtual knockout of cytochrome c oxidase II (COX II) expression (COX II is encoded by the mitochondrial genome) in human hepatoblastoma (HepG2) cells

(97). Also, in a rabbit model of ddC-induced neuropathy, it has been shown that there were significant mitochondrial alterations in Schwann cells (98). The inefficiency of excision of ddCMP from terminated DNA by Pol γ may contribute to the profound inhibition of mtDNA synthesis.

In the case of the slow or nonexistent hydrolysis of chain terminators, comparisons between Pol γ and HIV-1 RT would be effectively reduced to comparisons between their respective abilities to discriminate correct from incorrect during incorporation, since RT lacks a proofreading mechanism (32). An in-depth understanding of the mechanistic cause for the slow rate of removal is therefore of great interest in designing less toxic antiviral drugs.

MATERIALS AND METHODS

Nucleotides and oligonucleotides

Acyclovir-TP was purchased from Moravek Biochemicals (Brea, CA), dd2APyTP was provided by Dr. Larry McLaughlin (Boston College, Chestnut Hill, MA), and unmodified dNTP's and ddCTP were purchased from Sigma Aldrich Corp. (St. Louis, MO). Oligonucleotides were purchased from Integrated DNA Technologies (Coralville, IA).

Pol γ expression and purification

Overexpression and purification of recombinant human Pol γ were previously described (11;12). Holoenzyme was reconstituted at a 1:5 ratio of catalytic subunit to accessory subunit. Unless stated otherwise, all kinetic studies were conducted using a wild type Pol γ, but in cases of incorporation reactions an exonuclease-deficient mutant (E200A) was used.

Preparation of DNA

The 26mer primer sequence was 5′-GCCTCGCAGCCGTCCAACCAACTCA**X**-3′, where the bold **X** signifies the position where either dC or ddC was placed. The template sequence which was correctly base paired with the primer strand was 5′-GGACGGCATTGGATCGACAGTGAGTTGGTTGGACGGCTGCGAGGC-3′. The template sequence for the DNA containing eight different bases to create a frayed primer was 5′-GGACGGCATTGGATCGACAATATCAAGGTTGGACGGCTGCGAGGC-3′ Primer was 5′-^{32}P-labeled using T4 polynucleotide kinase, according to the manufacturer's instructions (Life Technologies, Gaithersburg, MD). The reaction was terminated by incubation at 95°C for 5 minutes, and excess nucleotide was removed using a Bio-Spin 6 column (BioRad, Hercules, CA). Primer was annealed to 45-mer template by combining at an equimolar ratio, heating to 95 °C, and slowly cooling to room temperature.

Polymerization and exonuclease reaction conditions

For reactions too fast to measure by manual mixing and quenching, a quench-flow apparatus (RFQ-3) from KinTek Corp. (Austin, TX) was used. Unless otherwise stated incorporation and exonuclease assays were performed at 37^{o}C in buffer containing 50 mM Tris-Cl, pH 7.5, 100 mM NaCl, 2.5 mM $MgCl_2$. For one experiment the reactions were performed in buffer containing 50 mM Tris-acetate pH 7.5, 100 mM potassium acetate, 2.5 mM $MgCl_2$, and 0.1 mM EDTA. The holoenzyme was reconstituted by incubating the two protein subunits for 5 min on ice in reaction buffer lacking magnesium. DNA was then added to the proteins, and the mixture was incubated for an additional 5 min on ice. Incorporation reactions were initiated by the addition of nucleotide and magnesium in the same reaction buffer at 37 °C and then quenched with 0.5 M EDTA. Alternatively, the excision reactions were initiated by the addition of 2.5

mM $MgCl_2$. All concentrations given are concentrations after mixing. Products were separated on 15% denaturing polyacrylamide sequencing gels, imaged on a Molecular Dynamics Storm 860, and quantified using ImageQuaNT software (Amersham Biosciences, Uppsala, Sweden).

Ground state dissociation constant and maximum rate of polymerization for nucleoside analog triphosphates

Single nucleotide incorporation assays were performed with various concentrations of nucleoside analogs to examine the nucleotide concentration dependence of the incorporation rate. Single-turnover conditions were employed where the concentration of enzyme was greater than the concentration of DNA. Specific reaction conditions are listed in each Figure legend. A time course was performed for each concentration of nucleoside analog triphosphate. To normalize data, the integrated amount of product (DNA_{n+1}) was divided by the sum of the substrate and product (DNA_n + DNA_{n+1}) and multiplied by the concentration of DNA used in the experiment. The concentration of extended product DNA was plotted against time and fit to a single ([product] = $A_1*e^{-k_1t}$ +C) or double ([product] = $A_1*e^{-k_1t}$ + $A_2*e^{-k_2t}$ + C), exponential equation (according to the Figure legends and results section). The observed rates were then plotted against nucleoside analog triphosphate concentration, and the data were fit to a hyperbola (observed rate = k_{pol} * [dNTP]/(K_d + [dNTP]) to obtain the K_d and the maximum rate of polymerization, k_{pol} for the nucleoside analog triphosphates.

RESULTS

ddC removal from correctly paired or frayed DNA

In our previous work on the toxicity of nucleoside analogs, we found that the rate for the exonuclease removal of ddC was too slow to measure under steady-state conditions (32). We revisited this phenomenon by examining in greater detail the

kinetics of exonuclease removal of ddC. With a defined primer and template of 26 and 45 bases, respectively, we designed one duplex to be completely complementary in the double stranded region and one duplex, with 8 mismatches on the 3′-terminus of the primer. The rationale for using frayed duplex stems from results obtained by Allison A. Johnson with Pol γ in our lab, where the rate of excision increased to a maximum of about 9 s^{-1} as the number of mismatches increased (0-7 mismatches) (27). Therefore, it appeared that primer melting was a least partially rate-limiting in the excision of correctly paired DNA, but as the number of mismatches increased, the rate-limiting step was more likely to take place after strand transfer from the polymerase site to the exonuclease site. In addition to the rate increasing, the reaction became biphasic with the amplitude of the fast phase increasing as the number of mismatches increased, suggesting that a percentage of primer was positioned in the exonuclease site at the start of the reaction with mismatched DNA.

Before examining the kinetics of ddC removal we measured the rate of removal of dC from both correctly paired DNA and frayed DNA. Wild type holoenzyme was preincubated under single-turnover conditions with either correctly paired or frayed DNA and mixed with Mg^{+2} to start the reaction (Figure 5.1A). The removal of correctly base paired dC was biphasic with rates of 0.86 ± 0.35 s^{-1} and 0.016 ± 0.004 s^{-1} and corresponding amplitudes of 21 ± 3 nM and 70 ± 3 nM, respectively. We did not expect the reaction of correctly paired DNA to be biphasic, but the amplitude of the fast phase was only 30 percent of the amplitude of the slow phase. The amplitude of the fast phase may represent the fraction of primer strand that was slightly frayed or present at the exonuclease site of Pol γ when the reaction was started. The exonuclease reaction with 8 base pair frayed DNA was also biphasic with rates of 1.6 ± 0.5 s^{-1} and 0.1 ± 0.07 s^{-1} and with amplitudes of 60 ± 10 nM and 25 ± 10 nM, respectively. The rate of the fast phase

increased only slightly, but the amplitude was increased to 60 nM compared to the correctly paired DNA. This is probably due to a larger percentage of the primer present at the exonuclease site when the reaction was started. The rate of the slow phase for frayed DNA was an order of magnitude larger than for the correctly paired DNA, presumably because the rate of melting for correctly paired DNA was slower than that of frayed DNA.

The reactions with ddC-terminated primers were dramatically different, in that they were much slower and removal only occurred at a single rate (Figure 5.1B). The rate for the removal of ddC-terminated correctly paired DNA was $3 \pm 0.4 \times 10^{-4}$ s^{-1}, 50-fold slower than the slow phase of dC removal. The removal of ddC from frayed DNA occurred at a rate of $4.4 \pm 0.5 \times 10^{-3}$ s^{-1}, 15-fold faster than with correctly paired ddC-terminated primer. Both reactions went 100 percent to completion with slower rates than the rate of dissociation of DNA from the enzyme active site (0.02 s^{-1}), suggesting that the DNA dissociates from the enzyme before removal occurs.

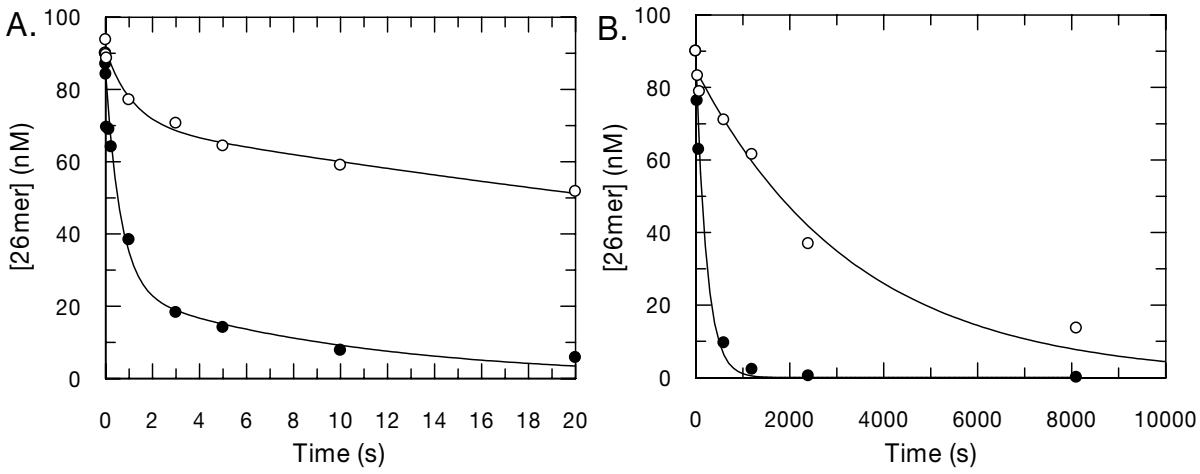

Figure 5.1: Exonuclease removal of dC and ddC-terminated primers with or without frayed termini

(A) Wild type holoenzyme (100 nM) was preincubated with 90 nM 26/45mer terminated with dC correctly base paired (○) or frayed at the 3′-terminus (8 mismatches) (●) and mixed with Mg^{+2} to start the reaction. Concentration of substrate as a function of time was plotted and fit to a double exponential equation. Both the correctly base paired and frayed DNA containing reactions were biphasic. The correctly paired dC DNA was excised at rates of 0.86 ± 0.35 s^{-1} and 0.016 ± 0.004 s^{-1} with amplitudes of 21 ± 3 nM and 70 ± 3 nM, respectively. The frayed dC-terminated DNA was excised at rates of 1.6 ± 0.5 s^{-1} and 0.1 ± 0.07 s^{-1} with amplitudes of 60 ± 10 nM and 25 ± 10 nM, respectively. **(B)** The same reaction conditions as in (A) were used, except the primer was terminated with ddC. Substrate was plotted as a function of time and fit to a single exponential equation. The reactions were not double exponentials as in (A), and were dramatically slower at a rate of 3 ± 0.4 x 10^{-4} s^{-1} for correctly paired ddC-terminated primer (○) and 4.4 ± 0.5 x 10^{-3} s^{-1} for ddC-terminated frayed DNA (●). Both had full amplitudes of about 90 nM.

Removal of ddC in the presence of dNTP

In the mitochondria, all four nucleotides are present which could affect the rate of removal of ddC. If ddC is incorporated, it is possible that the rate of excision be slowed by the presence of dNTP, because the next correct nucleotide could bind leading to a closed enzyme/DNA complex which is unable to catalyze the addition of the next nucleotide. This could result in a slower rate of exonuclease removal because the enzyme remains in the closed conformation and the melting of the primer strand over into the exonuclease site would be inhibited. In agreement, ddC removal with correctly paired DNA in the presence of 100 μM dNTP was slowed by almost four-fold to a rate of $8.0 \pm 0.7 \times 10^{-5}$ s^{-1} (Figure 5.2). However, the rate of removal of ddC with frayed DNA ($6.3 \pm 0.3 \times 10^{-3}$ s^{-1}) was nearly identical compared to the reaction without nucleotides ($4.4 \pm 0.5 \times 10^{-3}$ s^{-1}). Apparently, the presence of the next correct nucleotide was insufficient to lead to a large enough percentage of closed enzyme/DNA complex to inhibit strand transfer.

dC and ddC removal from correctly paired or frayed DNA in K^+-acetate buffer

Since K^+ is the normal intracellular cation K^+ instead of Na^+; the effect K^+ on the rate of excision of dC and ddC was inspected. Similar to the previous reactions, wild type Pol γ holoenzyme was preincubated under single-turnover conditions with correctly paired or frayed DNA terminated with either dC or ddC and mixed with Mg^{+2} to start the reaction (Figure 5.3A-Figure 5.3B). The removal of dC from both correctly paired and frayed DNA both occurred at single exponential rates of 0.011 ± 0.004 s^{-1} and $0.27 \pm 0.03 \times 10^{-3}$ s^{-1}, respectively. These rates were marginally slower, in that they match up better with the slow phase of the reactions performed with Na^+, but what may be more interesting is the lack of biphasic kinetics for either set of DNA. This suggests that most

or all of the primer may be at the polymerase site when the reaction was started with correctly paired DNA, or in the case of frayed DNA all of the primer may have been at the exonuclease site or the rate of excision and strand transfer were comparable and were not resolved. The rates of ddC removal for the correctly paired and frayed DNA were nearly identical to the reaction performed with Na^+.

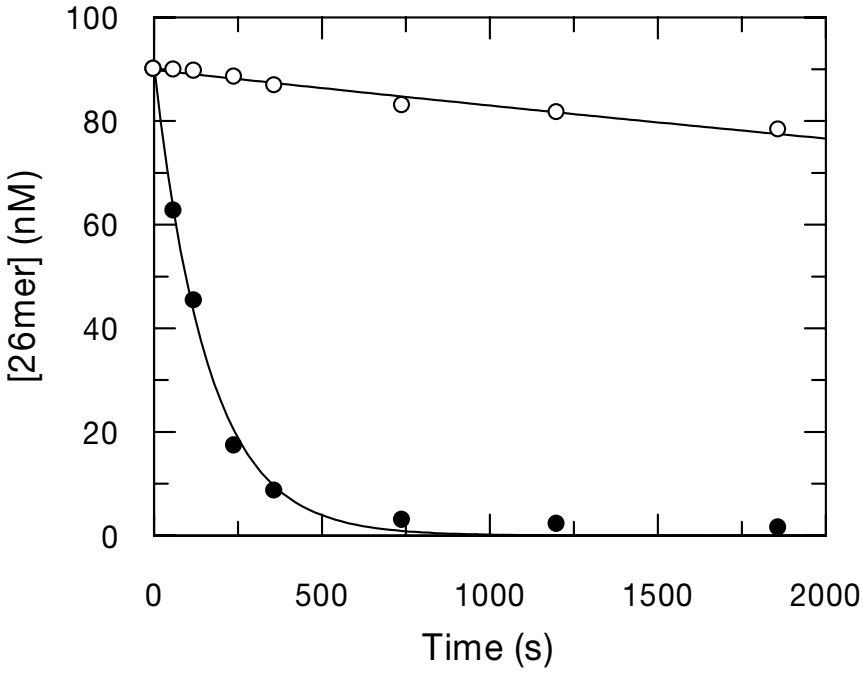

Figure 5.2: Exonuclease removal of ddC in the presence of dNTP with or without frayed termini

Wild type holoenzyme (100 nM) was preincubated with 90 nM 26/45mer terminated with ddC correctly base paired (○) or frayed at the 3′-terminus (8 mismatches) (●) and mixed with Mg^{+2} and 100 μM dNTP to start the reaction. Concentration of substrate as a function of time was plotted and fit to a single exponential equation. The correctly paired ddC-terminated DNA was excised at a rate of $8 \pm 0.7 \times 10^{-5}$ s^{-1}. The frayed ddC-terminated DNA was excised at a rate of $6.3 \pm 0.3 \times 10^{-3}$ s^{-1} with amplitudes of about 90 nM. The reaction with correctly paired ddC-terminated DNA was assumed to go to completion for fitting purposes.

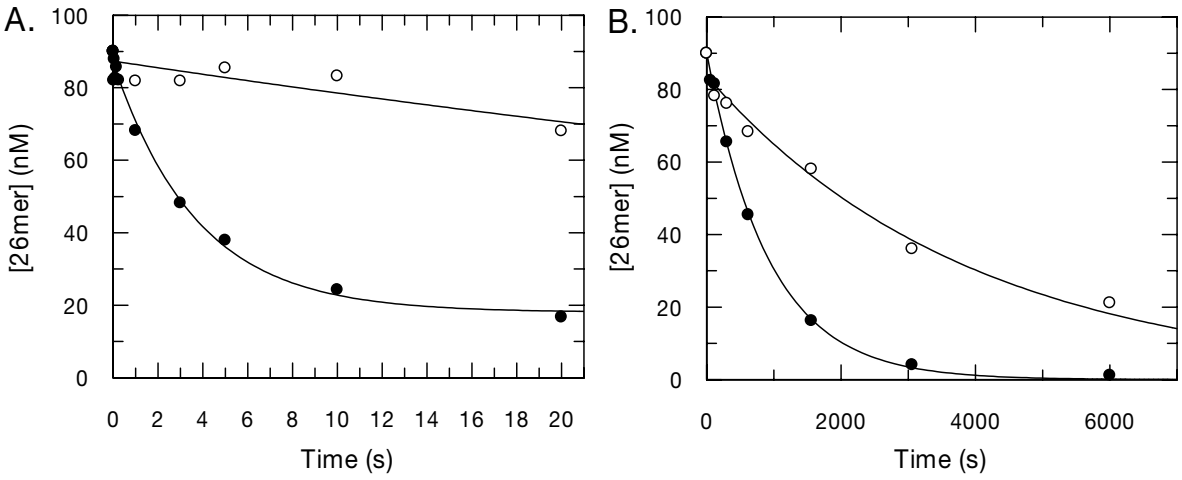

Figure 5.3: Exonuclease removal of dC and ddC in K^+-acetate buffer with or without frayed termini

(A) Wild type holoenzyme (100 nM) was preincubated with 90 nM 26/45mer terminated with dC correctly base paired (○) or frayed at the 3′-terminus (8 mismatches) (●) and mixed with Mg^{+2} to start the reaction. Concentration of substrate as a function of time was plotted and fit to a single exponential equation. The correctly paired dC-terminated DNA was excised a rate of $0.011 \pm 0.004\ s^{-1}$. Frayed dC-terminated DNA was excised at a rate of $0.27 \pm 0.03 \times 10^{-3}\ s^{-1}$. **(B)** The same reaction conditions as in (A) were used except the primer was terminated with ddC. The correctly paired ddC-terminated DNA was excised a rate of $3 \pm 0.3 \times 10^{-4}\ s^{-1}$. The frayed ddC-terminated DNA was excised at a rate of $1.10 \pm 0.04 \times 10^{-3}\ s^{-1}$.

Incorporation of dd2APyTP

dd2APyTP was synthesized in Larry W. McLaughlin's laboratory at Boston College where they obtained promising preliminary results for the efficient incorporation by HIV reverse transcriptase but not by mammalian polymerases. The analog had two differences from the natural nucleoside, dC; one was a modification of the nucleobase residue to eliminate the O2-carbonyl, and the second was that it was a synthesized from 2′,3′-dideoxyribose, so that is was a chain terminator (Figure 5.4A) (99). A 25/45mer was designed to have a G corresponding to the 26th primer position and preincubated with exonuclease-deficient holoenzyme under single-turnover conditions and mixed with Mg^{+2} and various concentrations of dd2APyTP to start the reaction (Figure 5.4B). The rates from the single exponential fits were plotted against concentration and fit to a hyperbola to obtain a K_d of 105 ± 10 μM and a k_{pol} of 0.004 ± 0.0002 s^{-1}, for a specificity constant (k_{pol}/K_d)of 3.8 ± 0.4 x 10^{-5} $\mu M^{-1}s^{-1}$. Surprisingly, a discrimination (calculated as $(k_{pol}/K_d)_{dCTP}/(k_{pol}/K_d)_{dd2APyTP}$) against dd2APyTP of about 1.2 million is the greatest we have seen for the various nucleoside analogs examined (32;60). Interestingly, the rate of removal, which was measured previously (99), was identical to the rate of removal of ddC, suggesting little to no role of the O2-carbonyl in the exonuclease removal of dd2APyMP.

Incorporation of acyclovir-TP

Previous studies with PMPA, an adenosine analog, (structure shown in Figure 4.1) showed that even when an analog lacked the 3′ carbon (no ribose ring) it could still be incorporated by Pol γ, albeit with severely reduced rates. Acyclovir (Zovirax) is an antiviral drug used to treat herpes infections of the skin, lip, and genitals; herpes zoster (shingles); and chickenpox. It can be administered as an ointment or orally. Acyclovir, a

guanosine analog, also lacks the ribose ring; in fact, it has neither the 2′ nor the 3′ carbons. Generally speaking the larger the modification to the ribose ring the lower the predicted toxicity is according to our toxicity index (32;60).

A 25/45mer coding for G incorporation (26^{th} primer position) was preincubated with exonuclease-deficient holoenzyme under single-turnover conditions and mixed with Mg^{+2} and various concentrations of acyclovir-TP to start the reaction (Figure 5.4B). The rates from the single exponential fits were plotted against concentration and fit to a hyperbola to obtain a K_d of 1.6 ± 0.3 μM and a k_{pol} of 0.31 ± 0.05 s^{-1}, for a specificity constant of 0.19 ± 0.05 $\mu M^{-1}s^{-1}$. The discrimination against acyclovir-TP of about 240 is surprisingly poor considering PMPA is discriminated against by a factor of 11,400. This suggests that toxic side effects would result if concentrations of acyclovir-TP reach concentrations similar to that of other nucleoside analogs such as ddC, ddI, and d4T in mitochondria.

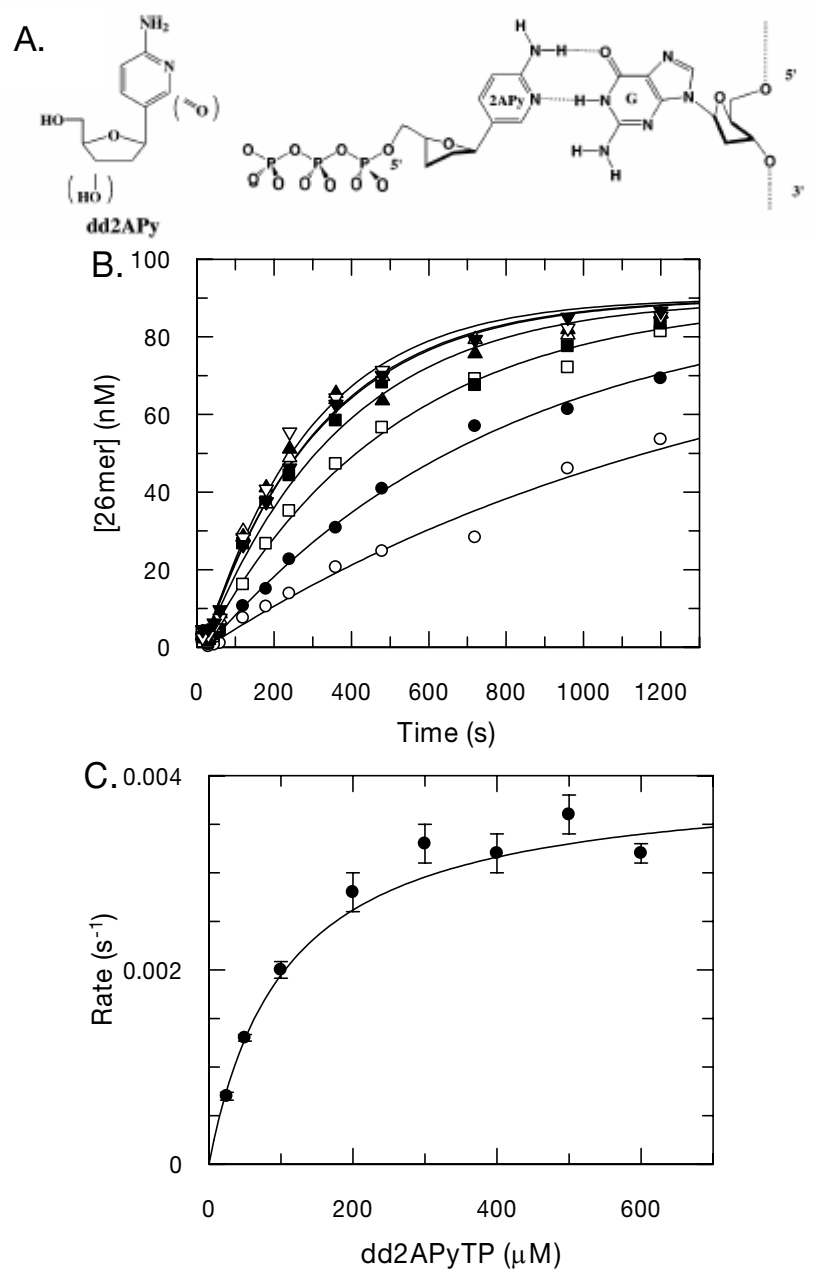

Figure 5.4: Incorporation of dd2APyTP

Figure 5.4: Incorporation of dd2APyTP

(A) Shown is the structure and base pairing arrangement for dd2APyTP. The analog lacks a carbonyl oxygen on the 2-carbon and also lacks a 3′-OH necessary for elongation making it a chain terminator (Figure from ref (99)). **(B)** Exonuclease-deficient holoenzyme (100 nM) was preincubated with 90 nM 25/45mer DNA duplex (G in the template at the 26^{th} position), and then rapidly mixed with Mg^{+2} and various concentrations of dd2APyTP (25 (○), 50 (●), 100 (□), 200 (■), 300 (△), 400 (▲), 500 (∇), and 600 (▼) μM). Each data set was fit by non-linear regression to a single exponential equation to obtain the rate of incorporation. **(C)** The single exponential rates were plotted as a function of dd2APyTP concentration. A fit of the data to a hyperbola yields a $K_d = 105 \pm 10$ μM and a $k_{pol} = 0.004 \pm 0.0002$ s^{-1}.

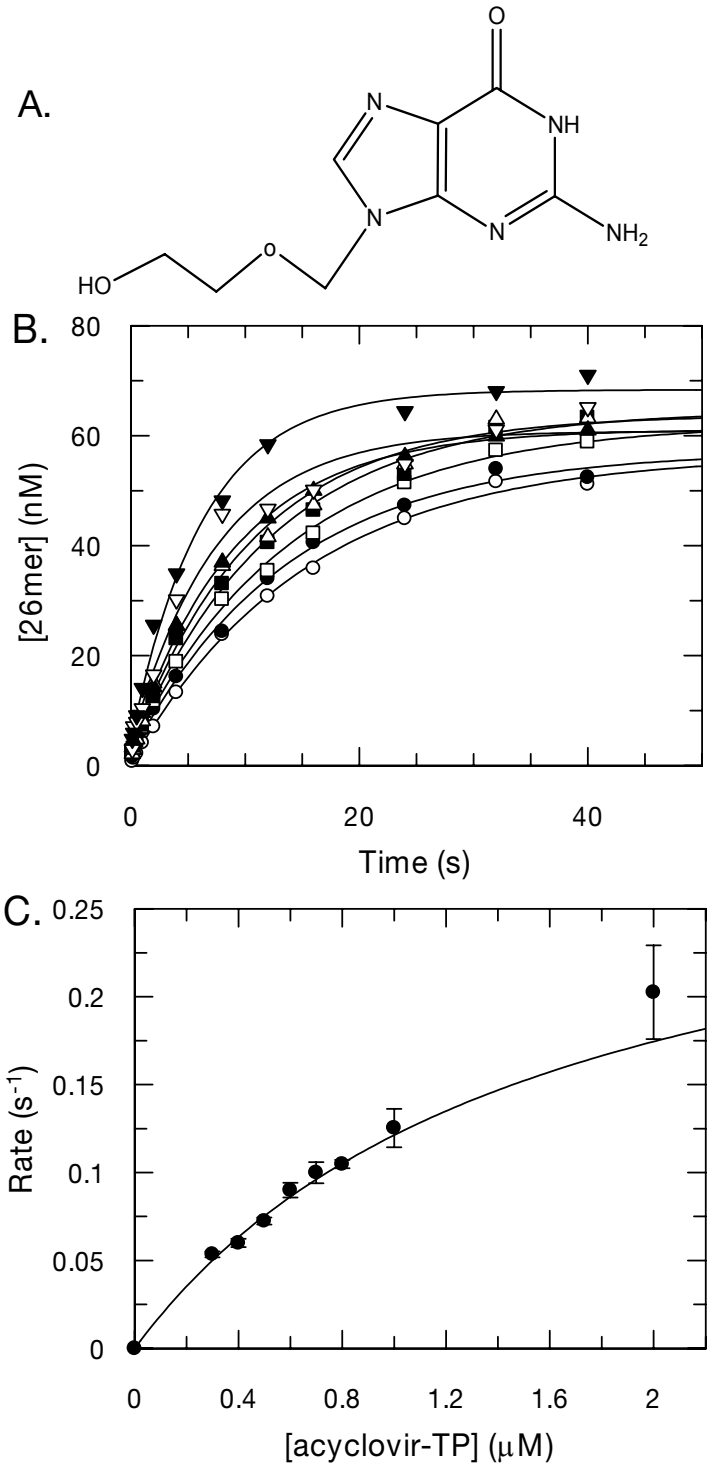

Figure 5.5: Incorporation of acyclovir-TP

Figure 5.5: Incorporation of acyclovir-TP

(A) Shown is the structure of acyclovir-TP. The 2′ and 3′ carbons are removed compared to dGTP. The triphosphate is the active form of the drug. **(B)** Exonuclease-deficient holoenzyme (100 nM) was preincubated with 90 nM 25/45mer DNA (C in the template at the 26^{th} position) duplex, and then rapidly mixed with Mg^{+2} and various concentrations of acyclovir-TP (0.3 (○), 0.4 (●), 0.5 (□), 0.6 (■), 0.7 (△), 0.8 (▲), 1(▽), and 2 (▼) μM). Each data set was fit by non-linear regression to a single exponential equation to obtain the rate of incorporation. **(C)** The single exponential rates were plotted as a function of acyclovir-TP concentration. A fit of the data to a hyperbola yields a $K_d = 1.6 \pm 0.3$ μM and a $k_{pol} = 0.31 \pm 0.05$ s^{-1}.

DISCUSSION

The rate of exonuclease removal of ddC was more accurately measured than previously and was shown to be $3.0 \pm 0.4 \times 10^{-4}$ s^{-1} The rate was slowed by about 4-fold in the presence of dNTP, and is probably a more accurate representation of the physiological rate. The rate increased 15-fold when frayed DNA was used. This illustrates the effect of kinetic partitioning between the polymerase and the exonuclease site of the enzyme. For instance, the rate of the slow phase of correctly paired dC removal was 0.016 ± 0.004 s^{-1} (50-fold faster than ddC removal), which most likely represents the rate of melting of primer strand and transfer into the exonuclease site. Although melting may not be rate limiting for ddC removal, the observed excision rate increased 15-fold when using frayed DNA. It is possible that there is an equilibrium between the exonuclease and polymerase sites with the majority of the correctly paired DNA at the polymerase site. Furthermore, the fact that the addition of the next correct dNTP slows the rate of removal about 4-fold seems to agree well, because the closed form of the enzyme would tend to slow melting and transfer of the primer to the exonuclease site. In any case, the rate of ddC removal is the slowest rate of removal of the nucleoside analogs we have examined, and is the most toxic of the nucleoside analogs approved for use as anti-HIV drugs.

The design of dd2APyTP in Dr. Larry McLaughlin's laboratory was based on recent work suggesting that mammalian polymerases make minor grove contacts with functional groups of the base residues of both the primer and templates and a change in the geometric shape of the base could lead to lower specificity of a nucleoside analog (99). The analogs approved to date have ribose ring modifications, and essentially native bases. From the kinetics of incorporation a discrimination against dd2APyTP of 1.2

million by Pol γ suggests that at least from the perspective of toxicity, could be a promising new drug lead. However, the rate of removal was identical to that of ddC. The contribution of the rate of removal for nucleoside analog toxicity is generally unknown, but after incorporation the polymerase will almost definitely dissociate from the chain terminated DNA. This is potentially a problem if the concentration Pol γ is relatively low in the mitochondria, because the slow rebinding of the polymerase would decrease the rate of excision further.

The incorporation of acyclovir was examined to inspect the effects of partially removing the ribose ring compared to the natural nucleotide, dGTP. In contrast to PMPA, the discrimination against acyclovir was significantly reduced (11,700 versus 240, respectively). This suggests that the high discrimination against PMPA is a result of the presence of the 2′ methyl group, the lack of a methylene group between the ribose oxygen and the nearest phosphate, or the effect is base specific (PMPA is an A analog and acyclovir is a G analog) or a combination of all three.

Chapter 6: Replication of Oxidatively Damaged DNA by Pol γ

INTRODUCTION

While several theories exist regarding the underlying molecular mechanisms that cause aging in mammals, the mitochondrial theory of aging recently has gained credence (61;100). According to the mitochondrial theory of aging, electrons from the electron transport chain, most likely from complex I, are able to reduce molecular oxygen to form superoxide anion radicals (O_2^-) during aerobic respiration. These reactive radicals go on to produce other reactive oxygen species (ROS) (61). ROS can be generated at a few cellular sites, but in healthy tissues, the majority are from metabolism. For that reason, they are always present at normal cellular activity levels. ROS attack a variety of different cellular macromolecules, including proteins, lipids and DNA. However, damage to mtDNA has been implicated as the most important in regard to aging, especially in postmitotic cells, such as neurons (70), in part because the damage caused at other sites is essentially reversible by virtue of the information contained within DNA. A cycle is created in the mitochondria under this continued state of oxidative stress leading to further damage to electron transport chain components, and ultimately causing an energy decline, carcinogenesis, and many age-related diseases (101).

One of the most common products of oxidative DNA damage is 8-hydroxy-2′-deoxyguanosine (8-oxodG), which is reported to be highly mutagenic and is commonly used as biomarker for oxidative stress. Basal levels of 8-oxodG in mtDNA between different species correlate negatively with longevity in many mammals and birds, which is not the case with nuclear DNA (nDNA) (71). Moreover, due to the proximity of mtDNA to the electron transport chain, the levels of oxidative damage are significantly higher in all tissues of mammals and birds examined than in the nucleus (72). It is now

established that caloric restriction increases the life span of rodents and is correlated with less mtDNA damage and age (102).

While much is known regarding the DNA repair pathways in the nucleus, comparatively little is known about the mitochondria. The repair of 8-oxodG is carried out by the base excision repair (BER) pathway, and its efficiency is evaluated by 8-oxodG glycosylase activity which increases over the life span of rodents but does not seem to stop the accumulation of 8-oxodG during aging (103;104).

The concern surrounding 8-oxodG stems from its mutagenic coding potential when copied by an assortment of mammalian and prokaryotic polymerases (73-75). For all studies done with DNA polymerases, dC and dA were inserted across from 8-oxodG with comparable but varying efficiencies which potentially results in a G to T transversion mutation. The molecular mechanism for the lack of specificity afforded by 8-oxodG is thought to be due to its ability to form either a normal Watson-Crick hydrogen bonding arrangement with dCMP or a Hoogsteen base pair with dAMP by flipping to the *syn* conformation (76;77).

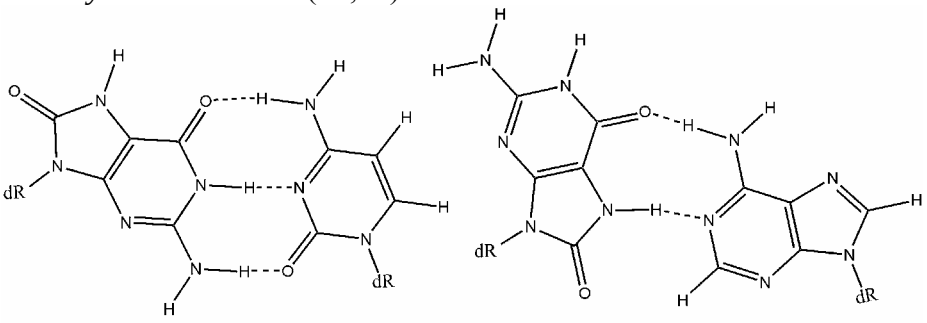

Arguably, the most important polymerase in regard to the replication of oxidatively damaged DNA is the human mitochondrial polymerase γ (Pol γ), which is responsible for the propagation and maintenance of the mitochondrial genome. Pertinent to Pol γ was a recent study done in mice where the researchers created a homozygous

knock-in that expressed a proofreading deficient version of Pol γ. The mice prematurely developed numerous signs of aging, presumably as a result of the reduction in the fidelity of replication of the mitochondrial genome (31).

We have examined in detail the kinetic parameters governing the fidelity of oxidatively damaged DNA replication by using a recombinant reconstituted human Pol γ and transient-state kinetic techniques. Due to growing evidence for the possibility and significance of damaged free nucleotides incorporated during the replication of DNA, we also investigated the kinetics of 8-oxodGTP incorporation (75;105-107).

MATERIALS AND METHODS

Nucleotides and oligonucleotides

8-oxodGTP was purchased from TriLink BioTechnologies (San Diego, CA), and unmodified dNTP were purchased from Sigma-Aldrich (St. Louis, MO). Oligonucleotides containing 8-oxodG (except for the primer terminated with 8-oxodG, which was enzymatically synthesized in our lab) were purchased from The Midland Certified Reagent Company (Midland, TX), and all other (unmodified) oligonucleotides were purchased from Integrated DNA Technologies (Coralville, IA).

Pol γ expression and purification

Overexpression and purification of recombinant human Pol γ were previously described (11;12). Holoenzyme was reconstituted at a 1:5 ratio of catalytic subunit to accessory subunit. Unless stated otherwise all kinetic studies were conducted using an exonuclease-deficient mutant (E200A).

Preparation of DNA

The 25mer primer sequence was 5′-GCCTCGCAGCCGTCCAACCAACTCA-3′, and the template sequence was 5′-

GGACGGCATTGGATCGACA**X**TGAGTTGGTTGGACGGCTGCGAGGC-3′, where the bold **X** in the template was modified according to the particular experiment performed (any modifications to the primer and template base sequences are detailed in the results section). Primer was 5′-^{32}P-labeled using T4 polynucleotide kinase, according to the manufacturer's instructions (Invitrogen, Carlsbad, California). The reaction was terminated by incubation at 95°C for 5 minutes, and excess nucleotide was removed using a Bio-Spin 6 column (BioRad, Hercules, CA). The primer was annealed to 45mer template by combining at an equimolar ratio, heating to 95°C, and slowly cooling to room temperature. Primers containing 3′-terminal 8-oxodG were enzymatically synthesized because they could not be chemically synthesized. A polymerase reaction was performed using 1 μM Pol γ, 100 μM duplex DNA (containing dC as the template base opposite 26th primer position), and 150 μM 8-oxodG in standard reaction buffer (50 mM Tris-Cl, pH 7.5, 100 mM NaCl, 2.5 mM $MgCl_2$). The reaction mixture was incubated at 37°C for 30 min, and then the product was gel-purified to obtain the 8-oxodG-terminated primer. Primer was labeled with ^{32}P on the 5′-end, and DNA duplex was annealed as described above.

Polymerization and exonuclease reaction conditions

For reactions too fast to measure by manual mixing and quenching, a quench-flow apparatus (RFQ-3) from KinTek Corporation (Austin, TX) was used. All incorporation assays were performed at 37^{o}C in buffer containing 50 mM Tris-Cl, pH 7.5, 100 mM NaCl, and 2.5 mM $MgCl_2$. The holoenzyme was reconstituted by incubating the two protein subunits for 5 min on ice in reaction buffer lacking magnesium. DNA was then added to the proteins, and the mixture was incubated for an additional 5 min on ice. Incorporation reactions were initiated by the addition of nucleotide and magnesium in the same reaction buffer at 37°C and then quenched with 0.5 M EDTA. Alternatively, the

excision reactions were initiated by the addition of 2.5 mM $MgCl_2$. All concentrations given are concentrations after mixing. Products were separated on 15% denaturing polyacrylamide sequencing gels, imaged on a Molecular Dynamics Storm 860 Imager, and quantified using ImageQuaNT software (Amersham Biosciences, Uppsala, Sweden).

Ground-state dissociation constant and maximum rate of polymerization for dNTP or 8-oxodGTP

Single nucleotide incorporation assays were performed with various concentrations of dNTP or 8-oxodGTP to examine the nucleotide concentration dependence of incorporation rate or amplitude. Single-turnover conditions were employed where the concentration of enzyme was greater than the concentration of DNA. Specific reaction conditions are listed in each Figure legend. A time course was performed for each concentration of dNTP. To normalize data, the integrated amount of product (DNA_{n+1}) was divided by the sum of the substrate and product ($DNA_n + DNA_{n+1}$) and multiplied by the concentration of DNA used in the experiment. The concentration of extended DNA product was plotted against time and fit to a single ([product] = $A_1*e^{-k_1t}$ +C) or double ([product] = $A_1*e^{-k_1t} + A_2*e^{-k_2t}$ + C) exponential equation (as stated in the Figure legends and results section). The observed rates, and in one case, amplitudes were plotted against dNTP concentration, and the data were fit to a hyperbola (observed rate (or amplitude) = k_{pol} (or A_{max}) * [dNTP]/(K_d + [dNTP]) to obtain the K_d and the maximum rate of polymerization, k_{pol} or maximum amplitude (A_{max}), for each dNTP or 8-oxodGTP.

K_d for DNA binding

A fixed concentration of enzyme was combined with increasing concentrations of DNA, allowed to equilibrate for 20 min on ice, and then reacted with an equal volume of nucleotide at 37°C. Reactions were quenched after 0.3 s by the addition of 0.3 M EDTA.

Final reaction conditions were 50 nM catalytic subunit, 500 nM accessory subunit, 300 μM dGTP, 50 mM Tris-HCl, pH 7.5, 100 mM NaCl, 2.5 mM $MgCl_2$, and a range of DNA concentrations. The amount of DNA product was plotted as a function of substrate DNA concentration, and the data were fit to the quadratic equation,

$$ED = \frac{(K_d + E_o + D) - \sqrt{(K_d + E_o + D)^2 - 4(E_o D)}}{2}$$

where E_o and D represent enzyme and DNA concentrations, respectively.

RESULTS

Incorporation of dATP prior to template 8-oxodG

Single-turnover conditions were employed, in that the enzyme concentration was in excess of DNA concentration. In order to understand in detail how Pol γ replicates DNA with oxidative damage, we designed a complementary primer and template combination of 24 and 45 bases, respectively. At the 25th position of the template is a dT followed by an 8-oxodG at the 26th, so that with a 24mer primer a correct single nucleotide incorporation reaction could be performed using dATP to inspect incorporation just prior to 8-oxodG.

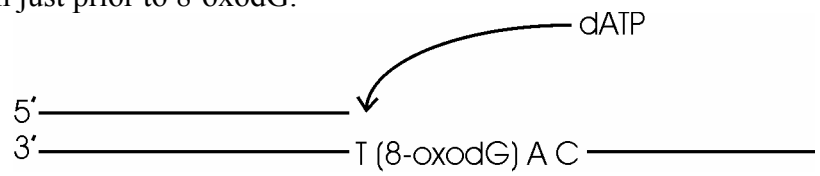

Exonuclease-deficient Pol γ holoenzyme was preincubated with the 24/45mer (8-oxodG) and rapidly mixed with increasing concentrations of dATP in a quench-flow apparatus, and at the specified times, quenched with 0.5 M EDTA. The time dependent formation of 25mer was fit to a single exponential equation and plotted in Figure 6.1A.

The single exponential rate for each reaction was plotted versus dATP concentration and fit to a hyperbola to obtain a ground-state dissociation constant (K_d) of 1.3 ± 0.2 μM and a maximum rate of polymerization (k_{pol}) of 53 ± 5 s^{-1} (Figure 6.1B). The specificity constant (k_{pol}/K_d) of 40 ± 7 $\mu M^{-1}s^{-1}$ is close to that of dATP incorporation onto undamaged DNA of 57 ± 6 $\mu M^{-1}s^{-1}$ (19). Therefore, the presence of 8-oxodG in the next template position does not alter the kinetics of incorporation.

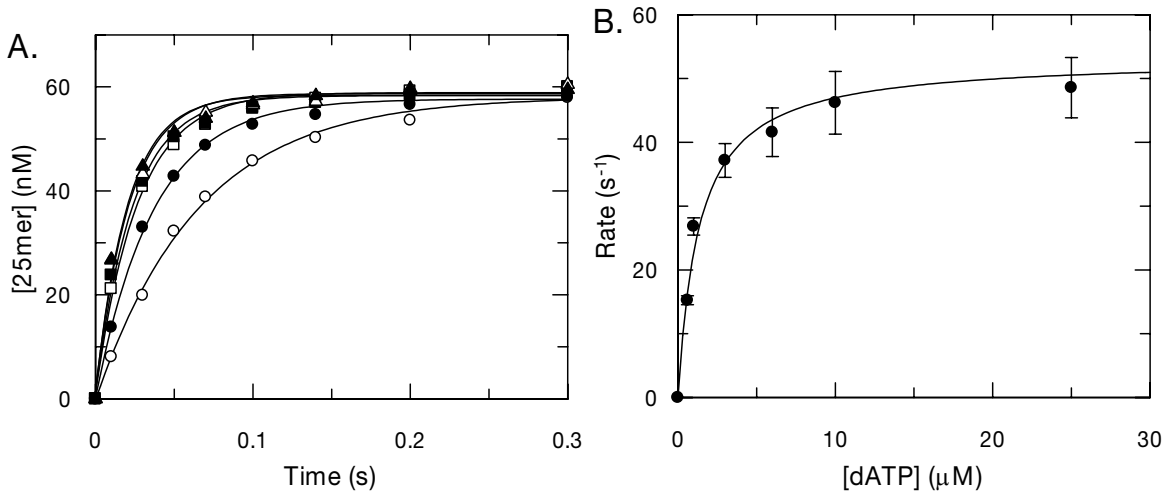

Figure 6.1: Incorporation of dATP prior to template 8-oxodG

(A) 100 nM exonuclease-deficient holoenzyme was preincubated with 90 nM 24/45mer ((**T**(8-oxodG)AC), the bold **T** signifies the position of incorporation) DNA duplex and then rapidly mixed with Mg^{+2} and various concentrations of dATP (0.6 (○), 1 (●), 3 (□), 6 (■), 10 (△), and 25 (▲) μM). Each data set was fit by non-linear regression to a single exponential equation to obtain the rate of incorporation. **(B)** the single exponential rates were plotted as a function of dATP concentration. A fit of the data to a hyperbola yields a $K_d = 1.3 \pm 0.2$ μM and a $k_{pol} = 53 \pm 5$ s^{-1}.

Incorporation of correct and incorrect base pairs onto 8-oxodG

To inspect the incorporation of the four dNTP directly onto 8-oxodG, we designed a primer and template combination of 25 and 45 bases, respectively, with 8-oxodG at the 26th position in the template.

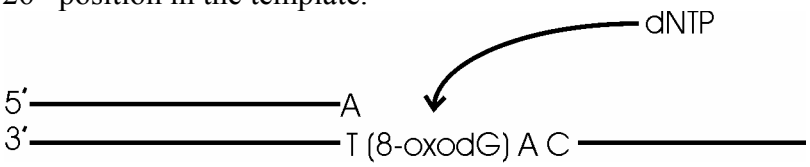

Exonuclease-deficient Pol γ holoenzyme was preincubated with the 25/45mer (8-oxodG) and rapidly mixed with increasing concentrations of each dNTP (separate experiments were performed for each dNTP) in a quench-flow apparatus, and at the specified times, quenched with 0.5 M EDTA. The time dependent formation of 26mer was fit to a single exponential equation and plotted in Figures 6.2-6.5A. The single exponential rate for each reaction was plotted versus dNTP concentration and fit to a hyperbola to obtain the values for each K_d and k_{pol} (Figures 6.2-6.5B). The results are summarized in Table 6.1.

	k_{pol} (s^{-1})	K_d (μM)	Specificity (k_{pol}/K_d)
dCTP	10 ± 0.8	100 ± 13	0.100± 0.001
dATP	3.4 ± 0.5	300 ± 70	0.011 ± 0.003
dGTP	0.07 ± 0.01	550 ± 150	0.00013 ± 0.00004
dTTP	0.0061 ± 0.0005	110 ± 20	0.000055 ± 0.000002

Table 6.1: Summarized results for the incorporation of correct and incorrect nucleotides onto 8-oxodG

The ground-state binding affinities and the rates of incorporation of each dNTP were reduced from that seen for unmodified dG in the template. The specificities of the incorporation of the four nucleotides onto 8-oxodG reveal that Pol γ prefers dCTP only 9-fold more than dATP when polymerizing over oxidatively damaged DNA. dGTP and dTTP are poor as substrates in comparison to dCTP with specificity constants nearly 800 and 2000-fold less, respectively. Accordingly, 8-oxodG will be highly mutagenic with an error frequency of 1/10.

Exonuclease removal of dCMP and dAMP paired with 8-oxodG

To inspect the likelihood that dC and dA are stably incorporated onto 8-oxodG we designed two primer and template combinations (26/45mer) where at the 26th position was either a correct dC:8-oxodG base pair or an incorrect dA:8-oxodG base pair and measured the rate of exonuclease removal of dC and dA.

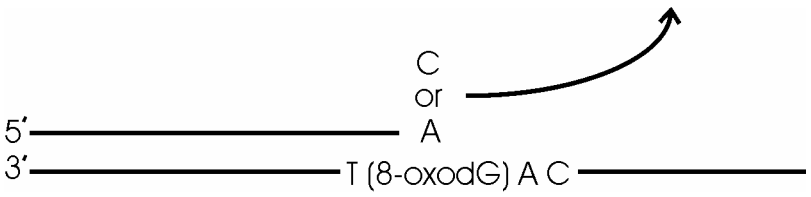

Wild-type Pol γ holoenzyme was preincubated with DNA under single-turnover conditions and mixed with Mg^{+2} to start the reaction. The concentration of substrate 26mer was plotted as a function of time and fit to a double exponential equation (Figure 6.2C is removal of dC, and Figure 6.3C is removal of dA). The removal of both dC and dA paired with 8-oxodG were biphasic with fast-phase rates of 0.08 ± 0.01 s^{-1} and 0.26 ± 0.02 s^{-1}, respectively. The amplitude of the fast-phase of each removal reaction was about 60 nM which is the amount of Pol γ/DNA complex present at equilibrium (under our single-turnover conditions). Therefore, the rate of removal for the slow phase of the reaction will be ignored because it is a function of the rate of DNA binding.

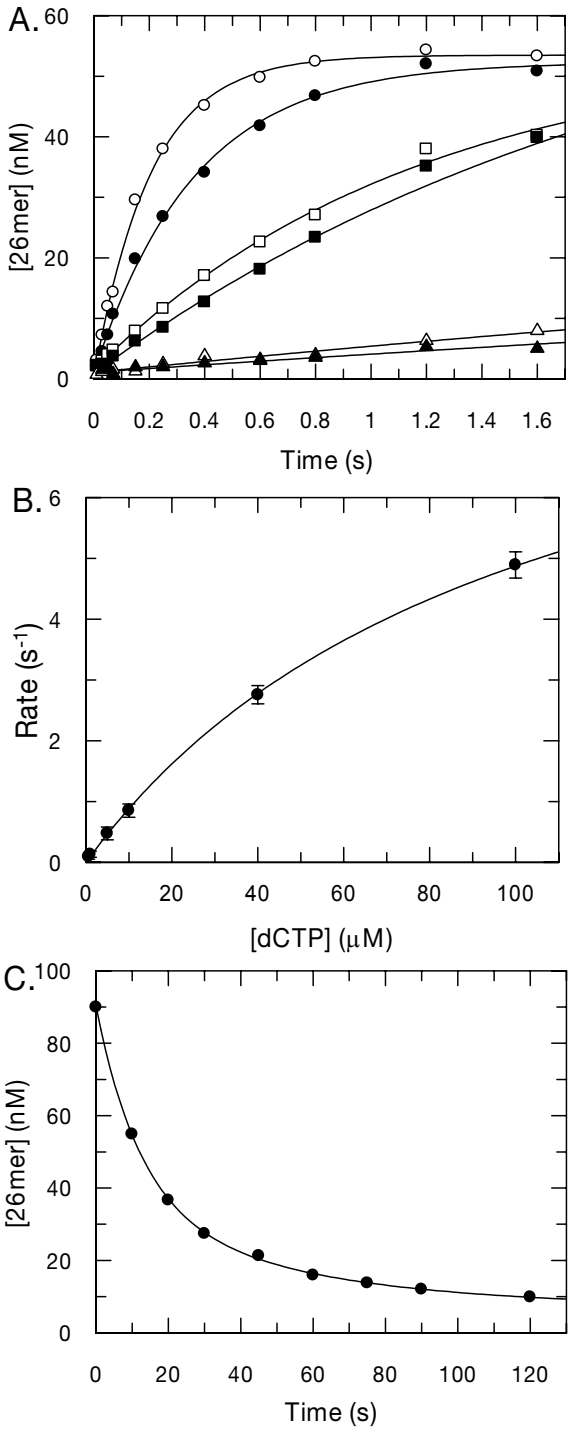

Figure 6.2: Incorporation of dCTP onto a template 8-oxodG

Figure 6.2: Incorporation of dCTP onto a template 8-oxodG

(A) 100 nM exonuclease-deficient holoenzyme was preincubated with 90 nM 25/45mer((T**(8-oxodG)**AC), the bold **(8-oxodG)** signifies the position of incorporation) DNA duplex and then rapidly mixed with Mg^{+2} and various concentrations of dCTP (0.6 (▲), 1 (△), 5 (■), 10 (□), 40 (●), and 100 (○) μM). Each data set was fit by non-linear regression to a single exponential equation to obtain the rate of incorporation. **(B)** The single exponential rates were plotted as a function of dCTP concentration. A fit of the data to a hyperbola yields a $K_d = 100 \pm 13$ μM and a $k_{pol} = 10 \pm 0.8\ s^{-1}$. **(C)** Shown is the excision of C, base-paired with 8-oxodG (template). 100 nM wild-type holoenzyme was preincubated with 90 nM 26**C**/45mer((T**(8-oxodG)**AC), the bold signifies bases that are directly across from one another) DNA duplex and mixed with Mg^{+2} to start the reaction. Concentration of substrate was plotted as a function of time and fit to a double exponential equation to obtain the rate of excision. The reaction was biphasic with rates of $0.08 \pm 0.01\ s^{-1}$ and $0.02 \pm 0.01\ s^{-1}$ and amplitudes of 54 ± 11 nM and 29 ± 9 nM, respectively.

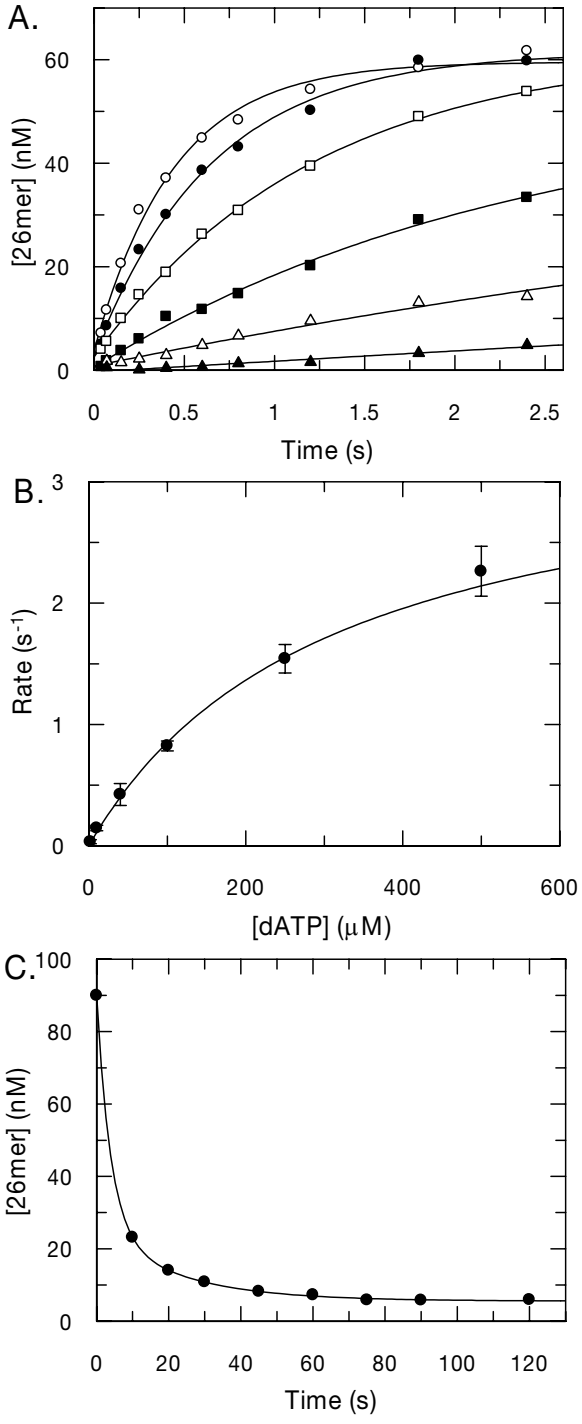

Figure 6.3: Incorporation of dATP onto a template 8-oxodG

Figure 6.3: Incorporation of dATP onto a template 8-oxodG

(A) 100 nM exonuclease-deficient holoenzyme was preincubated with 90 nM 25/45mer((T**(8-oxodG)**AC), the bold **(8-oxodG)** signifies the position of incorporation) DNA duplex and then rapidly mixed with Mg^{+2} and various concentrations of dATP (2 (▲), 10 (△), 40 (■), 100 (□), 250 (●), and 500 (○) μM). Each data set was fit by non-linear regression to a single exponential equation to obtain the rate of incorporation. **(B)** The single exponential rates were plotted as a function of dATP concentration. A fit of the data to a hyperbola yields a $K_d = 300 \pm 70$ μM and a $k_{pol} = 3.4 \pm 0.5$ s^{-1}. **(C)** Shown is the excision of A, base-paired with 8-oxodG (template). 100 nM wild-type holoenzyme was preincubated with 90 nM 26**A**/45mer((T**(8-oxodG)**AC), the bold signifies bases that are directly across from one another) DNA duplex and mixed with Mg^{+2} to start the reaction. Concentration of substrate was plotted as a function of time and fit to a double exponential equation to obtain the rate of excision. The reaction was biphasic with rates of 0.26 ± 0.02 s^{-1} and 0.045 ± 0.007 s^{-1} and amplitudes of 65 ± 3 nM and 20 ± 3 nM, respectively.

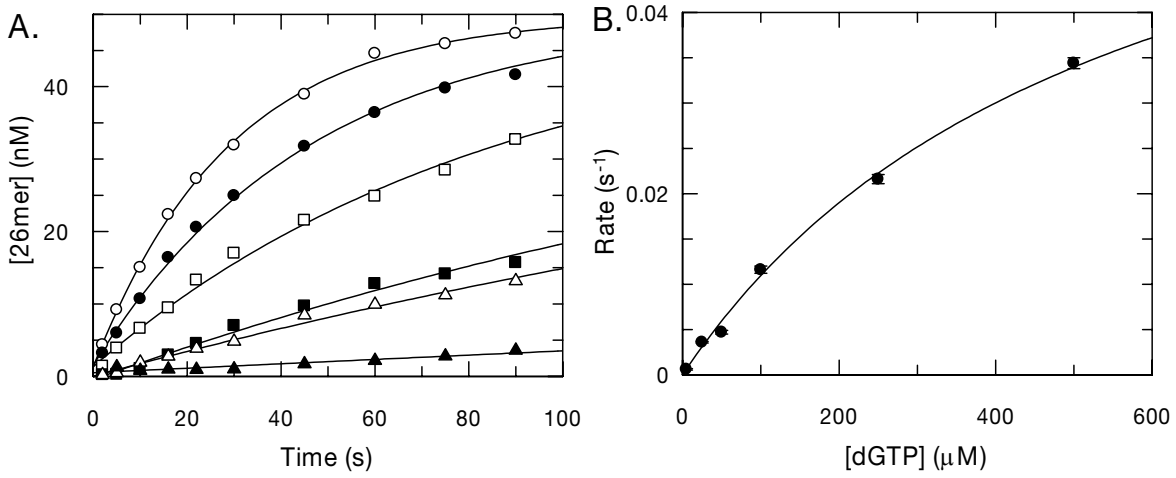

Figure 6.4: Incorporation of dGTP onto a template 8-oxodG

(A) 100 nM exonuclease-deficient holoenzyme was preincubated with 90 nM 25/45mer((T**(8-oxodG)**AC), the bold **(8-oxodG)** signifies the position of incorporation) DNA duplex and then rapidly mixed with Mg^{+2} and various concentrations of dGTP (5 (▲), 25 (△), 50 (■), 100 (□), 250 (●), and 500 (○) μM). Each data set was fit by non-linear regression to a single exponential equation to obtain the rate of incorporation. **(B)** The single exponential rates were plotted as a function of dGTP concentration. A fit of the data to a hyperbola yields a $K_d = 550 \pm 150$ μM and a $k_{pol} = 0.07 \pm 0.01$ s^{-1}.

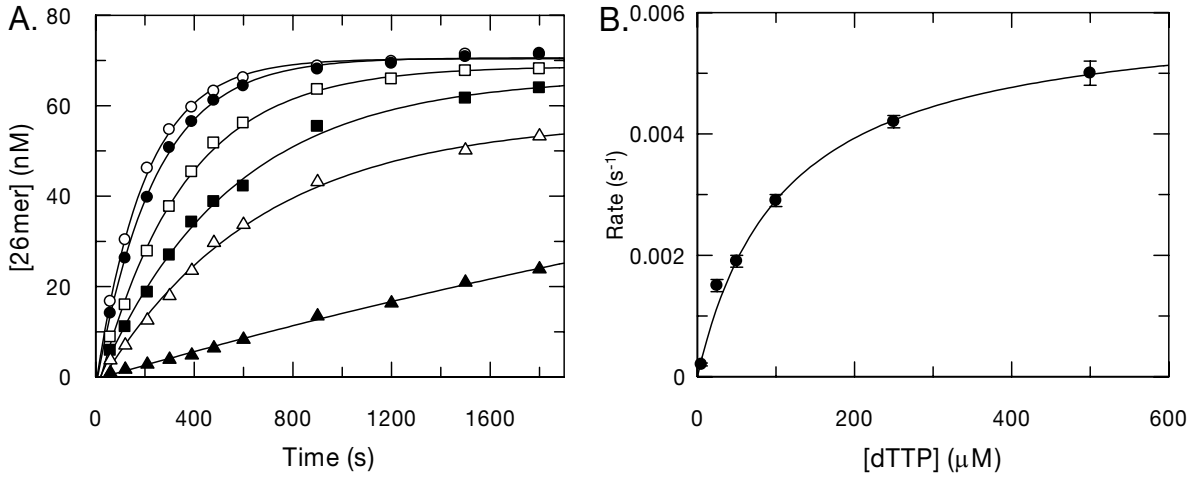

Figure 6.5: Incorporation of dTTP onto a template 8-oxodG

(A) 100 nM exonuclease-deficient holoenzyme was preincubated with 90 nM 25/45mer((T**(8-oxodG)**AC); the bold **(8-oxodG)** signifies the position of incorporation) DNA duplex and then rapidly mixed with Mg^{+2} and various concentrations of dTTP (5 (▲), 25 (△), 50 (■), 100 (□), 250 (●), and 500 (○) μM). Each data set was fit by non-linear regression to a single exponential equation to obtain the rate of incorporation. **(B)** The single exponential rates were plotted as a function of dTTP concentration. A fit of the data to a hyperbola yields a $K_d = 110 \pm 20$ μM and a $k_{pol} = 0.0061 \pm 0.0005$ s^{-1}.

Incorporation beyond correctly and incorrectly paired 8-oxodG

In order to assess the ability for Pol γ to replicate oxidatively damaged DNA, it is important to inspect DNA synthesis past the site of damage as well. This was accomplished by designing two primer and template combinations of 26 and 45 bases, respectively, starting synthesis at either a correct dC:8-oxodG or an incorrect dA:8-oxodG base pair.

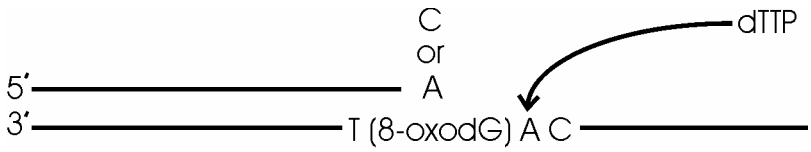

Incorporation of dTTP by Pol γ was slightly more efficient at burying a dC:8-oxodG base pair than a dA:8-oxodG mispair, with a K_d of 4.4 ± 1.0 μM and a k_{pol} of 19 ± 3 s^{-1} for the correct base pair (Figure 6.6) compared to a K_d of 10 ± 1 μM and k_{pol} of 13 ± 0.7 s^{-1} (Figure 6.7) for the mismatch. The specificity was about 4-fold greater following the correct base pair, but both were efficiently incorporated beyond. For reference, the normal incorporation of dTTP onto undamaged DNA by Pol γ occurs with a K_d of 0.6 μM at a k_{pol} of 25 s^{-1}, illustrating that the efficiency was not altered dramatically. Furthermore, the rate of incorporation of dTTP was much faster than the rate of removal of either dC (0.08 s^{-1}) or dA (0.26 s^{-1}) base-paired with 8-oxodG. Combining these results we calculate a 98 percent probability that a dA:8-oxodG mispair will be buried rather than removed.

$$\frac{k_{exo}}{k_{exo} + k_{pol,over}} = \frac{0.26}{0.26 + 13} = 0.019$$

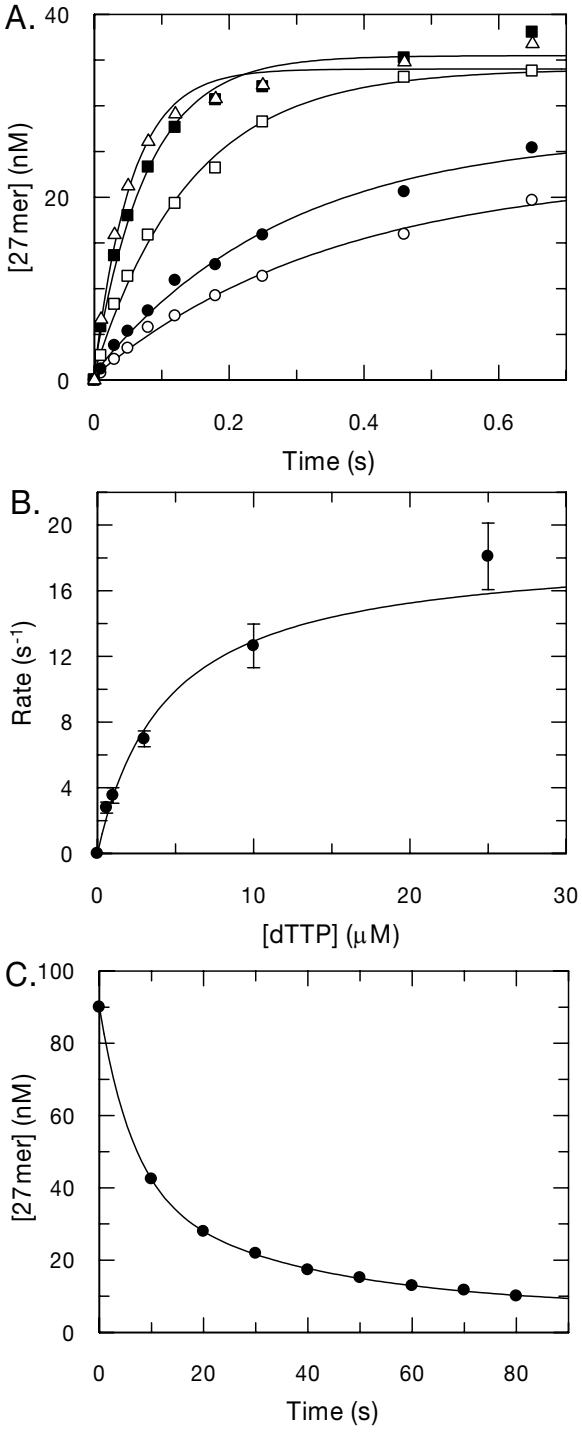

Figure 6.6: Incorporation of dTTP beyond a dC:8-oxodG base pair

Figure 6.6: Incorporation of dTTP beyond a dC:8-oxodG base pair

(A) 100 nM exonuclease-deficient holoenzyme was preincubated with 90 nM 26C/45mer((T(8-oxodG)**A**C), the bold **A** signifies the position of incorporation) DNA duplex and then rapidly mixed with Mg^{+2} and various concentrations of dTTP (0.6 (○), 1 (●), 3 (□), 10 (■), and 25 (△) μM). Each data set was fit by non-linear regression to a single exponential equation to obtain the rate of incorporation. **(B)** The single exponential rates were plotted as a function of dTTP concentration. A fit of the data to a hyperbola yields a $K_d = 4.4 \pm 1.0$ μM and a $k_{pol} = 19 \pm 3\ s^{-1}$. **(C)** Shown is the excision of T (T buries a C:8-oxodG (template) base pair). 100 nM wild-type holoenzyme was preincubated with 90 nM 27**CT**/45mer((T**(8-oxodG)A**C), the bold signifies bases that are directly across from one another) DNA duplex and mixed with Mg^{+2} to start the reaction. Concentration of substrate was plotted as a function of time and fit to a double exponential equation to obtain the rate of excision. The reaction was biphasic with rates of $0.16 \pm 0.01\ s^{-1}$ and $0.028 \pm 0.005\ s^{-1}$ and amplitudes of 50 ± 4 nM and 33 ± 3 nM, respectively.

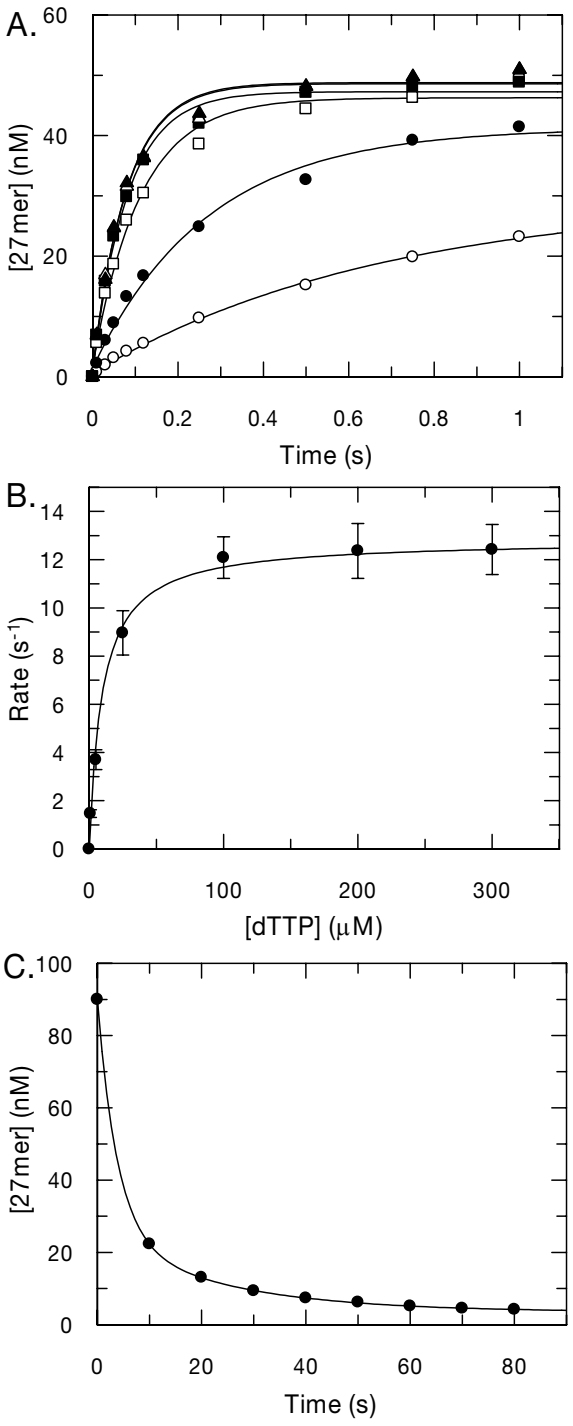

Figure 6.7: Incorporation of dTTP beyond a dA:8-oxodG base pair

Figure 6.7: Incorporation of dTTP beyond a dA:8-oxodG base pair

(A) 100 nM exonuclease-deficient holoenzyme was preincubated with 90 nM 26A/45mer((T(8-oxodG)**A**C), the bold **A** signifies the position of incorporation) DNA duplex and then rapidly mixed with Mg^{+2} and various concentrations of dTTP (1 (○), 5 (●), 25 (□), 100 (■), 200 (△), and 300 (▲) μM). Each data set was fit by non-linear regression to a single exponential equation to obtain the rate of incorporation. **(B)** The single exponential rates were plotted as a function of dTTP concentration. A fit of the data to a hyperbola yields a K_d = 10 ± 1 μM and k_{pol} = 13 ± 0.7 s^{-1}. **(C)** Shown is the excision of T (T buries an A:8-oxodG (template) base pair). 100 nM wild-type holoenzyme was preincubated with 90 nM 27**AT**/45mer((T**(8-oxodG)A**C), the bold signifies bases that are directly across from one another) DNA duplex and mixed with Mg^{+2} to start the reaction. Concentration of substrate was plotted as a function of time and fit to a double exponential equation to obtain the rate of excision. The reaction was biphasic with rates of 0.26 ± 0.01 s^{-1} and 0.043 ± 0.003 s^{-1} and amplitudes of 65 ± 1 nM and 22 ± 1 nM, respectively.

Removal of dT burying a correct or incorrect base pair with 8-oxodG

To have an accurate idea of the probability that a mutation occurs during replication of oxidatively damaged DNA, it was necessary to inspect the rate of removal of a correct base pair following either a correct dC:8-oxodG or an incorrect dA:8-oxodG base pair. Two primer and template combinations were designed where at the 26th position was either a correct dC:8-oxodG base pair or an incorrect dA:8-oxodG base pair and following that in the 27th position was a dT:dA base pair.

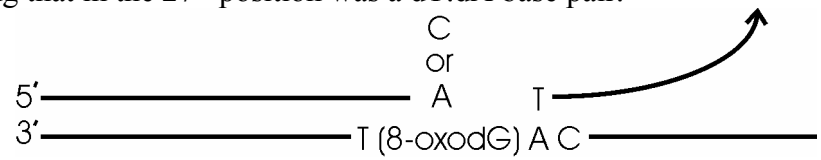

Removal of dT with both primer/template combinations was biphasic with fast-phase rates of 0.16 ± 0.01 s^{-1} and 0.26 ± 0.01 s^{-1}, respectively (Figure 6.6C is with dC:8-oxodG, and Figure 6.7C is with dA:8-oxodG). The amplitude of the fast phase of each removal reaction was, again, about 60 nM, which is the amount of Pol γ/DNA complex present at equilibrium (under our single-turnover conditions). Therefore, the rate of removal for the slow phase of the reaction will be ignored.

The ability of Pol γ to bury correctly and incorrectly base paired 8-oxodG

Continuing the single-step kinetic analysis of oxidatively damaged DNA polymerization by Pol γ, we designed an experiment that would assay for the ability of Pol γ to bury either a correct dC:8-oxodG (26th position) base pair followed by a T:A base pair (27th position) or an incorrect dA:8-oxodG (26th position) base pair followed by a T:A (27th position) base pair.

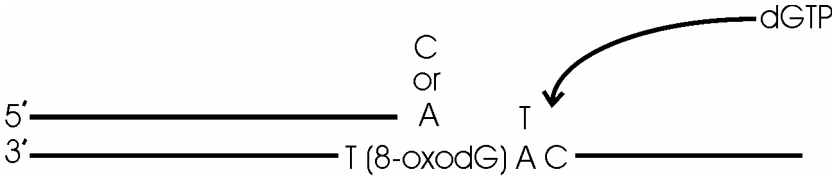

Pol γ is actually 3-fold more efficient at copying DNA with the mispair (Figures 6.8 and 6.9) at this step in polymerization. This was evidenced by a K_d of 7.9 ± 0.3 μM and a k_{pol} of 20.8 ± 0.6 s^{-1} for dGTP incorporation to bury a correct dC:8-oxodG base pair compared to a K_d of 3.2 ± 0.1 μM and a k_{pol} of 27.7 ± 0.5 s^{-1} for dGTP incorporation to bury an incorrect dA:8-oxodG base pair. Moreover, the amplitude of incorporation is about 10-15 nM higher for the reaction done with the mismatch, suggesting the enzyme binds tighter to the DNA with a mispair because the amplitude is a measure of the amount of productively-bound enzyme/DNA complex.

Dissociation constant for oxidatively damaged DNA

From the previous experiment it was discovered that the amplitude was lower than expected for dGTP incorporation onto the correctly base-paired 8-oxodG DNA primer/template combination. Therefore, an active site titration was performed in order to determine the dissociation constant for DNA binding. Exonuclease-deficient holoenzyme was preincubated with increasing concentrations of DNA and rapidly mixed with dGTP and Mg^{+2} to start the reaction. A time point of 0.3 seconds was taken for each DNA concentration because at a saturating concentration of dGTP, product formation was expected to be to full amplitude. Amplitude was plotted against DNA concentration and fit to the quadratic equation to obtain a K_d of 38 ± 12 nM (Figure 6.10). The quadratic equation was used to calculate a concentration of 51 ± 5 nM enzyme/DNA complex at equilibrium for the conditions used in the single-turnover experiment. The K_d for normal DNA binding is 25 ± 4 (data not shown), so a reduction in the amplitude is to

be expected, but the reduction was too large (30 nM amplitude) to be explained with this result.

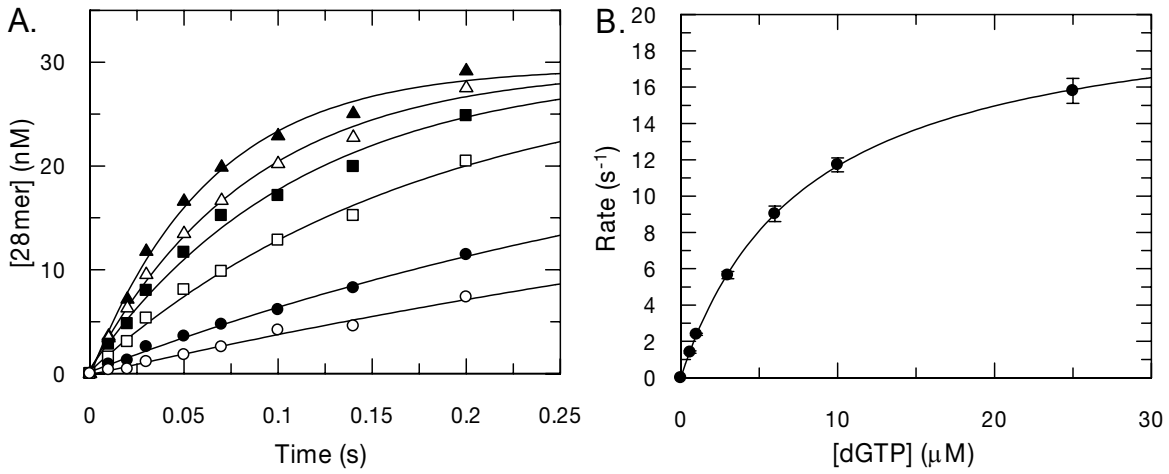

Figure 6.8: Incorporation of dGTP onto 27CT/45(8-oxodG)A**C**

(A) 100 nM exonuclease-deficient holoenzyme was preincubated with 90 nM 27CT/45mer((T(8-oxodG)A**C**), the bold **C** signifies the position of incorporation) DNA duplex and then rapidly mixed with Mg^{+2} and various concentrations of dGTP (0.6 (○), 1 (●), 3 (□), 6 (■), 10 (△), and 25 (▲) μM). Each data set was fit by non-linear regression to a single exponential equation to obtain the rate of incorporation. **(B)** The single exponential rates were plotted as a function of dGTP concentration. A fit of the data to a hyperbola yields a $K_d = 7.9 \pm 0.3$ μM and a $k_{pol} = 20.8 \pm 0.6$ s^{-1}.

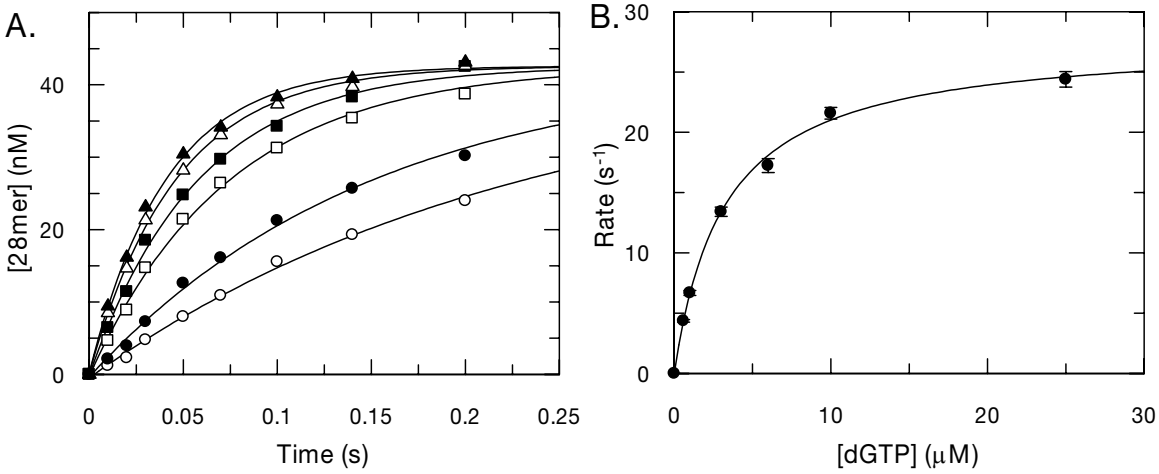

Figure 6.9: Incorporation of dGTP onto 27AT/45(8-oxodG)A**C**

(A) 100 nM exonuclease-deficient holoenzyme was preincubated with 90 nM 27AT/45mer((T(8-oxodG)A**C**), the bold **C** signifies the position of incorporation) DNA duplex and then rapidly mixed with Mg^{+2} and various concentrations of dGTP (0.6 (○), 1 (●), 3 (□), 6 (■), 10 (△), and 25 (▲) μM). Each data set was fit by non-linear regression to a single exponential equation to obtain the rate of incorporation. **(B)** The single exponential rates were plotted as a function of dGTP concentration. A fit of the data to a hyperbola yields a $K_d = 3.2 \pm 0.1$ μM and a $k_{pol} = 27.7 \pm 0.5$ s^{-1}.

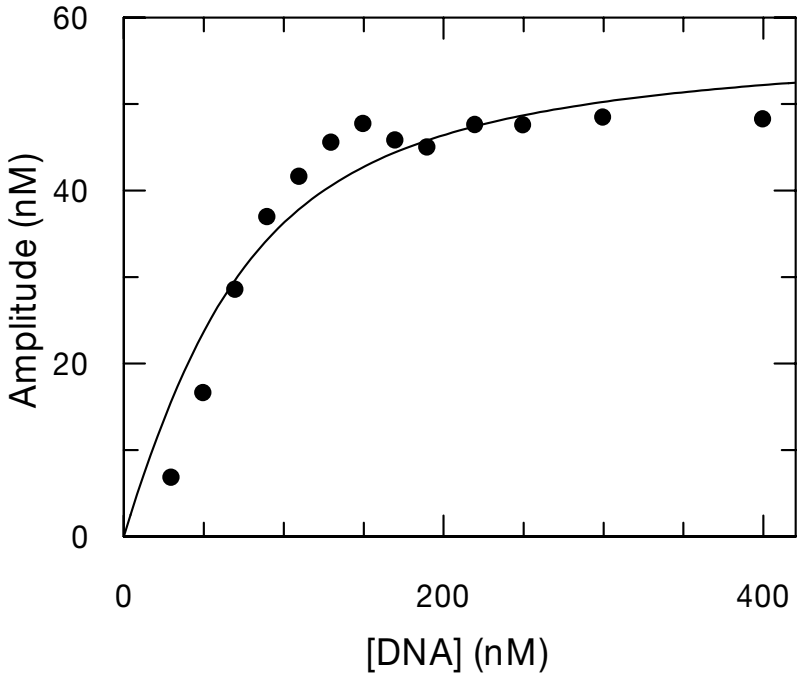

Figure 6.10: Active site titration of Pol γ with 27CT/45(8-oxodG)A**C**

Exonuclease-deficient holoenzyme (50 nM) was preincubated with increasing concentrations of 27CT/45mer((T(8-oxodG)A**C**), the bold **C** signifies the position of incorporation) DNA duplex and then rapidly mixed with Mg^{+2} and 200 μM dGTP. After 0.3 seconds, the reaction was quenched with 0.5 M.EDTA. The amount of product (amplitude) was plotted against DNA concentration and fit to the quadratic equation to yield a $K_d = 38 \pm 12$ nM for DNA binding.

Processive polymerization assay for replication of oxidatively damaged DNA

To assess the extent to which Pol γ can replicate full-length product with an oxidative lesion in the template in a single binding event we performed a processive DNA polymerization assay in the presence of a DNA trap. This was accomplished by using two primer and template combinations of 26 and 45 bases, respectively, starting synthesis at either a correct dC:8-oxodG or an incorrect dA:8-oxodG base pair and adding all four nucleotides to observe full-length product formation (dotted line).

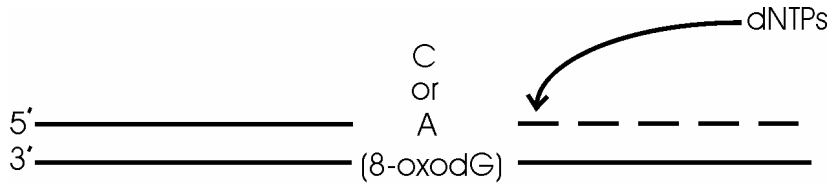

Exonuclease-deficient Pol γ holoenzyme was preincubated with 26/45mer DNA under single-turnover conditions and rapidly mixed with Mg^{+2}, 100 μM dNTP, and a 20-fold excess unlabeled DNA trap. The presence of the trap ensures that the full-length product observed is synthesized from a single enzyme molecule in a single binding event. Full-length product (45mer) was plotted as a function of time (Figure 6.11) and shows that the concentration of the resulting product agrees well with the results from the single nucleotide incorporation reactions. Interestingly, the amount of product obtained in the reaction starting with an dA:8-oxodG mismatch was significantly higher than the reaction starting with a correct dC:8-oxodG base pair.

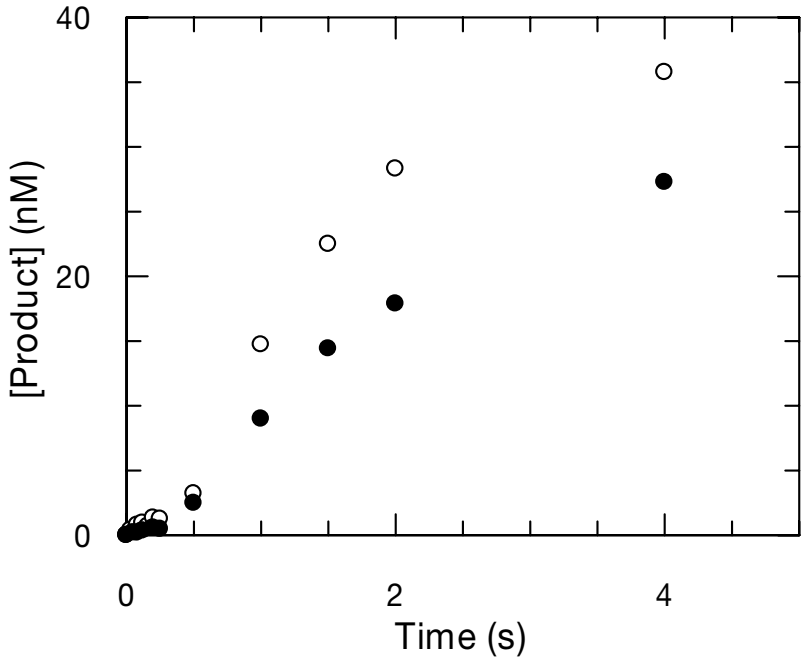

Figure 6.11: Processive polymerization assay with 8-oxodG in the template

100 nM exonuclease-deficient holoenzyme was preincubated with 90 nM 26**C**/45mer(**(8-oxodG)**, the bold signifies starting base pair position in the substrate DNA duplex) (●) or 26**A**/45mer((T**(8-oxodG)**AC) (○) DNA duplex and then rapidly mixed with Mg^{+2}, 100 μM dNTP, and an unlabeled 25/45mer DNA trap (20-fold excess). The concentration of full-length product was plotted as a function of time, showing that the reaction that started with an A:8-oxodG mismatch resulted in a higher concentration of full length product.

Incorporation 8-oxodGTP

Free dGTP has been shown to be even more susceptible to oxidation than dG in double-stranded DNA (106), which is of importance in the oxidative environment of the mitochondria. Therefore, we investigated the possibility that the mutagenic 8-oxodG accumulates in the mitochondrial DNA as a result of incorporation of 8-oxodGTP by Pol γ. Measurement of the kinetic parameters governing incorporation of 8-oxodGTP was carried out using an undamaged DNA primer and template of 25 and 45 bases (coding for G), respectively. Exonuclease-deficient holoenzyme was preincubated with DNA and rapidly mixed with increasing concentrations of 8-oxodGTP. Product formation as a function of time was plotted and fit to a double exponential equation (Figure 6.12A). There appears to be two dependencies occurring as a function of concentration of 8-oxodGTP, amplitude of the fast phase (Figure 6.12B), and rate of the slow phase (Figure 6.12C). The amplitude of the fast phase was fit to a hyperbola to obtain a K_d of 200 ± 30 μM while a fit of the slow phase rates revealed a K_d of 83 ± 7 μM and a k_{pol} = 0.4 ± 0.02 s^{-1}. The rate of the fast phase was relatively constant at about 2 s^{-1} and is reminiscent of data obtained with the 3' azide analogs (Chapter 4). An estimate of the specificity constant was obtained by using the K_d based on the amplitude dependence and the k_{pol} for the fast phase of the reaction and is equal to 0.01 ± 0.0015 $\mu M^{-1}s^{-1}$. See "Discussion" for a more detailed analysis of this data. Additional data regarding the incorporation of 8-oxodGTP collected by David M. Thal in our laboratory showed that the incorporation to form a mismatch with dA has a K_d of 2.4 ± 0.8 μM and a k_{pol} of 0.50 ±0.09 s^{-1} (data not shown) revealing its mutagenic potential even upon incorporation. The specificity constant is 21-fold greater than for the formation of the "correct" base pair (8-oxodG:dC).

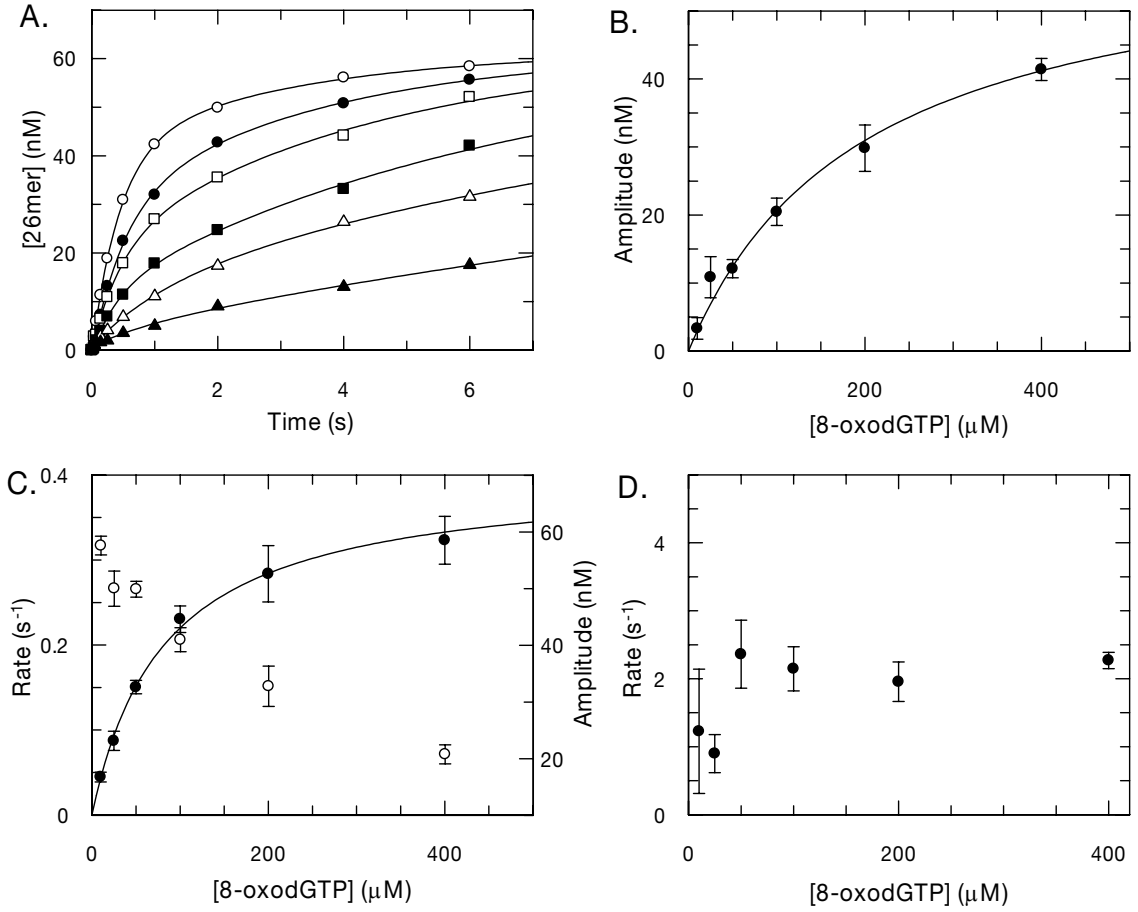

Figure: 6.12: Incorporation of 8-oxodGTP onto a template dC by Pol γ

(A) 100 nM exonuclease-deficient holoenzyme was preincubated with 90 nM 25/45mer (G incorporation) DNA duplex and then rapidly mixed with Mg^{+2} and various concentrations of 8-oxodGTP (10 (▲), 25 (△), 50 (■), 100 (□), 200 (●), and 400 (○) μM). Each data set was fit by non-linear regression to a double exponential equation to obtain the rate and amplitude of incorporation. **(B)** The single exponential amplitudes were plotted as a function of 8-oxodGTP concentration. A fit of the data to a hyperbola yields a K_d = 200 ± 30 μM and an A_{max} (maximum amplitude) = 62 ± 4 nM. **(C)** The rate from the slow phase of each reaction was plotted as a function of 8-oxodGTP concentration and fit to a hyperbola to yield a K_d = 83 ± 7 μM and a k_{pol} = 0.4 ± 0.02 s^{-1}.

Also shown is the amplitude of the slow phase as a function of concentration with the y-axis scale on the right side of the graph (○). **(D)** The rate from the fast phase of each reaction was plotted as a function 8-oxodGTP concentration to show that they remain relatively constant.

Exonuclease removal of 8-oxodGMP from the 3' terminus of the primer

To assess the probability that 8-oxodG is stably maintained in the mitochondrial genome once incorporated we examined the rate of excision using wild-type Pol γ and a 26/45mer (the primer was enzymatically terminated with 8-oxodG and correctly paired with dC). Plotted in Figure 6.13 is the concentration of substrate as a function of time with a fit to a single exponential equation. Interestingly, a rate of exonuclease removal of 0.075 ± 0.002 s^{-1} for the "correct" base pair was about 9-fold faster than the rate of excision for an 8-oxodGMP/dA mismatch (mismatch data collected by David M. Thal is not shown).

Incorporation of dTTP on a primer terminated with 8-oxodG

Once incorporated into a growing strand of DNA two competing rates dictate whether 8-oxodG will be buried or removed. Starting synthesis with a primer terminated with 8-oxodGMP (paired "correctly" with dC); we measured the kinetics of incorporation of the next correct nucleotide (dTTP). Product formation as a function of time was plotted and fit to a single exponential in Figure 6.14A. The single exponential rates were fit to a hyperbola to obtain a K_d of 9.3 ± 1.0 μM and a k_{pol} of 1.8 ± 0.1 s^{-1}, yielding a specificity constant of 0.19 ± 0.02 $uM^{-1}s^{-1}$ (Figure 6.14B). From the rate of polymerization and the rate of removal we can predict that if 8-oxodGMP is incorporated by Pol γ, it will be buried 96 percent of the time. Recent data by David M. Thal suggests that the efficiency of burying a mismatch of 8-oxodG with dA is similar (data not shown).

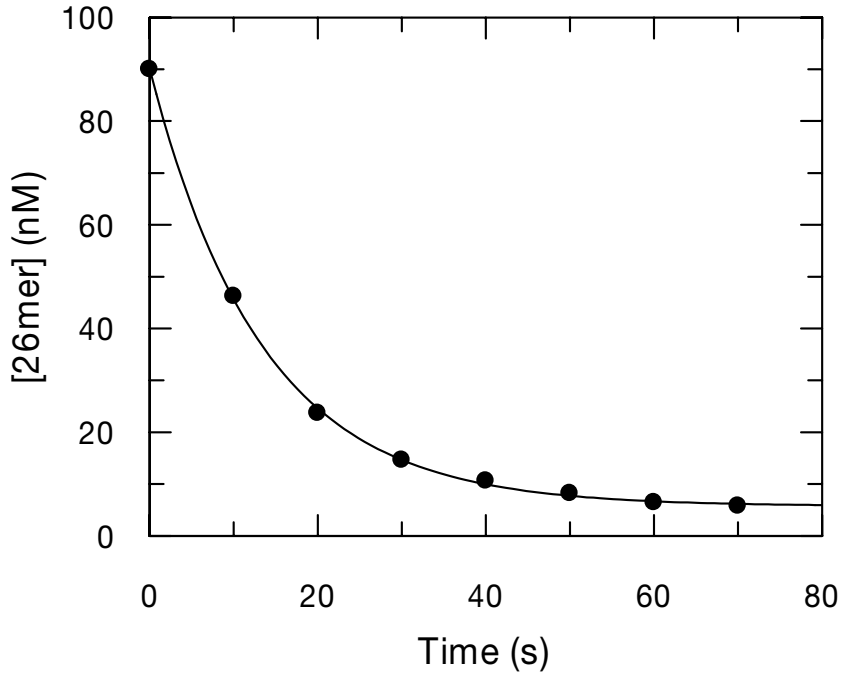

Figure 6.13: Exonuclease removal of 8-oxodGMP

100 nM wild-type holoenzyme was preincubated with 90 nM 26**(8-oxodG)**/45**C**mer (the bold signifies bases that are directly across from one another) DNA duplex and mixed with Mg^{+2} to start the reaction. Concentration of substrate was plotted as a function of time and fit to a single exponential equation to obtain a rate of excision of 0.075 ± 0.002 s^{-1} with an amplitude of 84.4 ± 0.7 nM

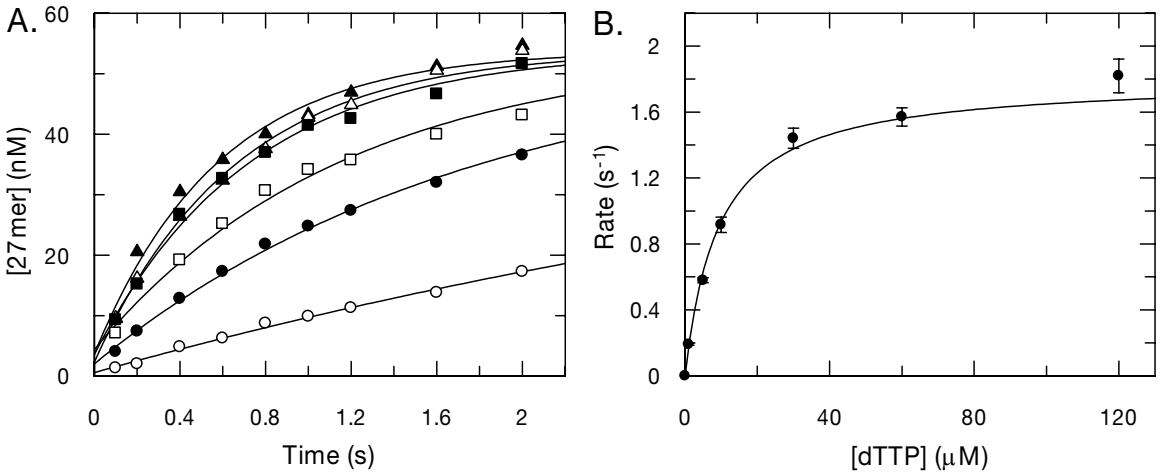

Figure 6.14: Correct incorporation of dTTP onto a primer terminated with 8-oxodGMP

(A) 100 nM exonuclease-deficient holoenzyme was preincubated with 90 nM 26(8-oxodG)/45C**A**mer (the bold **A** signifies the position of incorporation) DNA duplex and then rapidly mixed with Mg^{+2} and various concentrations of dTTP (1 (○), 5 (●), 10 (□), 30 (■), 60 (△), and 120 (▲) μM). Each data set was fit by non-linear regression to a single exponential equation to obtain the rate of incorporation. **(B)** The single exponential rates were plotted as a function of dTTP concentration. A fit of the data to a hyperbola yields a $K_d = 9.3 \pm 1.0$ μM and a $k_{pol} = 1.8 \pm 0.1$ s^{-1}.

Discussion

DNA damage is considered of paramount importance in aging, particularly in the mitochondria where the majority of the ROS are produced in healthy tissues. The levels of oxidative damage using 8-oxodG as a biomarker have been demonstrated to be 3- to 9-fold higher in mtDNA than nDNA in many species and the basal levels of damage were inversely correlated with the maximum life spans for the species examined (108). My studies show that the human mitochondrial DNA polymerase γ is capable of efficiently copying DNA with the oxidative lesion, 8-oxodG, present in the template.

Two pathways are shown in the following scheme. The left-hand pathway was constructed to present the experimentally determined kinetic parameters governing incorporation and exonuclease parameters at prior to and following 8-oxodG for the "correct" incorporation of dCTP across from 8-oxodG. The right-hand pathway presents the kinetic parameters of each incorporation and excision event for the "incorrect" incorporation of dATP across from 8-oxodG. The first step shown in the pathway (correct dATP incorporation) is the same for both and illustrates that there is a relatively small effect on the specificity constant for the incorporation of dATP just prior to 8-oxodG when compared to the incorporation onto an undamaged DNA substrate (40 ± 7 and 57 ± 6 $\mu M^{-1}s^{-1}$, respectively). Shown along the side of each pathway is the probability of that particular event to occur. For example, the "10% incorrect" beside dATP incorporation onto 8-oxodG represents that there is a 10% probability that dA will be inserted rater than the correct base dC. The percentages for the subsequent steps in the pathway represent the probability that incorporation will occur rather than proofreading excision. For example, there is a 98% probability that an incorrect dA:8-oxodG base pair will be buried by dTTP incorporation rather than the exonuclease removal of dA.

Furthermore, there is a 99% probability of continuing polymerization beyond dA:8-oxodG followed by a correct dT:dA base pair by the incorporation dGTP rather than the exonuclease removal of the correct dT. Thus, most mismatches opposite 8-oxodG will be extended and buried rather than removed by the proofreading exonuclease.

The most hindered incorporation event is the insertion of a nucleotide directly across from 8-oxodG. The specificity constant for dC incorporation across from 8-oxodG is reduced by about 470-fold (compared to incorporation onto dG) but is sufficiently fast for the polymerase to continue replication. However, the fidelity of replication is reduced significantly at the site of an oxidative lesion. Discrimination against the formation of the undamaged mispair, dA:dG, is 280,000 ± 80000 (in press H. Lee and K. A. Johnson), but the discrimination is reduced to 9 ± 0.3 (over 30,000-fold) for the base pair dA:8-oxodG. Pol γ discriminates relatively well against the incorporation of dGTP and dTTP onto 8-oxodG with discrimination values of 770 ± 240 and 1820 ± 70, respectively.

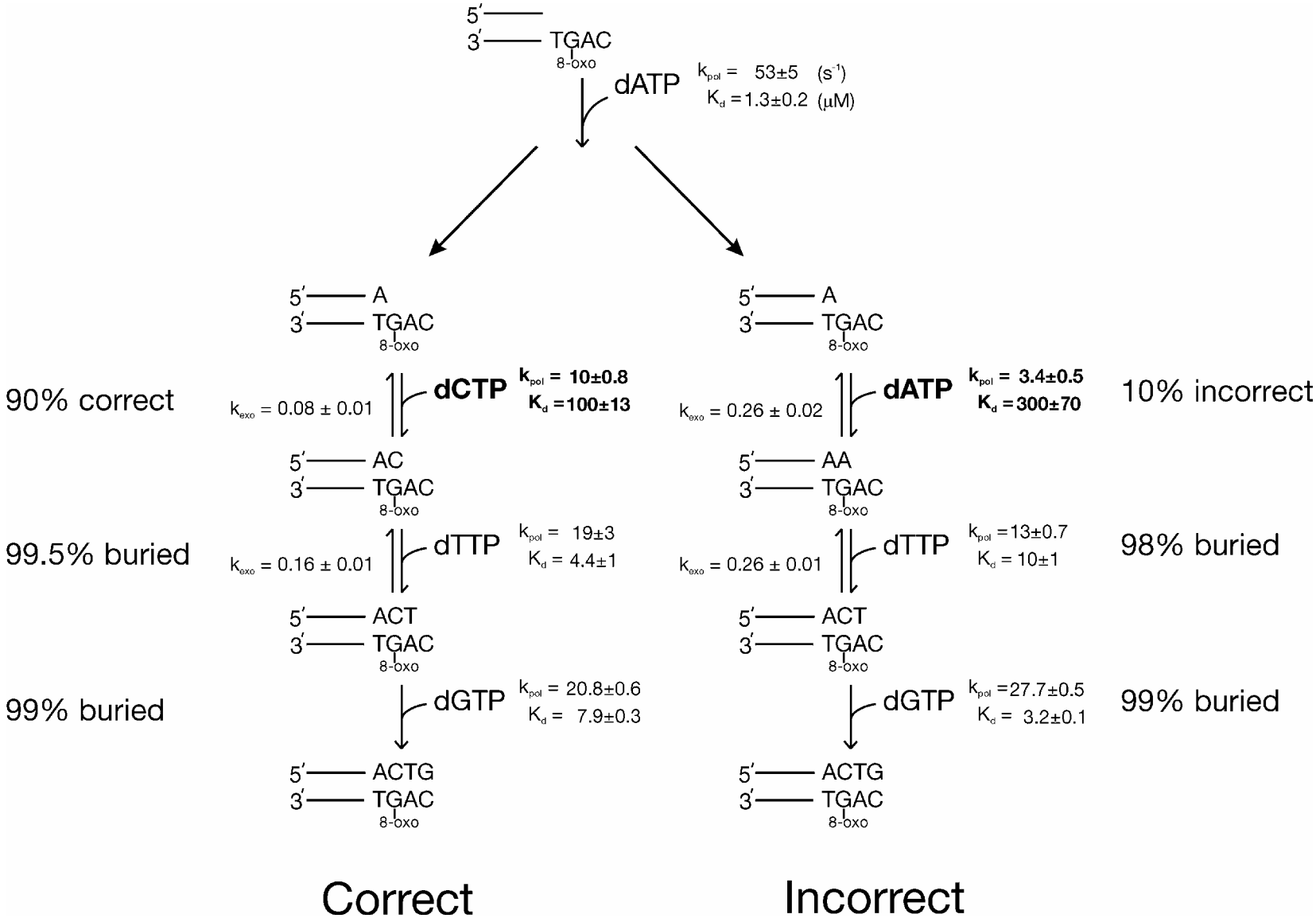
5′
3′ TGAC
8-oxo
dATP
k_{pol} = 53±5 (s^{-1})
K_d = 1.3±0.2 (μM)
5′ A
3′ TGAC
8-oxo
90% correct
k_{exo} = 0.08 ± 0.01
dCTP
k_{pol} = 10±0.8
K_d = 100±13
5′ AC
3′ TGAC
8-oxo
99.5% buried
k_{exo} = 0.16 ± 0.01
dTTP
k_{pol} = 19±3
K_d = 4.4±1
5′ ACT
3′ TGAC
8-oxo
99% buried
dGTP
k_{pol} = 20.8±0.6
K_d = 7.9±0.3
5′ ACTG
3′ TGAC
8-oxo
Correct
5′ A
3′ TGAC
8-oxo
k_{exo} = 0.26 ± 0.02
dATP
k_{pol} = 3.4±0.5
K_d = 300±70
10% incorrect
5′ AA
3′ TGAC
8-oxo
k_{exo} = 0.26 ± 0.01
dTTP
k_{pol} = 13±0.7
K_d = 10±1
98% buried
5′ ACT
3′ TGAC
8-oxo
dGTP
k_{pol} = 27.7±0.5
K_d = 3.2±0.1
99% buried
5′ ACTG
3′ TGAC
8-oxo
Incorrect

The processive polymerization assay starting the reaction at either the correct dC:8-oxodG or the incorrect dA:8-oxodG base pair in the presence of a DNA trap revealed that processive polymerization occurs without dissociation of the DNA from the enzyme active site. The total full-length product formed in that experiment was actually greater when starting with the mismatch and may be due to an increase in the rate of dissociation of DNA from the polymerase with the correct dC:8-oxodG (K_d = 25 compared to 38 nM). This could be due to a distortion in the DNA duplex with the "correct" base pair because of the steric hindrance between the 8-oxo-group and the phosphate backbone, which could also contribute to the lower coding specificity of 8-oxodG (the *syn* conformation is assumed when based paired with dA).

There is growing evidence that the incorporation of 8-oxodGTP is important to mutagenesis, carcinogenesis and aging (75;105). We examined the kinetics of incorporation for 8-oxodGTP onto both dC and dA. Shown in the following scheme is a summary of the kinetic parameters obtained to date governing the incorporation of 8-oxodGTP onto dC and dA and also shown are the kinetics of correct incorporation of dTTP following an 8-oxodG:dC base pair.

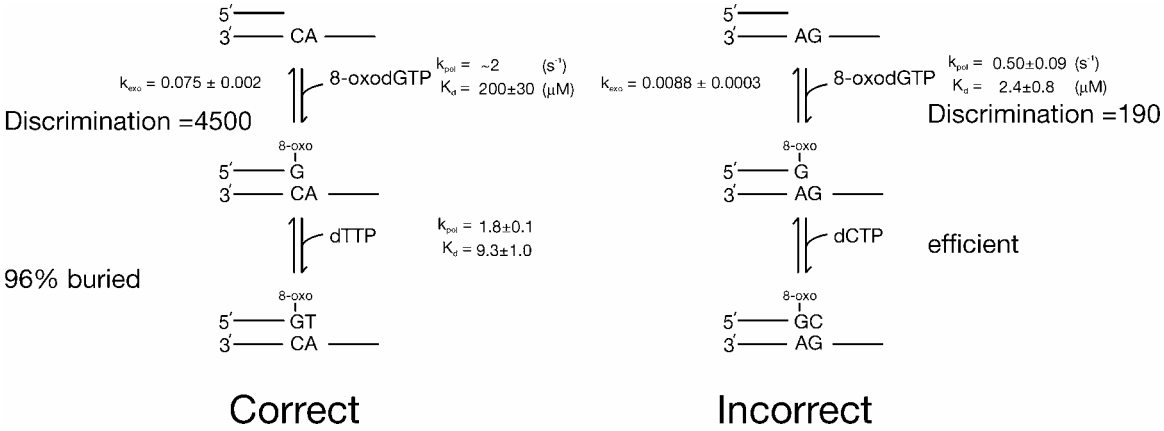

The incorporation of 8-oxodGTP onto dC was unusual, in that the reaction kinetics were biphasic. The amplitude of the fast phase of the reaction was dependent on concentration reminiscent of the 3′-azide analogs studied in Chapter 4. It was proposed that for AZTTP incorporation, phosphoryl transfer is reversibly linked to binding, resulting in a concentration dependent amplitude of incorporation. This explanation required that the conformational change after phosphoryl transfer was slow, trapping pyrophosphate in the active site, so that the reverse reaction of phosphoryl transfer (pyrophosphorolysis) equilibrated during incorporation. However, I observed an additional slower phase of incorporation of 8-oxodGTP that was not observed with AZTTP incorporation. The double exponential (8-oxodGTP incorporation), or lack thereof (AZTTP incorporation), may be due to the comparative difference between the rates of binding, phosphoryl transfer and pyrophosphate release. Regarding AZTTP incorporation, the rate of pyrophosphate release was much slower than incorporation so that the phosphoryl transfer step reached equilibrium at the active site. However, if pyrophosphate release was slightly faster, a double exponential could have been observed. To explain our 8-oxodGTP incorporation data a simulation was performed to test this possibility. The simulated curves with the experimentally obtained data are superimposed and shown in Figure 6.15.

A good fit was obtained using the same mechanism as shown in Figure 4.18 (AZTTP incorporation simulation) but with rates shown in the following scheme (Figure 6.15 legend). The conformational change following phosphoryl transfer (0.35 s^{-1}) is about the same rate as the slow phase of the reaction determined experimentally (0.40 ± 0.02 s^{-1}). This analysis supports a model in which the slow phase represents the rate limiting release of pyrophosphate allowing phosphoryl transfer to go to completion.

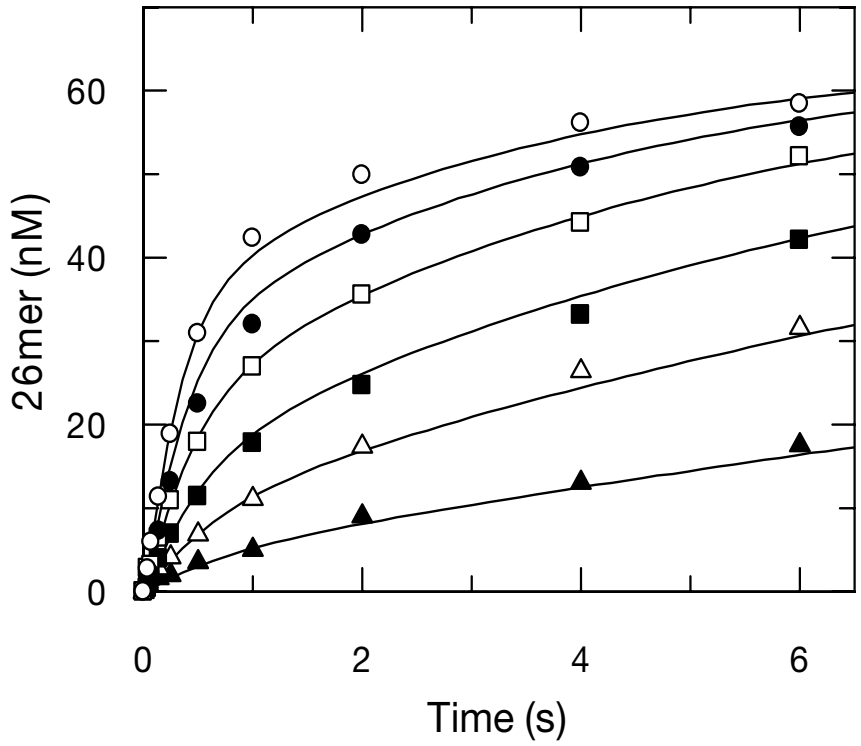

Figure 6.15: Simulated curves for the incorporation of 8-oxodGTP onto dC

Shown above is experimentally obtained data for the incorporation of 8-oxodGTP on to a template dC (dNTP in scheme) superimposed onto simulated data according to the mechanism and rates shown below. The experimental data was plotted earlier in Figure 6.12.

$$E_o \bullet DNA_n + dNTP \underset{k_{off} = 135\ s^{-1}}{\overset{k_{on} = 1\ \mu M^{-1}s^{-1}}{\rightleftharpoons}} E_c \bullet DNA_n \bullet dNTP \underset{k_{reverse} = 0.7\ s^{-1}}{\overset{k_{forward} = 2\ s^{-1}}{\rightleftharpoons}}$$

$$E_c \bullet DNA_{n+1} \bullet PPi \underset{}{\overset{k_{open} = 0.35\ s^{-1}}{\rightleftharpoons}} E_o \bullet DNA_{n+1} \bullet PPi \overset{fast}{\rightleftharpoons} E_o \bullet DNA_{n+1} + PPi$$

Whatever the case may be for the incorporation of 8-oxodGTP onto a template dC, a k_{pol} of about 2 s^{-1} can be estimated from the fast phase of the reaction, and an apparent K_d of 200 ± 30 μM can be used to estimate the specificity constant and the discrimination. Discrimination against 8-oxodGTP for incorporation across from dC and dA is 4500 ± 1300 and 190 ± 70, respectively. It is therefore 24-fold more likely that 8-oxodGTP will be incorporated as a mismatch; it is a surprisingly good substrate compared to dTTP. It is also unlikely that the mismatch will be repaired because the rate for removal of 8-oxodG across from either a dC or dA is slow in comparison to the rate of incorporation of the next correct nucleotide. For example, there is a 96 percent probability that after 8-oxodG is inserted across from a dC it is buried by the next correct nucleotide rather than exonuclease removal of 8-oxodG. Current efforts in the laboratory by David M. Thal are underway to measure the rate of incorporation of the next correct nucleotide on a primer/template with the mismatch, but preliminary data suggests that the mismatch will be buried with similar efficiency.

In summary, 8-oxodG in the template DNA strand dramatically reduces the fidelity of incorporation (30,000-fold), coding for dA 1/10 incorporation events. The polymerase is able to continue polymerization over 8-oxodG without dissociation, and the proofreading exonuclease activity is not effective at correcting the mismatch with dA. The incorporation of 8-oxodGTP appears to be especially mutagenic compared to 8-oxodG in the template. During the course of one's life this lack of discrimination against both the formation of dA:8-oxodG and 8-oxodG:dA mispairs along with the inefficient proofreading by Pol γ may contribute to the complicated process of aging.

References

1. Shoffner, J. M. and Wallace, D. C. (1994) *Annu.Rev.Nutr.* **14,** 535-568

2. Bourgeron, T., Rustin, P., Chretien, D., Birch-Machin, M., Bourgeois, M., Viegas-Pequignot, E., Munnich, A., and Rotig, A. (1995) *Nat.Genet.* **11,** 144-149

3. Bereiter-Hahn, J. (1990) *Int.Rev.Cytol.* **122,** 1-63

4. Robin, E. D. and Wong, R. (1988) *J.Cell Physiol* **136,** 507-513

5. Carrodeguas, J. A., Theis, K., Bogenhagen, D. F., and Kisker, C. (2001) *Mol.Cell* **7,** 43-54

6. Gray, H. and Wong, T. W. (1992) *J.Biol.Chem.* **267,** 5835-5841

7. Ropp, P. A. and Copeland, W. C. (1996) *Genomics* **36,** 449-458

8. Ito, J. and Braithwaite, D. K. (1990) *Nucleic Acids Res.* **18,** 6716

9. Ye, F., Carrodeguas, J. A., and Bogenhagen, D. F. (1996) *Nucleic Acids Res.* **24,** 1481-1488

10. Carrodeguas, J. A., Pinz, K. G., and Bogenhagen, D. F. (2002) *J.Biol.Chem.* **277,** 50008-50014

11. Graves, S. W., Johnson, A. A., and Johnson, K. A. (1998) *Biochemistry* **37,** 6050-6058

12. Johnson, A. A., Tsai, Y., Graves, S. W., and Johnson, K. A. (2000) *Biochemistry* **39,** 1702-1708

13. Lim, S. E., Longley, M. J., and Copeland, W. C. (1999) *J.Biol.Chem.* **274,** 38197-38203

14. Longley, M. J., Ropp, P. A., Lim, S. E., and Copeland, W. C. (1998) *Biochemistry* **37,** 10529-10539

15. Doublie, S., Tabor, S., Long, A. M., Richardson, C. C., and Ellenberger, T. (1998) *Nature* **391,** 251-258

16. Ahn, J., Kraynov, V. S., Zhong, X., Werneburg, B. G., and Tsai, M. D. (1998) *Biochem.J.* **331 (Pt 1),** 79-87

17. Eger, B. T. and Benkovic, S. J. (1992) *Biochemistry* **31,** 9227-9236

18. Einolf, H. J. and Guengerich, F. P. (2000) *J.Biol.Chem.* **275,** 16316-16322

19. Johnson, A. A. and Johnson, K. A. (2001) *J.Biol.Chem.* **276,** 38090-38096

20. Johnson, K. A. (1993) *Annu.Rev.Biochem.* **62,** 685-713

21. Kati, W. M., Johnson, K. A., Jerva, L. F., and Anderson, K. S. (1992) *J.Biol.Chem.* **267,** 25988-25997

22. Patel, S. S., Wong, I., and Johnson, K. A. (1991) *Biochemistry* **30,** 511-525

23. Johnson, K. A. (1992) *Philos.Trans.R.Soc.Lond B Biol.Sci.* **336,** 107-112

24. Hsieh, J. C., Zinnen, S., and Modrich, P. (1993) *J.Biol.Chem.* **268,** 24607-24613

25. Wong, I., Patel, S. S., and Johnson, K. A. (1991) *Biochemistry* **30,** 526-537

26. Moyle, G. (2000) *Clinical Therapeutics* **22,** 911-936

27. Johnson, A. A. and Johnson, K. A. (2001) *J.Biol.Chem.* **276,** 38097-38107

28. Donlin, M. J., Patel, S. S., and Johnson, K. A. (1991) *Biochemistry* **30,** 538-546

29. Pesole, G., Gissi, C., De Chirico, A., and Saccone, C. (1999) *J.Mol.Evol.* **48,** 427-434

30. Brown, W. M., George, M., Jr., and Wilson, A. C. (1979) *Proc.Natl.Acad.Sci.U.S.A* **76,** 1967-1971

31. Trifunovic, A., Wredenberg, A., Falkenberg, M., Spelbrink, J. N., Rovio, A. T., Bruder, C. E., Bohlooly, Y., Gidlof, S., Oldfors, A., Wibom, R., Tornell, J., Jacobs, H. T., and Larsson, N. G. (2004) *Nature* **429,** 417-423

32. Johnson, A. A., Ray, A. S., Hanes, J., Suo, Z., Colacino, J. M., Anderson, K. S., and Johnson, K. A. (2001) *J.Biol.Chem.* **276,** 40847-40857

33. Lewis, W., Copeland, W. C., and Day, B. J. (2001) *Lab Invest* **81,** 777-790

34. Cammack, N., Rouse, P., Marr, C. L., Reid, P. J., Boehme, R. E., Coates, J. A., Penn, C. R., and Cameron, J. M. (1992) *Biochem.Pharmacol.* **43,** 2059-2064

35. Chang, C. N., Doong, S. L., Zhou, J. H., Beach, J. W., Jeong, L. S., Chu, C. K., Tsai, C. H., Cheng, Y. C., Liotta, D., and Schinazi, R. (1992) *J.Biol.Chem.* **267,** 13938-13942

36. Chang, C. N., Skalski, V., Zhou, J. H., and Cheng, Y. C. (1992) *J.Biol.Chem.* **267,** 22414-22420

37. Gray, N. M., Marr, C. L., Penn, C. R., Cameron, J. M., and Bethell, R. C. (1995) *Biochem.Pharmacol.* **50,** 1043-1051

38. Hart, G. J., Orr, D. C., Penn, C. R., Figueiredo, H. T., Gray, N. M., Boehme, R. E., and Cameron, J. M. (1992) *Antimicrob.Agents Chemother.* **36,** 1688-1694

39. Schinazi, R. F., Chu, C. K., Peck, A., McMillan, A., Mathis, R., Cannon, D., Jeong, L. S., Beach, J. W., Choi, W. B., Yeola, S., and . (1992) *Antimicrob.Agents Chemother.* **36,** 672-676

40. Skalski, V., Chang, C. N., Dutschman, G., and Cheng, Y. C. (1993) *J.Biol.Chem.* **268,** 23234-23238

41. Skowron, G. and Merigan, T. C. (1990) *Am.J.Med.* **88,** 20S-23S

42. Robbins, B. L., Srinivas, R. V., Kim, C., Bischofberger, N., and Fridland, A. (1998) *Antimicrob.Agents Chemother.* **42,** 612-617

43. Kewn, S., Hoggard, P. G., Henry-Mowatt, J. S., Veal, G. J., Sales, S. D., Barry, M. G., and Back, D. J. (1999) *AIDS Res.Hum.Retroviruses* **15,** 793-802

44. Balzarini, J. (1994) *Pharm.World Sci.* **16,** 113-126

45. Squires, K. E. (2001) *Antivir.Ther.* **6 Suppl 3,** 1-14

46. Lewis, W., Papoian, T., Gonzalez, B., Louie, H., Kelly, D. P., Payne, R. M., and Grody, W. W. (1991) *Lab Invest* **65,** 228-236

47. Lewis, W., Gonzalez, B., Chomyn, A., and Papoian, T. (1992) *J.Clin.Invest* **89,** 1354-1360

48. Cheng, Y. C. and Parker, W. B. (1994) *J.NIH Res.* **6,** 57-61

49. Honkoop, P., Scholte, H. R., de Man, R. A., and Schalm, S. W. (1997) *Drug Saf* **17,** 1-7

50. Colacino, J. M. (1996) *Antiviral Res.* **29,** 125-139

51. Horn, D. M., Neeb, L. A., Colacino, J. M., and Richardson, F. C. (1997) *Antiviral Res.* **34,** 71-74

52. Barile, M., Valenti, D., Quagliariello, E., and Passarella, S. (1998) *Gen.Pharmacol.* **31,** 531-538

53. McKenzie, R., Fried, M. W., Sallie, R., Conjeevaram, H., Di Bisceglie, A. M., Park, Y., Savarese, B., Kleiner, D., Tsokos, M., Luciano, C., and . (1995) *N.Engl.J.Med.* **333,** 1099-1105

54. McKenzie, R., Fried, M. W., Sallie, R., Conjeevaram, H., Di Bisceglie, A. M., Park, Y., Savarese, B., Kleiner, D., Tsokos, M., Luciano, C., and . (1995) *N.Engl.J.Med.* **333,** 1099-1105

55. Touchette, N. (1993) *J.NIH Res.* **5,** 33-35

56. Lewis, W., Meyer, R. R., Simpson, J. F., Colacino, J. M., and Perrino, F. W. (1994) *Biochemistry* **33,** 14620-14624

57. Periclou, A. P., Nandy, P., and Avramis, V. I. (2000) *In Vivo* **14,** 377-388

58. Johnson, A. A. and Johnson, K. A. (2001) *J.Biol.Chem.* **276,** 38090-38096

59. Staschke, K. A. and Colacino, J. M. (1994) *J.Virol.* **68,** 8265-8269

60. Lee, H., Hanes, J., and Johnson, K. A. (2003) *Biochemistry* **42,** 14711-14719

61. Shigenaga, M. K., Hagen, T. M., and Ames, B. N. (1994) *Proc.Natl.Acad.Sci.U.S.A* **91,** 10771-10778

62. Miquel, J., Economos, A. C., Fleming, J., and Johnson, J. E., Jr. (1980) *Exp.Gerontol.* **15,** 575-591

63. Bowling, A. C., Mutisya, E. M., Walker, L. C., Price, D. L., Cork, L. C., and Beal, M. F. (1993) *J.Neurochem.* **60,** 1964-1967

64. Shigenaga, M. K., Hagen, T. M., and Ames, B. N. (1994) *Proc.Natl.Acad.Sci.U.S.A* **91,** 10771-10778

65. Hudson, E. K., Hogue, B. A., Souza-Pinto, N. C., Croteau, D. L., Anson, R. M., Bohr, V. A., and Hansford, R. G. (1998) *Free Radic.Res.* **29,** 573-579

66. Barja, G. and Herrero, A. (2000) *FASEB J.* **14,** 312-318

67. Morre, D. M., Lenaz, G., and Morre, D. J. (2000) *J.Exp.Biol.* **203 Pt 10,** 1513-1521

68. Bulpitt, K. J. and Piko, L. (1984) *Brain Res.* **300,** 41-48

69. Chen, D., Cao, G., Hastings, T., Feng, Y., Pei, W., O'Horo, C., and Chen, J. (2002) *J.Neurochem.* **81,** 1273-1284

70. Barja, G. (2004) *Trends Neurosci.* **27,** 595-600

71. Gao, D., Wei, C., Chen, L., Huang, J., Yang, S., and Diehl, A. M. (2004) *Am.J.Physiol Gastrointest.Liver Physiol* **287,** G1070-G1077

72. Herrero, A. and Barja, G. (1999) *Aging (Milano.)* **11,** 294-300

73. Pinz, K. G., Shibutani, S., and Bogenhagen, D. F. (1995) *J.Biol.Chem.* **270,** 9202-9206

74. Shibutani, S., Takeshita, M., and Grollman, A. P. (1991) *Nature* **349,** 431-434

75. Kamiya, H. (2003) *Nucleic Acids Res.* **31,** 517-531

76. Gannett, P. M. and Sura, T. P. (1993) *Chem.Res.Toxicol.* **6,** 690-700

77. Krahn, J. M., Beard, W. A., Miller, H., Grollman, A. P., and Wilson, S. H. (2003) *Structure.(Camb.)* **11,** 121-127

78. Ausubel, F. M., Grent, R., Kingston, R. E., Moore, D. D., Seidman, J. G., Smith, J. A., and Struhl, K. (1997) *Current Protocols In Molecular Biology*

79. Fairbanks, G., Steck, T. L., and Wallach, D. F. (1971) *Biochemistry* **10,** 2606-2617

80. Brune, M., Hunter, J. L., Corrie, J. E., and Webb, M. R. (1994) *Biochemistry* **33,** 8262-8271

81. Weymouth, L. A. and Loeb, L. A. (1978) *Proc.Natl.Acad.Sci.U.S.A* **75,** 1924-1928

82. Loeb, L. A. and Kunkel, T. A. (1982) *Annu.Rev.Biochem.* **51,** 429-457

83. Lewis, W., Papoian, T., Gonzalez, B., Louie, H., Kelly, D. P., Payne, R. M., and Grody, W. W. (1991) *Lab Invest* **65,** 228-236

84. Lewis, W., Gonzalez, B., Chomyn, A., and Papoian, T. (1992) *J.Clin.Invest* **89,** 1354-1360

85. Honkoop, P., Scholte, H. R., de Man, R. A., and Schalm, S. W. (1997) *Drug Saf* **17,** 1-7

86. Colacino, J. M. (1996) *Antiviral Res.* **29,** 125-139

87. Horn, D. M., Neeb, L. A., Colacino, J. M., and Richardson, F. C. (1997) *Antiviral Res.* **34,** 71-74

88. Barile, M., Valenti, D., Quagliariello, E., and Passarella, S. (1998) *Gen.Pharmacol.* **31,** 531-538

89. Pan-Zhou, X. R., Cui, L., Zhou, X. J., Sommadossi, J. P., and Darley-Usmar, V. M. (2000) *Antimicrob.Agents Chemother.* **44,** 496-503

90. de la Asuncion, J. G., del Olmo, M. L., Sastre, J., Pallardo, F. V., and Vina, J. (1999) *Hepatology* **29,** 985-987

91. de la Asuncion, J. G., del Olmo, M. L., Sastre, J., Millan, A., Pellin, A., Pallardo, F. V., and Vina, J. (1998) *J.Clin.Invest* **102,** 4-9

92. Birkus, G., Hitchcock, M. J., and Cihlar, T. (2002) *Antimicrob.Agents Chemother.* **46,** 716-723

93. Feng, J. Y., Johnson, A. A., Johnson, K. A., and Anderson, K. S. (2001) *J.Biol.Chem.* **276,** 23832-23837

94. Feng, J. Y., Johnson, A. A., Johnson, K. A., and Anderson, K. S. (2001) *J.Biol.Chem.* **276,** 23832-23837

95. Whittington, R. and Brogden, R. N. (1992) *Drugs* **44,** 656-683

96. Adkins, J. C., Peters, D. H., and Faulds, D. (1997) *Drugs* **53,** 1054-1080

97. Birkus, G., Hitchcock, M. J., and Cihlar, T. (2002) *Antimicrob.Agents Chemother.* **46,** 716-723

98. Anderson, T. D., Davidovich, A., Feldman, D., Sprinkle, T. J., Arezzo, J., Brosnan, C., Calderon, R. O., Fossom, L. H., DeVries, J. T., and DeVries, G. H. (1994) *Lab Invest* **70,** 724-739

99. Fraley, A. W., Chen, D., Johnson, K., and McLaughlin, L. W. (2003) *J.Am.Chem.Soc.* **125,** 616-617

100. Dufour, E. and Larsson, N. G. (2004) *Biochim.Biophys.Acta* **1658,** 122-132

101. Alexeyev, M. F., Ledoux, S. P., and Wilson, G. L. (2004) *Clin.Sci.(Lond)* **107,** 355-364

102. Barja, G. (2002) *Ageing Res.Rev.* **1,** 397-411

103. Souza-Pinto, N. C., Hogue, B. A., and Bohr, V. A. (2001) *Free Radic.Biol.Med.* **30,** 916-923

104. Stevnsner, T., Thorslund, T., Souza-Pinto, N. C., and Bohr, V. A. (2002) *Exp.Gerontol.* **37,** 1189-1196

105. Yoshimura, D., Sakumi, K., Ohno, M., Sakai, Y., Furuichi, M., Iwai, S., and Nakabeppu, Y. (2003) *J.Biol.Chem.* **278,** 37965-37973

106. Kamiya, H. and Kasai, H. (1995) *J.Biol.Chem.* **270,** 19446-19450

107. Kamiya, H. and Kasai, H. (2000) *Nucleic Acids Res.* **28,** 1640-1646

108. Barja, G. and Herrero, A. (2000) *FASEB J.* **14,** 312-318

Vita

Jeremiah Wayne Hanes was born in Benkelman, Nebraska on November 7th, 1977, the son of Tim and Sherry Hanes. After graduating from Dundy County High School in May 1996, he attended The University of Nebraska at Lincoln. Jeremiah received the degree of Bachelor of Science in May 2000 and then went to The University of Texas at Austin for graduate studies in August 2000.

Permanent address: P.O. Box 233, Max, NE, 69037

This dissertation was typed by the author.